UTS UNIVERSITY OF TECHNOLOGY SYDNEY

Design of a scalable, single-use photo-bioreactor for the growth of algae in axenic conditions

Julian R. Kofler

PhD by research

Submitted in fulfilment of the requirements for
The degree of Doctor of Philosophy

Climate Change Cluster
School of Life Sciences
University of Technology Sydney
2021

Certificate of original authorship

I, Julian R. Kofler, declare that this thesis is submitted in fulfilment of the requirements for the award of Doctorate of Philosophy, in the Faculty of Science at the University of Technology Sydney.

This thesis is wholly my own work unless otherwise reference or acknowledged. In addition, I certify that all information sources and literature used are indicated in the thesis. This document has not been submitted for qualifications at any other academic institution. This research is supported by the Australian Government Research Training Program.

Signature:

Production Note:
Signature removed prior to publication.

Julian R. Kofler
08/12/2021

Acknowledgements

Many people contributed to shape this PhD journey, and to them I am very grateful. First, I would like to thank my main supervisor Peter Ralph, he gave me an amazing opportunity, guidance, and continuous advice. I learned a lot from his great leadership. Special thanks go to Leen Labeeuw, my co-supervisor, she continuously kept my thoughts and ideas in the right direction, preventing me from going down every rabbit hole I encountered in my research. Thank you both for the fruitful discussions about my work.

I would like to thank the tech staff at UTS for all the help provided. Thanks to Lochlan de Beyer for all the methodological guidance and dedication regarding photobioreactors set up. Lochlan's passion and craftmanship inspired me to find the perfect set up for my project. Many thanks to Paul Brooks, he was always ready to help out and to find the bits and pieces missing for my experimental setups.

The support of my peers was very important for the successful completion of my PhD work. Thanks to all the members of Algae Biosystems and Biotechnology group for the constant discussions and feedback received. I would like to offer my special thanks to Alonso Zavaleta, his expertise in photochemistry and photobiology perfectly complemented my research efforts. Thank you for your contributions and guidance.

I wish to acknowledge and give thanks for the funding I have received from the UTS International Research Scholarship, as well as GE Healthcare.

I am deeply grateful to my family for their continuous support. I always knew that there is someone out there rooting for me. This includes Cristina, my fiancée, that challenged and supported me and kept me sane during the hard times.

Preface

Julian R. Kofler was supported by the UTS International Research Scholarship, as well as an Australian Research Council (ARC) Linkage project (LP150100751) in cooperation with GE Healthcare Life Sciences.

Some of the research conducted for this thesis forms part of collaborative work. Special thanks go to Tim O'Meara (GE Healthcare) for his consistent support. We wish to thank Alonso Zavaleta Fernandez de Cordova (Alonso Zavafer), Harvey Bates, and Luca Maestrini for methodological guidance in chapter 2.

Thesis format

This thesis is comprised of an introduction chapter (Chapter 1), three data chapters (Chapter 2 to 4) and a conclusion chapter (Chapter 5). A detailed project overview is given subsequently after Chapter 1. At time of thesis submission, Chapter 1 (review portion) and 2 are in final draft for publication.

List of publications

The method that forms the basis for Chapter 2 has been submitted:

Alonso Zavafer, Harvey Bates, Leen Labeeuw, **Julian R. Kofler**, Peter J. Ralph, (2021). Normalized chlorophyll fluorescence imaging: a method to determine irradiance and photosynthetically active radiation in phytoplankton cultures. *Algal Research, (in review)*

Table of Contents

List of Figures

List of Tables

List of Abbreviations

AUS	Australia
BR	Bioreactor
C3G	C3 glomerulopathy
CAD	Computer aided design
CAPEX	Capital expenditure
CFD	Computational fluid dynamics
CHO	Chinese Hamster Ovary
D/L	Dark to light
D50	Penetration depth of 50% light attenuation in microalgae culture
D90	Penetration depth of 90% light attenuation in microalgae culture
DCFI	Direct Chlorophyll Fluorescence Imaging
DNA	Deoxyribonucleic acid
EFSA	European Food Safety Authority
EPA	Environmental Protection Agency
EPO	Erythropoetin
ETR	Electron transport rate
EU	European Union
FDA	Food and Drug Administration
FFT	Fast Fourier transformation
GEM	Genetically engineered microalgae
GESD	Generalized extreme studentized deviate
GM	Genetically modified
GMO	Genetically modified organism
GMP	Good manufacturing practice
GRAS	Generally recognized as Safe
HCL	Hydrochloric acid
ISAAA	International Service for the Acquisition of Agri-Biotech
ISPE	International Society for Pharmaceutical Engineering
LED	Light emitting diode
NaOH	Sodium hydroxide
NCFI	Normalized Chlorophyll Fluorescence Imaging
OGTR	Office of the Gene Technology Regulator
OPEX	Operating expenses
PAM	Pulse amplitude modulation
PAR	Photosynthetically Active Radiation
PBR	Photo-bioreactor
PCB	Printed circuit board
PE	Polyethylene
PPFD	Photosynthetic photon flux density
PSII	photosystem II
PTM	Post-translational modification
qPCR	quantitative Polymerase Chain Reaction
ROI	Regions of Interest
SD	Standard deviation
USDA	U.S. Department of Agriculture
WFI	water for injection

Abstract

Microalgal cultivation systems for biopharmaceutical production are currently limited and current biopharmaceutical bioreactors are not optimized in terms of efficient light and substrate supply for algae. This project aims to address this gap, by establishing a process to convert and optimize a bioreactor system which is already established in the biopharmaceutical sector into a photo-bioreactor (PBR) system, facilitating axenic microalgae growth at an industrial scale in a regulated environment. The system to be converted is an industrially used single-use bioreactor, for which an optimization platform was designed including both physical and digital components. The physical part consisted of a 200 L PBR and a scaled down 20 L PBR, both mimicking physical characteristics of the industrial bioreactor, thereby enabling the rapid testing of new illumination systems. Different methods, such as gassing-in method (mass transfer), pH- and dye-method (mixing time) and optical particle tracing (hydrodynamic flow) were utilized to characterise the system and validate the down-scaling process, which revealed similar cultivation features compared to the industrial bioreactor. The predominant focus of the optimization platform was the supply of light: as such, accurate and precise data of the light attenuation were needed. A novel, practical, and easily applicable optical method using modified cameras for measuring the light distribution of complex light sources was developed to address this – Direct Chlorophyll Fluorescence Imaging (DCFI). DCFI was applied to *Phaeodactylum tricronutum* and *Chlorella vulgaris* cultures at different cell concentrations for a variety of LED wavelengths, yielding precise light maps of the light distribution into the culture. These light maps and the particle tracing data were combined in a computer aided design (CAD) process which enabled the calculation of the best configuration of the artificial light system (LEDs) according to the optimal light experience for the microalgae cells. The CAD forms the digital component of the optimization platform and completes the system. The optimization platform and the underlying methodology builds the foundation for a streamlined approach to convert existing bioreactor systems or to optimize alternative PBR systems. As such, this technology can help in establishing microalgae as a cultivation system in the biopharmaceutical sector.

Chapter 1

Use of genetically engineered microalgae (GEMs) for pharmaceutical applications

REVIEW

Author Contributions

Julian R. Kofler wrote the manuscript. Leen Labeeuw advised and assisted in editing. Lik Theng Ho assisted in editing. Peter J. Ralph advised and assisted in editing.

1.1 Introduction

Biopharmaceutical production is a steadily growing industry, with a global market value of $USD 188 billion in 2017 [1], and a predicted value of $USD 278.2 billion in 2020 [2]. Biopharmaceuticals are medical drugs which are produced or refined in biological systems. Bacteria, yeast and mammalian cells are the prevalent biopharmaceutical hosts used in this industry, although it is primarily dominated by mammalian cells with 79% of approved products in 2015-2017 [1]. Mammalian cells are industrially favoured for their high yield, the robust tools for genetic modification readily available, and their complex post-translational modification (PTM). The PTM, including protein folding and the N-glycosylation of the amino acids, are essential for the activity of complex proteins: absence or limitations of the PTM can change the protein characteristics, their function and structure [3]. Yeast and bacteria lack PTM machinery [4], hence complex protein production in these hosts need to be additionally modified in the downstream processes to obtain the native protein activity, which gives mammalian cells an edge is this regard. However, challenges with using mammalian cells are the costly growth media, the delicate cultivation conditions and the high susceptibility to culture crashes, which makes yeast and bacteria with its lower production cost, simple handling, and the exceptional culture scalability, preferable for proteins with simple post-modifications.

Microalgae are a relatively new pharmaceutical production platform, with outstanding advantages compared to the conventional production hosts (see Table 1-1), meaning they could be cost efficient and reliable production systems. Microalgae are a diverse group of photosynthetic organisms. Taxonomically, microalgae belong to almost every major supergroup in the eukaryotic tree of life. However, in industry terms, cyanobacteria (photosynthetic prokaryotes) are also referred to as microalgae[5]. Eukaryotic microalgae are capable of correctly assembling and folding complex proteins with the potential secretion of final product into the culture media [6], all of which ultimately diminishes down-stream processing [7]. In terms of operational costs, microalgae have lower raw material costs compared to other hosts: for example, in the case of a human antibody production system, the cost is approximately $USD 150 g^{-1} for mammalian cells in comparison to less than $USD 0.05 g^{-1} for microalgae [8]. Microalgae have been recognised as a food source for centuries, which facilitate some of the species to be classified as “Generally Recognized as Safe” (GRAS) [9]. This status is given to organisms that present no harm for human consumption, and can therefore reduce the processing cost and toxicity concerns of biopharmaceuticals using these

hosts [10][11]. Regarding their cultivation, microalgae are less demanding than mammalian cells. They can endure broader fluctuations of temperature, pH, and substrate limitation during cultivation without the risk of culture crashes, which makes large scale systems more feasible [12]. Furthermore, microalgae do not carry the risk of endotoxin contamination [13], nor are there currently any known transferable human/mammalian pathogenic plant viruses [14][15]. Terrestrial plants share these benefits, yet their significantly longer cultivation time and higher scale-up costs are disadvantageous when compared to microalgae [16]. Pharmaceutical interest in microalgae is also reflected in the increase of publications in this field. In the last decade, the number of publication of microalgae in relation with biopharmaceuticals increased annually by around 10% to nearly 6000 publications in 2020 (Figure 1-1).

Table 1-1: Comparison of diverse biopharmaceutical expression systems. Modified from [15][16][17]

Expression Systems	Bacteria	Yeasts	Cultured Mammalian Cells	Animals	Plants	Microalgae	Plant cell culture
Protein folding accuracy	Low	Medium	High	High	High	High	High
Glycosylation	None	Incorrect	Correct	Correct	Minor Differences	Minor Differences	Minor Differences
Product quality	Low	Medium	High	High	High	High	High
Protein yield	Medium	High	High	High	High	High	High
Production scale	Limited	Limited	Limited	Limited	Worldwide	High	Limited
Production time	Short	Medium	Long	Long	Long	Short	Medium
Scale-up capacity	High	High	Very low	Low	Very high	High	Medium
Scale-up cost	High	High	High	High	Medium	Low	-
Overall cost	Medium	Medium	High	High	Low	Low	Medium
Contamination risk	Endotoxins	Low	High	High	Low	Low	Low risk
Safety	Low	Unknown	High	High	High	High	Non-specific

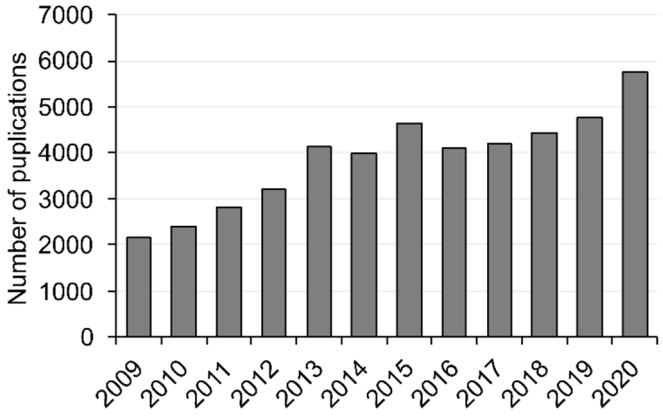

Figure 1-1: Annual publications in the field of microalgae and biopharmaceuticals from Google scholar. Key words: "Microalgae & biopharmaceuticals", "Microalgae & pharmaceuticals", or "Microalgae & recombinant protein"

1.1.1 Current work on genetically modified algae

Genetic engineering has emerged as a compelling strategy for optimizing the product yield in the biotechnology sector [18]. Nearly 40 years ago, the first successful DNA transformation of the microalgae *Chlamydomonas reinhardtii* was described [19], and since then genetic modification of microalgae has massively gained traction. Biopharmaceutical production in microalgae has been shown in over 50 cases, including antibodies, recombinant proteins, and vaccines [16][20][21]. One noteworthy example is Erythropoetin (EPO), a hormone that stimulates red blood cell production and is used for anaemia and cancer treatment. EPO was one of the most widely sold biopharmaceuticals in 2009 [22] and has an anticipated global market value of $USD 14.4 billion by 2024 [23]. The hormone was produced in *Chlamydomonas reinhardtii* and reached a concentration of 100 μg L^{-1} in initial trials [24], although this is still comparably lower than commercially used CHO cell lines that produce typically 50 mg L^{-1} [25]. Analysis of the glycosylation are still pending, but the hormone produced had a molecular weight of 33 kDa compared to 34 kDa of the native protein, suggesting that complex glycosylation took place. Another example of antibody expression in microalgae is the anti-Hepatitis B antibody produced in *Phaeodactylum triconutum,* which secreted up to 2.55 g L^{-1} [6]. The antibody showed a different binding affinity to the two receptors compared to the native mammalian protein due to a deviation of protein N-glycosylation. Future work will focus on glycoengineering of the microalgae to enhance this protein activity [26].

Genetic engineering of microalgae typically targets the chloroplast or the nucleus. The chloroplast is an organelle of prokaryotic origin [13] with high protein expression levels, eukaryotic-like ribosomes, but no post-translational glycosylation machinery [27]. In the nucleus, expression is much lower, yet specific post-translational modification can be targeted [28]. Furthermore, the total soluble protein concentration is higher in the chloroplast, with up to 10% of soluble protein, compared to the nucleus (0.2%) [28]. Selection of the genetic engineering site is particularly relevant in cases such as the recombinant protein production of Pfs25, a malaria transmission blocking vaccine [29]. Pfs25 consists of structurally complex subunits with disulfide bonds that does not need post-translational glycosylation. The particular expression process in the *Chlamydomonas reinhardtii* chloroplast folds the Pfs25 protein with its disulfide bonds, but does not glycosylate the protein. Typically the production of this protein in other hosts lead to unwanted glycosylation or incorrect folding [29], which makes the chloroplast expression in microalgae an appealing platform for genetic modification for this type of protein. This demonstrates the capability of microalgae to work with both proteins that require PTM, and those that do not, with the potential of genetic modification to establish microalgae as industrially relevant production hosts. However, the low titre achieved also showcases the substantial amount of work that still needs to be done.

1.1.2 Legislation covering genetically modified algae

The environmental impact of genetically modified organisms (GMO) on other species and the surrounding biodiversity are difficult to test or predict, and therefore pose an unknown risk in the event of an environmental release [30][31]. During cultivation, either special containment measurements must be in place to prevent the release of the GMO or extensive proof of the GMO safety has to be provided to mitigate these potential risks [32]. Currently, several genetically modified (GM) plants are internationally cultivated or are approved to be cultivated outdoors for food or biomass production [33]. According to International Service for the Acquisition of Agri-Biotech (ISAAA), Australia and European Union have about 107 (EU) and 135 (AUS) commercially accepted GM plants, including cotton, maize, potato, and soybean, with 17 of these accepted GM crops currently grown outdoors in Australia [34]. In the U.S., 203 plant GM species are commercially allowed for outdoor cultivation, which might reflect the higher acceptance of GM plants in the U.S. [35]. The approval process for uncontained cultivation is substantial, including risk assessments and conformity to national

regulations, which, combined with the low public acceptance of GMO products in some countries, has encouraged producers to avoid the whole GMO issue altogether.

There is no globally agreed upon definition for what constitutes a genetically modified organism. Regulations in U.S., European Union, and Australia distinguish GMOs depending on the method of manipulation, the transferred content, and the stability of the modification over several generations [36][37]. Gene modifications can be either from mutations induced by chemicals and radiation, or by targeted gene editing. Chemical mutagenesis is frequently not included in the GMO category, with the argument that this process solely accelerates naturally appearing mutations, does not introduce foreign DNA into the cell genome, and leaves no sign of the artificial modification in the strain [36][38][39]. These methods are rather random and need elaborate strain screening [40]. Targeted gene editing technics are more precise in modifying specific regions of the DNA and are preferred for their greater control, the reduced need for strain screening, and the ability to introduce foreign DNA into the cell genome [41]. Typically, these techniques rely on vectors (i.e., plasmids) that are introduced into the cell, which modifies the genome or the post-translational system of the cell [42]. Similar to chemically induced treatments, these techniques can be designed to leave minimal trace of an artificial modification in the strain [43].

The definition of what is classified as GMO is determined by each country or region. In Europe, the European Food Safety Authority (EFSA) is responsible for the regulation of GMO crops and assessment of GMO applications. EFSA's Panel on Genetically Modified Organisms carries out risk assessments of GMO applications based on molecular characterisation, comparative analysis, evaluation of potential toxicity and allergenicity, and evaluation of potential environmental impact [44]. Currently, European regulations classify organisms based on the methodology used for modification. Methods that exceed the accelerated natural mutation approach, for instance by introducing foreign DNA into the cell, are categorized as GMO. This includes targeted mutations, even if the final strain shows no sign of the mutation (e.g. knock-out) [45].

Australia and the US have similar regulations regarding GMOs. In Australia, the regulation of genetically modified organisms and the regulatory scheme is operated by the Office of the Gene Technology Regulator (OGTR). This department supplies information about how GMOs are regulated in Australia [46]. In the United States, GM crops are regulated by three regulatory agencies, with each performing different roles, i.e. the Environmental Protection Agency (EPA), the Food and Drug Administration (FDA), and the U.S. Department of Agriculture (USDA) [47]. Australia and the U.S. give the GMO classification primarily based on the

resulting strain and on the traceability of the artificial modification and transgenes in the strain [48][49]. Targeted mutagenesis that show no trace of an artificial modification beyond naturally occurring mutations can potentially avoid the label. Several organisms in the U.S. receiving a gene modification with these techniques were not classified as GMO and can be normally cultivated [50]. One example of this is the white button mushroom (*Agaricus bisporus*) engineered to reduce the browning of sliced mushrooms. This was achieved by disabling a core sequence responsible for the encoding of polyphenol oxidase enzyme with the CRISPR-Cas9 technique. The USDA stated that without a trace of the artificial modification, the GMO regulation does not apply to this strain [51]. By the end of 2020, more than 125 engineered plants were exempt from regulation [52].

These cases represent mainly higher plants for food application, but they have paved the way for modified microalgae and their uncontained cultivation. Current work on microalgae modified with accelerated mutation could avoid the GMO label entirely, and even GMO classified microalgae could possibly be cultivated outdoors, as seen with higher plants, if they satisfy GMO regulations in a particular country.

The GMO regulations concern the containment of potential GMOs and their possible release. Biopharmaceutical production however also has to consider additional guidelines affecting the product quality. The most common and worldwide recognized regulatory guideline is Good Manufacturing Practice (GMP). GMP covers all aspects of production and ensures that products are consistently produced and controlled to a certain standard of quality. Minimum requirements and thresholds for the production process are provided, which have to be met in order for the product to be released on the market [53]. GMP highly emphasizes contamination prevention and the impact of the used materials and chemicals on the final product. In terms of production, each piece of equipment which is used has to qualify for their intended use. This can be challenging for new microalgal technologies since the cultivation systems have limited manufacturing data to build on to demonstrate that they adhere to the strict guidelines. Conformity to GMP guidelines are crucial for the production and commercialisation of biopharmaceuticals, and needs to be addressed early in the development process. As such, microalgal specific technologies either have to go through rigorous testing in order to demonstrate that the whole novel production system is GMP compliant, or has to convert existing technologies, and only have to prove that the modification achieve compliance.

1.1.3 Current methods for large scale algal production

Efficient cultivation systems need to supply certain substrates to the culture to prevent substrate limitation. In regard to microalgae production, this means light and CO_2. CO_2 is the fundamental component for the synthesis of more complex molecules. A photobioreactor (PBR) that is incapable of providing a sufficient mass transfer will limit culture growth, especially in cases of high culture volumes and high cell concentrations. Microalgae in these scenarios directly absorb dissolved CO_2 from the media, meaning cells in less aerated or mixed regions of the PBR will be starving. Light, i.e., photons, are the source of energy for the cells, rendering it as another significant limitation factor of growth – and the most challenging one to ensure. Light attenuation in microalgae cultivation increases during the cultivation due to self-shading of the cells. Microalgae cells near the illuminated surface absorb the light, leaving cells deeper in the culture starving for photons [54]. This effect can be countered by enlarging the illuminated surface in relation to culture volume, which can be challenging for industrial scale productions. Mixing is also relevant in this regard as it improves the photosynthetic photon flux density (PPFD) within the culture by distributing photons to more cells [55]. Efficient photobioreactors systems need to consider not only possible light limitation, but also light inhibition, in which cells suffer increased photo-damage by high exposures of photons, which will also limit microalgae growth.

The most common designs of PBRs for microalgal cultivation can be categorized into open and closed systems. These two types of systems have different advantages and disadvantages that depend on the cultivated species, the production scale, and final product.

1.1.3.1 Open systems

Open systems can be broadly separated into two designs: raceway and open-pond systems. At industrial scale, these systems cover vast open areas which are typically uncontained, and therefore in direct contact with the environment. The exposed culture surface usually serves as the interface for the transmission of sunlight and CO_2, which leads to constraints on the amount of optimization that can be done to improve these parameters [56]. Light distribution can only be adjusted by reducing the depth, which improves the surface to volume ratio. Mass transfer in open pond occurs solely on the water surface, while in raceway ponds additional agitation of the culture with paddles, jets, and airlift system improves the mass transfer, although it also increases the energy demand. Due to their low CAPEX and OPEX, these open systems are widely used for low value products such as oil, biomass, and pigments [57]. However, open

systems hold inherent disadvantages for the use of genetically engineered microalgae (GEM), especially for pharmaceutical production.

Maintaining controlled culture conditions in open systems is difficult due to the large culture volume and the impact of external environmental conditions (e.g. seasonality, precipitation, etc.), which presents a challenge for the production of high value products in a GMP environment. Relevant culturing parameters such as pH, temperature, and light exposure are highly dependent on environmental conditions, which can be difficult to control. One improved design was able to maintain the temperature in a 8,500 L raceway pond by adjusting the culture volume flow and preventing overheating due to sun irradiance by keeping parts of the pond covered [58][59]. Control of the pH has been accomplished in a pilot-scale airlift raceway pond by active aeration used to buffer the pH, but also to keep the culture in motion [60]. However, fine control is still limited in open systems.

By the very nature of an open design, the culture is in direct contact with the environment which elevates the risk of product contamination. Natural competitors, bacteria, or viruses can overgrow or infest the GEM, resulting in decreased productivity or the loss of the complete batch [61]. Cultivation of higher plants for biopharmaceuticals face similar challenges to meet GMP compliance with potential microbial contaminations in the soil. In order to contain sources of contamination, higher plants are grown in fully automated and sterile hydro-cultures facilities, thereby reducing contamination risks and costs [62]. Theoretically, this approach could also be applied to open pond cultivation with glasshouses and containment facilities as a quasi-sterile environment, yet clearly, this would reduce the open pond advantage of low CAPEX and OPEX. A more appropriate solution is something like the Pharma-Planta project, a GMP compliant production of monoclonal antibodies in higher plants for a stage 1 clinical trial [63]. In this project, genetically engineered tobacco plants were grown in partially controlled, but not completely contained, greenhouse facilities on common soil and municipal water [64], hence in non-sterile environment. The approval of the European regulatory bodies was gained by splitting the production in specific up- and downstream process phases. The first phase, including cultivation, harvesting, and primary processing, took place in the greenhouse facility, an unsterile- and non-GMP environment, yet with standard operational procedures for processes and materials to keep the product quality risks to a minimum. In phase two, the plant extract was transferred to a GMP-certified facility and further processed [63]. This approach was adopted into the “Guideline On The Quality Of Biological Active Substances Produced By Stable Transgene Expression In Higher Plants” [65]. Although this strategy includes only higher plants, the guideline could be used as a primer for the cultivation of GEM in open ponds

using less strict clean room conditions, or even uncontained cultivation. However, open cultivation systems still have a high contamination load that could possibly affect the product.

A commonly used technique to control contamination of ponds is the use of selective media and culture conditions that work in favour of the desired microalgae. Depending on the strain, this can be done with high salinity, pH, chemicals, pesticides, or antibiotics and resistance genes in the microalgae [66]. However, with increased cultivation volume, the chemical dosage required is elevated which can reduce the economic feasibility. On the other hand, the chemical consumption of the system can be controlled by identifying the dominant contamination source in the culture. By knowing the main contaminant, the chemical and pesticide usage can be adjusted for the contamination type and its severity [61]. Another approach is the use of selective nutrients in the media that can only be utilised by the desired host, which makes pesticides and antibiotics unnecessary. A strain of *Chlamydomonas reinhardtii* was designed to grow specifically in a selective media. The microalgae was modified to express phosphite oxidoreductase, enabling it to grow on both phosphite and phosphate as a phosphorus source [67]. Even though phosphite is ubiquitous in the environment [68], it is present in far smaller concentrations compared to phosphate. While natural phosphite metabolism does occur in some bacteria and yeasts [69], laboratory experiments demonstrated that the modified algae with phosphite-only media has an advantage over most microbial competitors. Even after the introduction of native contaminants, the microalgae culture was able to thrive for 16 days [67]. So far, this has only been demonstrated at laboratory-scale, but the potential for application in outdoor cultures could reduce the overall load of contaminants [70]. However, it does not completely prevent them, which might leave traces of contamination in the final product.

Prevention of product contamination is important for the economic feasibility and safety concerns of the product, but equally relevant is the risk of a release of GEM into the environment and the resulting impact on the surrounding ecosystem. Typically, microalgae are introduced by wind and fauna from the open pond into the natural habitat, with one of the main concerns being that the GEM could outcompete local species in their natural habitat, or introduce foreign DNA into the natural system via horizontal gene transfer or sexual transfer [71][72]. Large-scale trials were conducted in the U.S. to estimate the proliferation of GEM in the environment and its consequences on the natural systems [73]. *Acutodesmus dimorphus* was genetically augmented for enhanced fatty acid biosynthesis and the expression of a recombinant green fluorescent protein. Cultivated in an open pond, the spread of the GEM was monitored in water filled ponds, situated around the cultivation pond at different distances. qPCR detected the GEM primarily in traps that were in the path of the prevailing wind direction

from the culture, up to the 50 m away. However, the study did not prove that GEM outcompeted the natural species after 50 days. In fact, other studies showed that GEM might be less fit compared to wild types, due to their higher genetic load and special nutrient requirements [30]. This suggests that released GEMs would not pose a threat for the natural environment; however, the impact on the ecosystem as a whole is not predictable and might differ according to the type of GEM released [74].

One strategy is to reduce the survivability of the GEM which can be done with different genetic modifications. The aforementioned phosphite method was used in the cyanobacterium *Synechococcus elongatus,* which was genetically modified to grow selectively on phosphite as the essential phosphorus source [75]. In this case, this was done to reduce its survivability in the natural habitat of the area where it was to be cultivated. In case of an accidental release into the environment, the inability to absorb natural phosphate and the insufficient supply of phosphite in nature would lead to its extinction. Another approach is the use of suicide genes that would further increase the biosafety of a strain. The switch would induce a self-destruction mechanism in the cell under specific environmental conditions, such as the presence or absence of a substrate or molecules. These systems rely on a strong genetic promoter that starts expressing essential or terminative proteins that induce cell destruction [76]. Several applications are possible, depending on culture and environmental conditions, such as: i) permanently induced expression of an essential protein while in the culture media, leading to a termination when no longer in that specific media (e.g. in the wild); or ii) induction of a terminating protein when exposed to certain environmental conditions [77]. The feasibility of these death switches was shown in the cyanobacterium *Synechocystis* sp., with the metal-ion induced promoter (copM). The promoter was induced at high metal ion concentration in the media and expressed a non-specific nuclease NucA (originally from another cyanobacteria, *Anabaena*). Variations in the metal-ion concentration of the media resulted in nuclease expression, thereby resulting in DNA degradation in the cell which ultimately led to cell death [76]. A similar approach is the constitutive expression of a toxin and the induced expression of an antitoxin in the cyanobacterium *Synechocystis* sp.. By removing the inducing signal for the antitoxin expression, the cell cannot neutralize the expressed toxins anymore, which results in cell termination. Both methods could be successfully utilized as a death switch [76]; however, they are highly dependent on a strong inducible promoter and the technology transfer into eukaryotic microalgae may pose a challenge for these methods.

Future cultivation of GEM in outdoor systems will depend upon risk assessments which should consider the fitness of the strain in the environment, possible gene transfer, and toxicity to the natural habitat. Evaluations have to be performed on a case by case basis, and the potential benefit has to be weighed against potential environmental ramifications [78]. The cultivation of GEM in open ponds might be viable in the future, however, open systems need further developments in their design to meet the regulatory challenges for pharmaceutical production.

1.1.3.2 Closed photobioreactors

Closed PBR systems represent a more promising production platform for biopharmaceutical production in microalgae. These systems can be similar to existing bioreactors (such as fermenters) which are already widely used for the GMP regulated production of bacteria, yeast, and mammalian cells. The design of a closed photobioreactor differs from commonly used stainless steel systems however, since there is the additional need to provide light to the culture for microalgae to grow. Typically, the PBR shell is made of transparent material (e.g., plastic, glass), thereby enabling light to penetrate into the culture through the side walls. Another option is internal illuminations systems – light sources that are submerged into the culture in order to distribute light more evenly [79][80]. These systems increase the illuminated surface of the PBR and diffuse light into the culture with optical fibres or transparent rods, and have been shown to have a positive impact on the culture growth rate [81][82]. A potential drawback of these systems is the possible interference with the mixing, which is an important aspect of closed systems. Closed systems typically need active mixing to perform efficiently. Mixing ensures the homogeneity of the culture and can be supplied via impellers, aeration, or media agitation by pumping [83]. Mixing supports the mass transfer of the crucial CO_2 required for photosynthesis, which is typically supplied via membrane or direct aeration [84].

There are many PBR designs in use for different applications, with the main types categorized as: tubular, flat panel, and fermenter-type bioreactors, with detailed descriptions found in various reviews [56][85]. Most closed systems have a high cultivation reproducibility due to the tight environmental control, good mass transfer, and comprehensive monitoring systems, even at larger scales. The drawback of these systems is the higher energy consumption, which can be 500 times higher for a tubular PBR compared to an open system [86]. Contamination risks in closed systems are significantly lower. Nevertheless, a second

containment level should be in place to prevent the transfer of GEM through spills, in the unlikely event of an incident [77].

Product contamination in traditional durable bioreactor (BR) systems occur mainly because of incomplete cleaning, sterilization, or incorrect process handling [87]. Even for an established processes such as fermenters, the cleaning and sterilization procedures are extensive and, especially in the GMP environment, require thorough process design and documentation [88]. Since cleaning and sterilization measures are a high cost factor [89], there is increased research and development focused on minimizing these. One solution is the use of single-use technology, which is becoming increasingly popular in GMP production [90]. In single-use systems, any reactor parts that comes into direct contact with the pharmaceutical product are replaced with new, pre-sterilized components after each production run, which eliminates the need for cleaning and in-place sterilization. Additionally, the technology offers more process flexibility with its adjustable and rearrangeable components, and reduced turnaround time between batches [91]. Analysis for monoclonal antibody production reported 22% lower OPEX compared to a traditional stainless steel facility [92]. This technology can be utilized in single process steps or for whole systems, which can lead to an efficient mix of durable stainless-steel and single-use systems [87]. The retrofit of a clinical plant with single-use systems lowered the annual costs of water for injection (WFI) and labour costs by $USD 250,000 and $USD 60,000, respectively [92]. Besides economic factors, environmental impacts of single-use systems must be considered. Single-use systems have the disadvantage of more plastic waste, yet the overall environmental impact of single-use is lower compared to traditional fixed-in-place technology due to the lower water, detergent and energy usage over the lifespan of the equipment [93] [94].

For microalgae cultivation, single use systems provides additional advantages: the plastic layer used in these applications are typically transparent, allowing more flexibility for illumination systems attached outside the bags [95][96][97]. Furthermore, the cultivation of marine microalgae in saltwater media would increase the maintenance effort for stainless steel systems due to higher potential for corrosion and salt residues – factors that can be avoided with single-use systems [98]. An industrial example for the pharmaceutical production of phototrophic microorganisms in single-use systems is the moss cultivation by Greenovation [99]. These single cell moss strains are currently producing drugs for several orphan diseases (Fabry disease, C3 glomerulopathy (C3G), and Pompe disease). They are cultivated in single-use wave bag bioreactors (up to 500 L) which are artificially illuminated and operated in an approved GMP environment [100]. There are several novel challenges inherent in single-use

technology, such as the diffusion of leachables from the plastic materials into the culture [101]. These leachables can negatively impact the growth of the microalgae, the product yield, or its quality. However, the moderate cultivation conditions for most phototrophic microalgae cultivation, absence of organic solvents and ambient cultivation temperatures (often around 23˚C), in addition to careful selection of the single-use material might diminish the potential for material leachate [102]. The utilization of single use systems in pharmaceutical production are furthermore promoted by new guidelines such as the EU GMP Annex 1 guideline and organisations such as the International Society for Pharmaceutical Engineering (ISPE), with the caveat that the interaction between the product and product contact surface is carefully understood [103][104].

Industrialization of microalgae for biopharmaceuticals is not yet fully realised, mostly due to the absence of a highly productive strain (e.g., high product titre). Nevertheless, from a regulatory and economic perspective, closed systems seem to be the preferable choice for high value production, especially in case of GMOs, for the foreseeable future.

1.1.4 Bottlenecks/ Challenges in commercialisation

1.1.4.1 Upstream: Challenges in production strain creating

The establishment of microalgae as a valid production host in the biopharmaceutical sector currently has several limitations. One important challenge is the genetic modification of the algae with a robust transformation process. Currently *Clamydomonas reinhardtii* is the only microalgal species for which chloroplast transformation is well established, which highlights the pressing need for a more diverse toolbox for genetic modification. Furthermore, it is not uncommon that foreign genes introduced to a transformant cannot be expressed, potentially due to the lack of stable transformation systems due to codon bias [86][87]. The codon-optimization method has been improved in *C. reinharditti* [107] and software for codon-pairing is available [108]; however, there is still a need for further development with other microalgae species. Random integration of transgenes [109] and unstable transgene expression by gene silencing [110] also poses problems for successful nuclear transformation. Alternatively, CRISPR-Cas9 system could be utilised for targeting transgenes into specific regions of the genome, offering a solution for random integration of transgenes through nuclear transformation [111][112][113]. As the regulation of GMP production relies on master cell banks with identical clones that have been previously characterised and approved [114], any source of genetic instability arising within GEM may limit their use in GMP production. Some

microalgae can be stored over a long period of time via cryopreservation, although cryopreservation protocols are not necessarily interchangeable between algae species and are not developed for all species [115]. Optimization of the cryopreservation process based on the microalgal strain is necessary to increase the viability of the cells after thawing; this is particularly challenging for GEM strains that are potentially more sensitive to the process [116]. Furthermore, the freezing process can also influence the functional performance of the strain, which might affect the productivity [117]. Chloroplast transformation may present a more promising strategy for precise engineering and high-level expression of transgenes due to its ability to target transgenes into specific genomic regions *via* homologous recombination [118][119]. However, this method of transformation can sometimes exclude post-translation modification of proteins [24], resulting in the production of untargeted proteins.

The surge in the development of molecular tools, including methods to enhance gene expression and transformation, have the potential to improve algal biopharmaceutical production. Genome information is currently restricted to a few species, commonly used in research and industry. The application of new sequencing techniques may provide opportunities for sequencing new microalgae species, some of which might be easier to manipulate or natively show higher production rates [120]. This should allow for higher product titre per algal cell, which are currently still lagging behind the more well-established hosts.

1.1.4.2 Cultivation challenges

Economic viability of microalgae depend on how the PBR supports the productivity of the algae. Typically, high biomass yield translates into a high overall product titre. One of the most challenging aspects of microalgae cultivation is the supply of light. Self-shading of the cells, due to absorption and scattering of light, results in a gradual decrease in the light penetration, which is particularly true in later stages of cultivation with high cell densities. Major constraints for achieving substantial biomass arise from light limitation, a state in which the cells do not receive sufficient photons for photosynthesis, and light inhibition, a state of increased photo-damage due to over exposure from too many photons [121][122]. Growth rate limitations at industrial scale are predominantly caused by inferior light supply [123], hence, there is a need for special consideration of the illumination source when designing photo-bioreactors. Optimal growth can only be achieved by balancing the light saturation with the mass transfer, such that

the cells are exposed to sufficient photons without over- or under-saturating them and have sufficient access to the substrates required.

1.1.4.3 Downstream challenges

Downstream processing is key for transforming algal biomass into the desired product(s). The economic viability of microalgae-based products depends on reducing the technological limitations of downstream processing of microalgae products [124]. Downstream processing is a major cost factor and can exceed 80% of the total production cost of biopharmaceuticals in higher plants and microbial production hosts [125][126]. Once the product is extracted, the processing can be quite similar to other host systems. The harvesting and extraction process however will be unique to algae. The high-water content of algal biomass during the cultivation step makes dewatering unavoidable as a first step to reduce the overall volume and the corresponding processing cost. For microalgal biomass production (e.g. for biofuels), this cell harvesting step can take up to 30% of the production costs [127], highlighting the need for process optimization that could be done at this step. This can be achieved by improved harvesting technologies [128], and/or by increasing biomass concentration in the growth culture phase by improving the cultivation systems .

1.1.5 Conclusion

Microalgae are a promising alternative to established hosts, with the promise of a cheap and robust production system for biopharmaceuticals. However, the technology is currently in the preliminary stages of research and validation. There is ongoing research into improving production strains, which will most certainly rely on genetic modification to improve productivity and product expression.

Outdoor cultivations at this point are unlikely, considering the heightened regulation of GMO containment and product quality requirements. However, GMP requirements could potentially be satisfied by separating the production processes and ensure the product quality in the downstream process, as seen with higher plants [63], while the risk of environmental release could be minimised by physical containment or genetic restraints. Still, genetic containment is in its infancy, and mechanical isolation increases the investment cost, hence counteracting the cost advantage of open systems. Since significant work is still required to improve the product titre, avoidance of the GMO label for production strains will be rather unlikely, even with the utilization of new engineering technologies. Modification of

biopharmaceutical strains can be considerable and might include transgenes, which nearly always means that they are currently classified as GMO. Closed systems for cultivation pose a better option in this scenario. The production can be tightly controlled, and regulatory requirements are easier to apply, which suggests closed PBR systems, especially single-use systems, are a promising cultivation system for future biopharmaceutical microalgal production.

1.2 Project outline

Microalgae are an exciting new host system for the production of biopharmaceuticals. However, currently the growth systems utilized in the biopharmaceutical industry are not optimized for the efficient cultivation of microalgae, as they are not designed with autotrophic organisms in mind. This can lead to poor conversion of existing bioreactors, which leads to suboptimal growth resulting in low product titre, further increasing down-stream costs. For microalgae to compete with traditional production hosts in the biopharmaceutical market, investment and operational costs of production must be lowered. Designing such a photo-bioreactor (PBR) is a challenge. A completely new design may take time to achieve the necessary certification [129]. As such, one option is to use an existing bioreactor widely used in the pharmaceutical industry and adapt it for use with microalgae.

In order to design such a system, an optimization platform to convert an existing bioreactor was established in this thesis. The platform includes physical PBRs, a computer assisted design (CAD) process, and a methodology for conversion and optimization of an existing bioreactor into a PBR (Figure 1-2). The methodology for the conversion was designed to be flexible, with the intent to adapt bioreactors of different geometry, volume-scale, and different microalgal species. Several aspects needed to be considered for the initial bioreactor system: compliance with current (GMP) regulations, containment of GMOs, and process control. The proposed PBR system is based on a GE Xcellerex bioreactor system: a single-use application consisting of a control unit, a cooling jacket, and a single-use bag with integrated impeller-aeration system and modifiable tube connectors. The Xcellerex is a fermenter-type closed bioreactor that is tightly controllable, and is commonly used to cultivate bacteria and mammalian cells in the pharmaceutical industry (GMP environment) [130].

System optimization was predominantly focused on improving the light distribution into the PBR. The aim was to design a PBR that provides sufficient light of the correct wavelength to the cells, so that the culture can grow optimally without suffering from light limitation or excess

level of light. Designed like a fermenter, the shape of the initial bioreactor system suffers from its the relatively low surface to volume ratio. The cylindrical shape, with its large diameter, limits the ability to supply light through surface illumination. Light attenuation due to self-shading of the cells leads to a lack of light supply after a few centimetres, especially in cultures with high cell density. Typically, a narrow PBR vessel is favoured to increase the surface area (supplied light) per culture volume. However, the light exposure of the cells is dynamic and depends on the flow pattern of the culture within the bioreactor. A favourable mixing pattern and an optimized illumination system could compensate for this design flaw by improving the light distribution in the converted BR.

Typically, light attenuation is obtained by manually measuring the light intensity inside a PBR or calculating the light attenuation through models such as the Beer-Lambert law. However, these methods have limitations for complex PBR shapes or illumination systems, and can be time consuming to empirically determine the relevant constants for each new species and density. Therefore, a more practical method was developed for this thesis which enabled the creation of high-resolution light maps (**Chapter 2**). The Direct chlorophyll fluorescence imaging method (DCFI) captures emitted fluorescence from algae cultures with cameras and converts the images into light intensity images. These images (light maps) were of a resolution of 10 µm and can be further transformed into three dimensional volumes. An initial calibration step is needed for each new species, but it can then be used for that species across a wide range of PBR designs.

Modifications of a sophisticated existing system, such as the Xcellerex, can be costly and time-consuming, since material costs are high and physical modifications cannot be easily applied. Therefore, the optimization platform was designed to freely retrofit the process parameters, and illumination system. The optimization platform consists of three parts: 1) a 200 L cage bioreactor, used to test final modification before changes are applied to the Xcellerex system; 2) three scaled-down PBRs of 20 L culture volume, used to evaluate modification impacts on growth in a more rapid manner; and 3) a computer model of the system to optimize the cell exposure to light and accelerate testing of modification on design and cultivation parameter. Optimizations can be rapidly made *in silico*, and then translated into the 20 L and the 200 L PBR for testing. The improved setup can then be transferred into the industrial system (Figure 1-2).

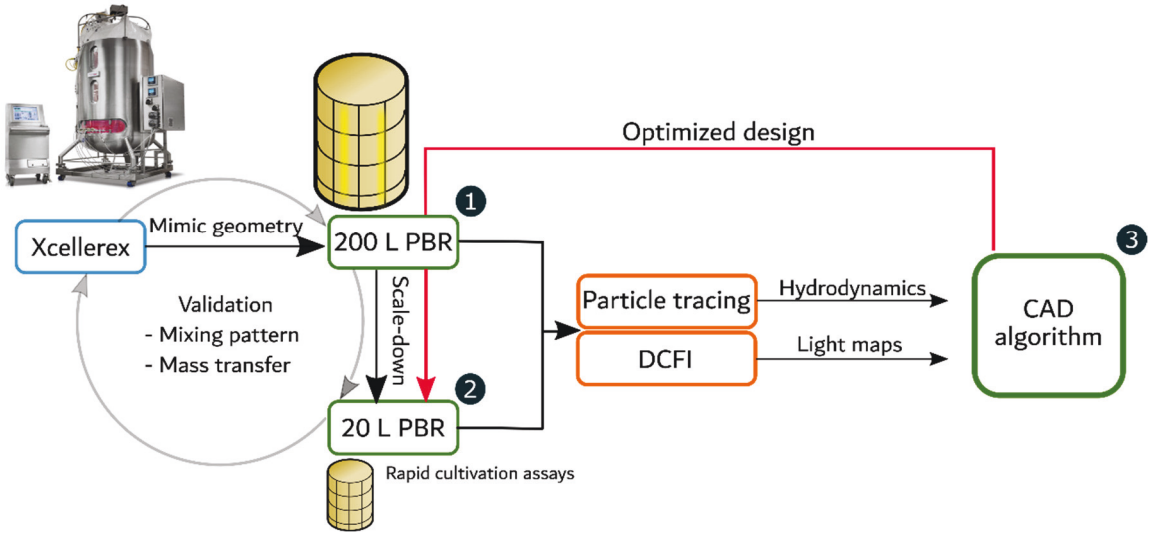

Figure 1-2: Project overview. The PBR systems (part 1 and 2) were based on the industrial GE Xcellerex system geometry and physical parameters were validated. Characteristics of hydrodynamic flow (particle tracing method) and the light distribution (DCFI method) were measured, and the resulting hydrodynamic data were combined with the light maps in a CAD process to calculate the optimal LED configuration. This optimized design can then be transferred and tested back in the PBR systems.

The 200 L cage PBR (Part 1) was designed with the dimensions of the original Xcellerex system. Similar performance of the optimization platform is essential to translate modifications to the industrial system. The ability to replicate the industrial bioreactor was tested for the 200 L PBR with the mass transfer and mixing time (**Chapter 3**). Furthermore, the scale-down approach of the 200 L PBR to the 20 L PBR was validated. The 20 L PBRs (Part 2) were dimensionally scaled down to keep the illuminated surface / volume ratio proportional to the 200 L PBR. This scale-down approach was chosen to keep the surface area ratio consistent during scaling. However, this scaling method cannot ensure a similar light distribution into the PBR since the light penetration of the LEDs can, even with adapted light intensity, not easily be scaled. Correct scaling of certain process parameters, such as mass transfer rate and mixing time, was crucial in order to correlate the 200 and 20 L PBRs. **Chapter 3** additionally analyses the hydrodynamics of the optimization platform by applying a particle tracing method to track movement within the bioreactor and highlight laminar and turbulent zones within the PBR.

The computer model (**Chapter 4**) combined the hydrodynamic data with the light maps to calculate the dynamic light exposure of the cells during cultivation. Culture mixing induced by aeration moves cells continuously through different light zones of the bioreactor. By tracing the liquid flow through these light zones, a light history of the cell can be estimated, facilitating

the calculation of the duration and intensity of the light exposure, as well as the total exposed light experienced during cultivation. Both the mixing rate and the arrangement of the illumination system can impact these light exposures. The results of this model can be used to configure the artificial illumination system to optimally fit different mixing rates and microalgae species, thereby potentially leading to increased growth, while reducing the material and energy costs of the system.

The project designed an optimization platform capable of converting the single-use Xcellerex bioreactor into an efficient PBR system. Furthermore, the established platform allows ongoing optimizations efforts while the converted industrial PBR is used in production.

The specific aims of this project are:

Aim 1: Characterization of the illumination system used for the bioreactor conversion

Objectives:

- Identification of suitable illumination system for industrial cultivation
- Development of a method to accurately measure the illumination system
- Characterisation of the illumination system in regards to light distribution and light attenuation.

Aim 2: Validation of the optimization platform and verification of the down-scaling approach

Objectives:

- Design of the physical components based on the industrial bioreactor system
- Analysis of mass transfer and mixing time of the optimization platform and verification against the industrial bioreactor
- Analysis of the hydrodynamic flow pattern with an empirical particle tracing method

Aim 3: Calculation of the ideal light source configuration based on the light exposure of microalgae cells

Objectives:

- Developing a computer aided design process to combine light distribution measurements with particle tracing data and calculating ideal light configuration for different settings.

Chapter 2
Light attenuation in a photo-bioreactor; a practical approach of light mapping algae culture to optimize illumination of photo-bioreactors

Author Contribution

Julian R. Kofler designed and performed all experiments and wrote the manuscript. Alonso Zavaleta Fernandez de Cordova advised, supported the experiments, and assisted in writing. Luca Maestrini gave methodological guidance. Leen Labeeuw advised, supported the experiments, and assisted in writing. Peter J. Ralph advised, materially supported the experiments, and assisted in writing.

2.1 Introduction

Microalgae are photosynthetic microorganisms that are capable of producing complex molecules with CO_2 and light in a nutrient rich medium. They are primarily cultivated for lipid or biomass production, but are also gaining increased interest as a biopharmaceutical production platform [21]. The production cost of recombinant proteins in algae is predicted to be lower compared to traditionally used host systems, such as mammalian or yeast cells, which makes this technology attractive to industry [131]. Furthermore, microalgae are simpler to culture with reduced contamination risks and high volume scalability [16].

Microalgae are typically cultivated in photo-bioreactors (PBR) which use natural or artificial illumination to supply essential photons to the cells. PBRs range from closed benchtop bioreactors to open raceway ponds for industrial applications, where the desired product imposes restrictions on the type of bioreactor used. Different light distribution occurs in these bioreactors depending on the shape of the bioreactor, the light source, and the microalgae species. Furthermore, the cell concentration influences the light attenuation: incoming photons are absorbed and scattered by algae cells, gradually diminishing photon availability for cells further from the light source (self-shading) [132]. This is particularly true in later stages of cultivation with increased cell concentrations. For example, in *Chlorella vulgaris* cultures a decrease of 35% and 92% in photosynthetic photon flux density (PPFD) was observed at cell densities of 0.09 g L^{-1} and 1.34 g L^{-1} respectively within 2 cm of the light source [133]. This light gradient through the culture creates several zones in the PBR: a dark zone, a light saturated zone, and an optimal growth zone. Dark zones can be defined as the area in which the PPFD is not sufficient for photosynthesis. Microalgae in this zone experience light undersupply, resulting in diminished or no growth. On the other hand, in the light saturated zone the exposure to high irradiances induces light inhibition in these cells. Typical photon saturation thresholds vary around 150–400 µmol m^{-2} s^{-1} depending on the species and wavelength [134]. Beyond this irradiance, stress can occur where the photosystem is damaged and the cells redirect energy into cell repair and light protection (photoinhibition), resulting in reduced cell division [135]. The optimal growth zone is located between these two areas, in which the cells are exposed to enough photons for photosynthesis, yet are not saturated, with enough time for the photosystem to regenerate after high light exposure [136].

However, not only is the intensity (quantity) of light crucial, but the wavelength (quality) also impacts cell growth. Algae have specific light absorption spectrums that are influenced by

the occurrence of specific pigments in the cells. These pigments absorb light of different wavelengths, enabling the cells to grow using a broader light spectrum. Typically, algae have a low absorption in the green spectrum and a high absorption of blue and red light (see Table 2-1) [137]. This absorption, together with the scattering characteristics of microalgae, are fundamental for light penetration into the liquid culture. Less absorbed wavelengths can penetrate deeper into the culture compared to strongly absorbed wavelengths [138]. The mix of different light qualities, or their exclusion, should be considered when designing PBR lighting.

Table 2-1: Light absorption peaks and pigments typically be found in different algae species.

Algae species	Cell pigments	Absorption peaks (nm)			Ref.
Phaeodactylum tricornutum	Chl a, Chl b, Fucoxanthin	435	500	680	[139]
Chlorella vulgaris	Chl a, Chl b,	435	485	680	[139]
	β-carotene, astaxanthin, and lutein	410–430	450	640–660	[140]
Chlamydomonas reinhardtii	Chl a, Chl b, Carotenoids	440	495	630, 680	[141][142]
Summary		420–440	450–500	630–680	

Microalgae growth and cell composition can differ with the light quality. Illuminating *Chlorella vulgaris* with blue light caused an increase in cell size, whereas red light resulted in small-sized cells with high division potential [143]. Colours such as blue, green, and purple showed a significantly lower growth rate compared to white in *Chlorella* sp.. Curiously, purple light, created by combining blue and red light (2:8 parts), had significantly lower growth rates than solely red light, implying that the supplemented blue light had a severe inhibiting effect [144]. However, *Chlamydomonas reinhardtii* requires blue light to grow, even in very low quantities such as when mixed in with other lights [138][145]. Interestingly, mixing in other wavelengths (e.g. yellow) can reduce the overall light stress in the algae, thereby promoting growth overall [146]. In general, blue and red illumination promotes the best growth in *Chlamydomonas reinhardtii* and many other microalgae [147]. Further examples are listed in Table 2-2.

Table 2-2: Impact of wavelength on different algae species.

Wavelength (nm)	Algae	Effect	Ref
~430-460	*Dunaliella tertiolecta*, *Thalassiosira rotula*	Increased protein synthesis, carbon uptake and respiration	[148]
460	*Phaeodactylum tricronutum*	Increase in protein concentration, but decrease in carbohydrate concentration compared to 660 nm	[149]
520	*Chlorella vulgaris*	Decreased fatty acid production	[144]
550	*Nanochloropsis sp.*	Increased fatty acid methyl ester production	[150]
~600-650	*Dunaliella tertiolecta*, *Thalassiosira rotula*	Increased protein synthesis, carbon uptake and respiration	[148]
> 700	*Duneliella bardawil*	Decreased lag phase at cultivation start and increase in growth rate. Increases carotenoid production (irradiance protection). Decreased cell density	[151]

Light quantity and light quality have to be balanced in order to provide beneficial wavelengths to the cells without inducing photoinhibition [152], which emphasises the need for precise illumination systems to optimise cell growth. Knowledge about the type of irradiance and the abundance of specific wavelengths are crucial to optimize the PBR. Typically these details are understood by mapping the illuminated culture manually with Photosynthetically Active Radiation (PAR) sensors [153][154][155], or by calculating the light attenuation based on the Lambert-Beer-Law [156]. In the case of manual mapping, the PAR sensor has to sample the whole PBR in order to generate an accurate overview of the light distribution, with separate iterations for different species and culture conditions. This can result in extensive labour requirements for a complex PBR system, especially for high resolution light maps [153]. The mathematical approach does not account for certain PBR reflections or the complex light profile of a non-homogeneous LED light source. Photon flux is calculated as homogeneously distributed from the surface, which is sufficient for reactor systems illuminated by sunlight, but not for PBRs with artificial light sources (such as LEDs) directly attached to the reactor vessel, or PBRs with complex geometry. Particular optical characteristics such as absorption and scattering of the different microalgae must be incorporated, and must be obtained empirically. These properties are species-specific and factors like the growth medium, culture health, acclimatisation to variations in light quality and quantity [157] have to be considered for a detailed calculation of light distribution.

In this study, a practical method of fluorescence imaging was designed and applied to create light profiles of LEDs in a cylindrical bag photo-bioreactor. These light maps describe the PPFD inside the PBR, resulting in a precise light pattern of the LEDs and potential light reflections of the reactor walls. The resolution from using this method is higher and more precise than light maps obtained by manual mapping with a PAR sensor. When compared with conventional imaging measurements that uses visible light [158], the fluorescence imaging technique has the advantage that only fluorescence emissions of microalgae are recorded. Regions of the PBR that show fluorescence emission can be assumed to have photosynthetic activity with sufficient irradiance of the specific PAR wavelengths. This method is adaptable to complex photo-bioreactor geometries and could be used to identify light saturated areas. The setup was designed to be easy to use with a domestic camera system and enables rapid measurement of different illumination systems and microalgae species. Two microalgae species and three LEDs (red, blue, and white) were analysed in regards to light penetration and light distribution at different cell concentrations. The algae species were chosen for their contrasting characteristics in morphology, cell size and cell composition, and served as initial model species to validate the method.

2.2 Method

2.2.1 Theoretical background

The underlying principle behind this method was first proposed for terrestrial leaves [159], and modified for algae using Normalized Chlorophyll Fluorescence Imaging (NCFI) ([160] unpublished). This method was further refined and adapted for this project. NCFI overlayed a normalized fluorescence image with a grid of PAR measurements. Both datasets are correlated by known Cartesian coordinates, thereby pixel values could be converted into PPFD, resulting in a converted fluorescence image (light map). Unlike the NCFI approach, the Direct Chlorophyll Fluorescence Imaging (DCFI) method links the captured pixel value directly with the measured PPFD by taking calibration images of the sensor position in the PBR and relating them with the corresponding pixel values in the fluorescence image. These calibration images allow for a more flexible placement of the sensor, which allows for easier utilization of the method in bigger and more complex PBR geometries. As such, the method does not require precise distance measurement and needs less effort compared to the NCFI, since the image processing does not require additional normalization or cropping steps in order to convert the

fluorescence images. These changes to NCFI made it necessary to design a new data processing procedure to process the fluorescence images.

The method measures light distribution indirectly through the fluorescence characteristics of microalgae. Microalgae are excited by a particular wavelength and their emitted fluorescence is recorded. The wavelength absorption of the microalgae depends on the pigment composition of the cell [161]. Pigments are photon collecting molecules that absorb specific wavelengths. Their concentration and composition in the cell vary among species and may change according to the health of the culture [12]. Photons captured by pigments are absorbed, causing its electrons to be converted to a higher energy level. This energy is transferred to the reaction centre of the photosystem and is used in photosynthesis, dissipated as heat, or is emitted as fluorescence [162]. Chlorophyll fluorescence is a dynamic process that depends on the photosynthetic state, but if the sample is saturated under continuous illumination it reaches a steady state of emission. In such a saturated state, fluorescence is directly proportional to light intensity [159]. The emitted fluorescence is captured by the camera images, and by superimposing the location of light intensity measurements in the fluorescence image, it is possible to relate the pixel value with the light intensity. With several of these measurements, at different sites around the bioreactor, it is possible to obtain a calibration formula which, when applied to the fluorescence image, converts them into a 2D light map, with a converted PPFD value for each pixel.

2.2.2 Microalgae species and growth conditions

This method was applied to two microalgae species, *Chlorella vulgaris* CS-41 (Australian National Algae Culture Collection), and *Phaeodactylum tricornutum* CCMP632 (National Centre for Marine Algae and Microbiota). *C. vulgaris* is a freshwater algae with a cell size of 1–5 µm, has a spherical shape, and shows a greenish reflectance spectrum with a low absorption in greenish spectrum [163]. *P. tricornutum* is a marine diatom, with a cell size of 5–10 µm; it is a fusiform diatom, and shows a brownish reflectance spectrum [164]. These species were chosen for their cell size, shape and different absorption spectra. Furthermore, *P. tricornutum* incorporates silica into its cell walls that might affect light scattering and the shape of the light path [165]. Absorption spectra of both species were measured with a spectrophotometer (Cary 60 UV-Vis Spectrophotometer, Version 2.00, Scan Version 5.1.0.1016, Agilent Technologies Inc). *C. vulgaris* was maintained in MLA media (4-part concentrate, Algaboost™). *P. tricornutum* was maintained in F/2 media [166] based on natural seawater with a salinity of 34-

35 ppt (Rose Bay, Sydney). Stock cultures were maintained at 21°C under constant halogen light. Experimental cultures were grown in 10 L aerated flasks till exponential phase (white halogen light 100 µmol m^{-2} s^{-1}, 20:4 hours light:dark cycle, 23°C). Cultures were collected at different points of the exponential phase and diluted with sea- or dechlorinated tap water, as needed. Cell counting for each biological replicate was done before each experiment using a haemocytometer. Microscopic imaging and ImageJ (version 1.52p, [167]) was used to measure the cell size. Effective quantum yield of photosystem II (PSII) was recorded at the beginning of the experiment with a pulse amplitude modulated (PAM) fluorometer (Walz). Cultures with an effective quantum yield of 0.7–0.8 for *C. vulgaris* and 0.6–0.7 for *P. tricornutum* were used for the experiment. Additionally, the culture was light-adapted for at least 5 minutes to reach a steady chlorophyll emission (S-phase), before each experiment [168]. The culture was manually stirred before the measurement to ensure uniform distribution of light adapted cells.

2.2.3 Experimental setup

The measurement chamber was designed to simulate the vertical half of a bag PBR with the radius of 13.5 cm and a height of 10 cm. It was made of a metal mesh structure to support a plastic bag (Polyethylene (PE)) (Figure 2-1). The design was based on a 200 L plastic bag bubble column bioreactor in regards to its geometry and material. The chamber was filled with microalgae culture until the water level was 2 to 3 cm above the non-reflecting plate. Low reflective material was used in the measurement chamber as the bottom layer to prevent unwanted reflections and create a flat surface (Figure 2-1). The LED was located on one edge of the measurement chamber, 0.5 cm above the low reflecting layer. The side perspective of the measurement chamber created a light contour of the light source that was used for calibration and the analysis of the light behaviour in the culture. The top view, captured a precise cross-section of the light cone that was used later to calculate the light exposure (Chapter 4).

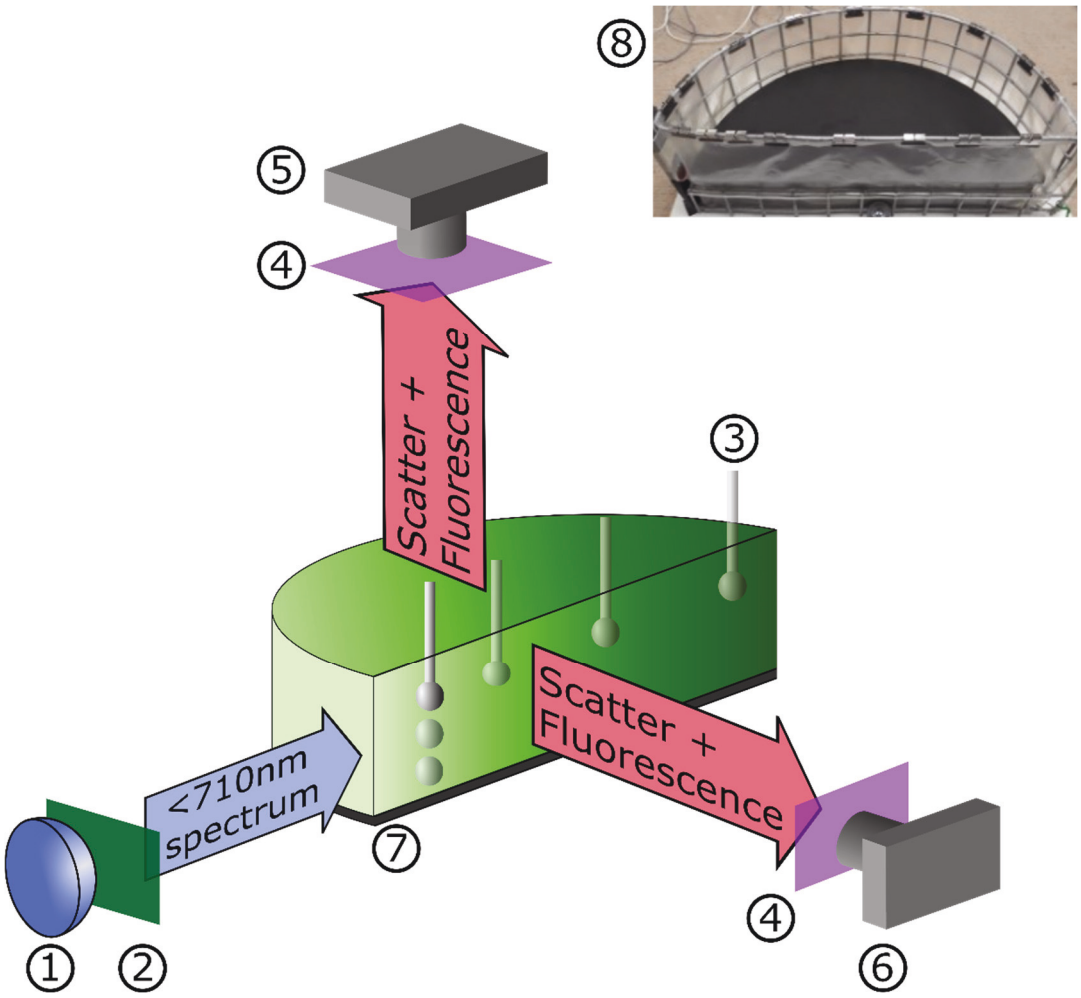

1) LED
2) Short pass filter <710 nm
3) PAR sensor position
4) Long pass filter >840 nm
5) Camera top
6) Camera side
7) Low reflecting material
8) Image of the measurement chamber

Figure 2-1: Experimental setup of the DCFI measurement. LED light is emitted through a short pass filter (< 710 nm) into the microalgae culture. The culture either processes the photons, scatters them, or re-emits them with higher wavelength (fluorescence). The scattered light is filtered out by a long pass filter (>840 nm) so only fluorescence light reaches the camera sensor. Grey spheres in the measurement chamber show the representative positions of the PAR sensor. Also displayed is the actual measurement chamber.

In the first step of this experiment, the light intensity and the position of the sensor was recorded. The required PAR measurements (4-Pi-quantum sensor, LI 250A, LI-COR) were conducted inside the measurement chamber at different positions, by placing the sensor on the plastic layer of the side profile (Figure 2-1). At each position, the measured PPFD value in the culture and an image of the side profile was captured (calibration image). This procedure was

repeated for several positions of different light regimes. In the second step, fluorescence images of the side and the top profile without the light sensor were taken. For this step, the algae culture was light-adapted for at least 5 minutes, ensuring that the chlorophyll fluorescence reached stable emission (S-phase). While keeping the light setups constant, the side images (calibration image) of step one and two can be superimposed and the pixel values of the sensor positions in the fluorescence image can be extracted. The conversion is done with a calibration formula, obtained by plotting the pixel values with the PAR measurements (section 2.2.2). This calibration has to be done once for each species, LED colour and cell concentration, but can then be applied to similar set ups (e.g., same algae with same LED) without additional measurements.

2.2.4 Camera

Two cameras (modified Canon EOS 1500D, with Canon EF 50mm f/1.8 STM lens) were positioned in front of the side and on top of the measurement chamber, creating a side and top profile of the LED (Figure 2-1). Images with both cameras were captured simultaneously. In each experiment, the camera setup was held constant. The internal optical filter of the cameras was replaced with a full spectrum filter to allow the detection of fluorescence wavelengths > 900 nm. The camera modification was tested with a spectrometer, and the image sensor was able to detect wavelengths of 1780 nm. Camera lenses can create optical distortions at the edges of the camera field of view, so to avoid flawed measurements, the cameras were situated further away (80 cm side camera and 110 cm top camera) from the measurement chamber and positioning the chamber in the image centre. Additionally, the lens distortion was tested by recording a grid image (chessboard) and analysing the distortion with ImageJ. No distortion was detected. Images were taken with a wide variety of shutter speeds at an aperture of 1.6, ISO6400, and no image correction. Files were stored in raw .cr2 format. Dark current for both cameras was measured as a mean pixel value of ~200 in 16-bit images with a shutter speed between 640 – 0.5 s^{-1}.

2.2.1 Optical filter and LEDs

The LED wavelengths were chosen for their known impact on microalgae metabolism and to reduce potential light stress of the cells induced by other wavelengths of the PAR spectrum [169]. The specific LEDs had peak emissions at wavelengths that matched the absorption spectrum of the algae (Figure 2-2). Blue LED of 450 nm (16,000 µmol m^{-2} s^{-1}, 0.7 Ampere,

PCB chip with lens) was used because of its high absorption rate in microalgae, and good market availability. The high wavelength band in the blue spectrum was chosen as it is described to have a lower photoinhibition effect on cells [170][171]. Red LED of 670 nm (6,000 µmol m^{-2} s^{-1}, 0.7 Ampere, PCB chip with lens) was selected for its high absorption in the red spectrum. Additionally, a cool white LED (3997K, 1,000 µmol m^{-2} s^{-1}, 12 Volt light stripe, Ultra high 2835 SMD LED strip, Optic Fibre & LED Lighting Solutions Pty Ltd) was used. Unlike warm lighting with higher K-values and stronger emission in the green and red spectrum, cool white light predominantly emits in the blue light spectrum and provides less intense irradiance of higher wavelengths. The emission spectrum of the LEDs was analysed with a spectrometer (JAZ, Ocean optics).

Since LEDs can emit wavelengths that might interfere with the fluorescence recording, different optical filters were used to prevent unwanted wavelengths reaching the cameras. An optical short-pass filter (300 - 700 nm, Edmund Optics) in front of the LED ensured the supply of exclusively PAR to the culture (Figure 2-1). A long-pass filter (> 800 nm, Edmund Optics) in front of the camera lens blocks interfering wavelength from the LED, along with scattering of the culture, thereby allowing the recording of the fluorescence emission only. Potential interference with the light transmission of the PE bag were excluded by testing the absorption spectrum with a spectrophotometer. The resulting absorption spectra showed negligible absorption in the relevant regions of 400 – 1200 nm (data not shown).

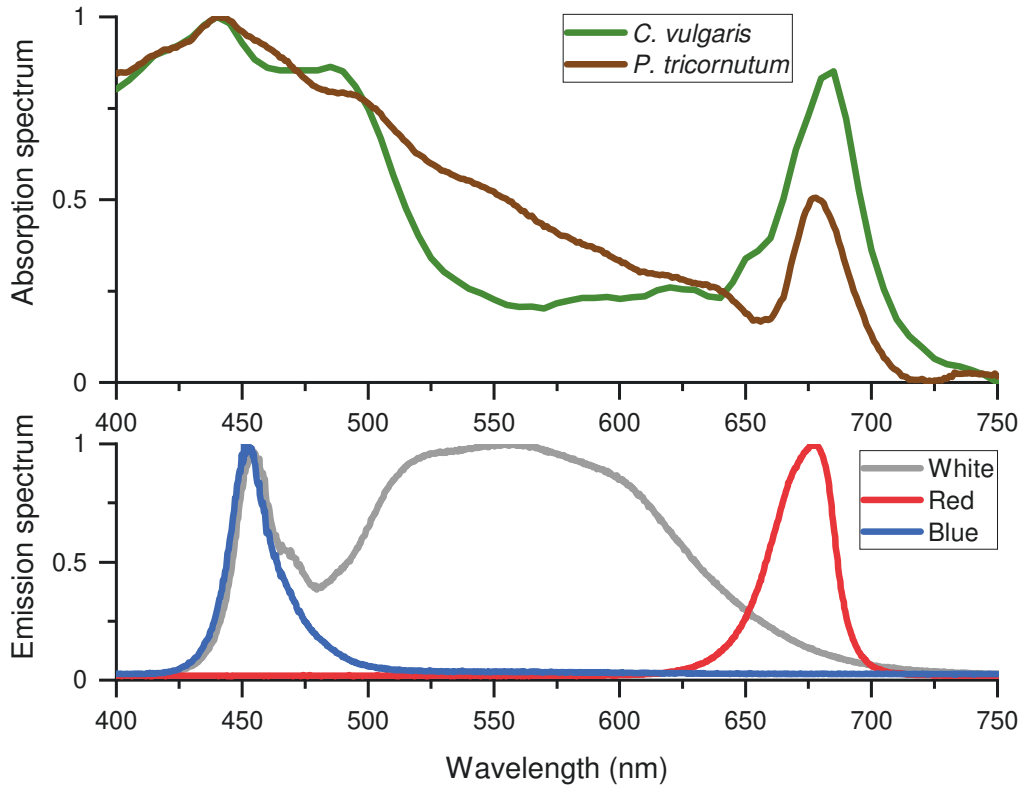

Figure 2-2: Absorption spectrum of *C. vulgaris* and *P. tricornutum*, together with the emission spectrum of blue, red and white LEDs. High peaks in the absorption spectrum relate to a high absorption in this wavelength area, whereas peaks in the emission spectrum represent the photon flux in the specific wavelength region. Spectrum values are normalized to the minimum and maximum values.

2.2.2 Data processing

The raw .cr2 images were converted into .TIFF format using Digital Photo Professional (ver. 4.10.40.0., Canon). The image processing was done with ImageJ. The minimum and maximum pixel values of the fluorescence images affected the final results, due to higher noise to signal ratio in fluorescence images with a pixel values below 10% of the maximum value, and information loss through photon overflow at the sensor for pixel values close to the maximum value (65,535 for 16-bit images). Therefore, only fluorescence images with overall pixel values between 10 – 90% of the maximum pixel value were chosen. The cameras captured colour images with three colour channels. The red, green, and blue colour channels of the side profile image were split and exclusively the red colour channel was further processed. Thereafter, a circular Regions of Interest (ROI) with the size of the sensor head (in this instance 0.05 cm^2) were applied to mark the PAR sensor positions in the images. These circular ROIs were used to measure the average pixel value of the fluorescence image and thereby match the pixel

values of the image with the light intensity measurements. Pixel values and light intensity were plotted with MATLAB (R2019a, Update5, The MathWorks) using a power trend line. The trend line (Eqn 1) was utilized to calculate light intensity (I) with the pixel value (x) of the fluorescence image:

$$I = a * x^b + c \qquad 1)$$

Where (a) represents the coefficient, (b) the power and (c) the offset of the trendline. As it was assumed that at light intensity zero the pixel values will have a zero value, the offset (c) was defined as zero. This zero intersect is an approximation, as the camera chip has naturally a dark current that creates a constant baseline noise resulting in a minimal pixel value above zero. However, the noise level is dependent on several factors, such as chip temperature, chip acclimatisation to light and camera settings [172], which were not assessed in this study. As such the calculations were estimated with a minimal pixel value of zero. These power trend line equations were applied to each pixel in the corresponding fluorescence image, resulting in the conversion of a fluorescence image into a PPFD image (light map). Digital line profiles were used to analyse light attenuations of the images by extracting the image pixels (MATLAB). This yielded the pixel intensity together with its correlated position in the measurement chamber. The line profile stretched horizontally from the LED centre across the length of the measurement. Statistical analyses were done with R (Version 1.2.5033) [173]. Normality of the data were tested with Shapiro-Wilk, non-parametric Kruskal-Wallis test with a pairwise comparison between group levels using the Pairwise Wilcoxon Rank Sum tests. Correction for multiple testings were done with the Benjamini & Hochberg method. Discrepancies between tested groups were defined as significant at $p < 0.05$.

2.3 Results and Discussion

2.3.1 Method validation

The proposed DCFI method is strongly reliant on the initial data processing step in which the pixel values are correlated with the measured light intensity values. The conversion of the fluorescence image into a light map is done by locating the position of the light intensity measurements in the image and extracting the mean pixel value of that region in the fluorescence images. These mean pixel values of fluorescence intensity and the measured irradiance of each position in the measurement chamber were plotted (Figure 2-3), resulting in a trend line using the calibration formula (Eqn 1). Applying this formula to the fluorescence image converts the

pixel values into light intensity values, which translates the fluorescence image into a light map. Pixel value and light intensity show a direct correlation. Outliers that were clearly attributable to interfering reflections in the fluorescence image were manually removed. These unwanted fluorescence reflections were created by the measurement chamber and can interfere with the results, emphasizing the need for a properly designed test chamber to avoid unfavourable optical properties.

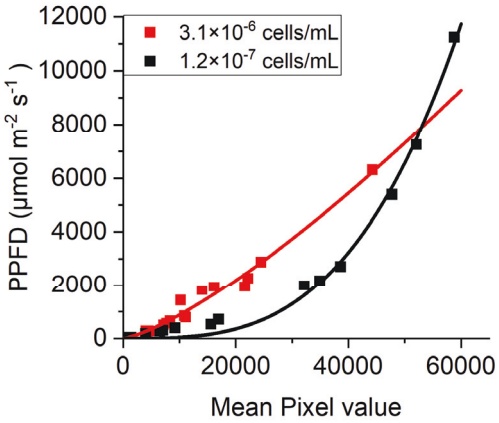

Figure 2-3: Representative graph of the relationship between the mean pixel value in specific ROI and PAR measurements of the PAR sensor for different *P. tricornutum* concentrations. Datapoints show the irradiance measurement with correlated pixel value of the fluorescence image. The lines represent the associated calculated trend line.

While the camera setup was consistent during the experiment, diverse fluorescence intensities were observed with the differing cell concentrations, algae species, and LEDs, which led to over- or under-saturation of the image. In order to prevent this over- or under-exposure, a range of shutter speeds were applied to each experimental setup. The reproducibility with different shutter speeds and their effect on the final light maps was analysed with an experimental dataset. The line profile of light maps with a short (0.00125 s), a long (0.025 s), and an optimal (0.00625 s) exposure time were compared in Figure 2-4 (B). The plotted line profiles correlated with the actual PAR measured, indicating that images with different shutter speeds can be correctly converted into light maps. However, the faster shutter speed (0.00125 s) demonstrates higher signal fluctuations since the ratio of standard noise for the camera chip increases with the reduction of signal intensity due to the shorter duration of chip exposure. This renders images with lower signal intensities more prone to noise, which can be seen in the corresponding light map (Figure 2-4 A). On the other hand, excessive image exposure resulted

in light maps that suffer information loss due to the over-saturation of the image sensor. These over-saturated fluorescence images led to unrepresentative light maps (Figure 2-4 (0.025 s shutter speed)). Conversion of these fluorescence images led to reduced noise levels in the light map, but had incorrect maximum values due to the imprecise conversion formula (i.e., trend-line). In order to avoid both cases, and to create reliable trend lines, fluorescence images with an overall pixel intensity below 10% and above 90% of maximum pixel intensity were excluded for the analysis.

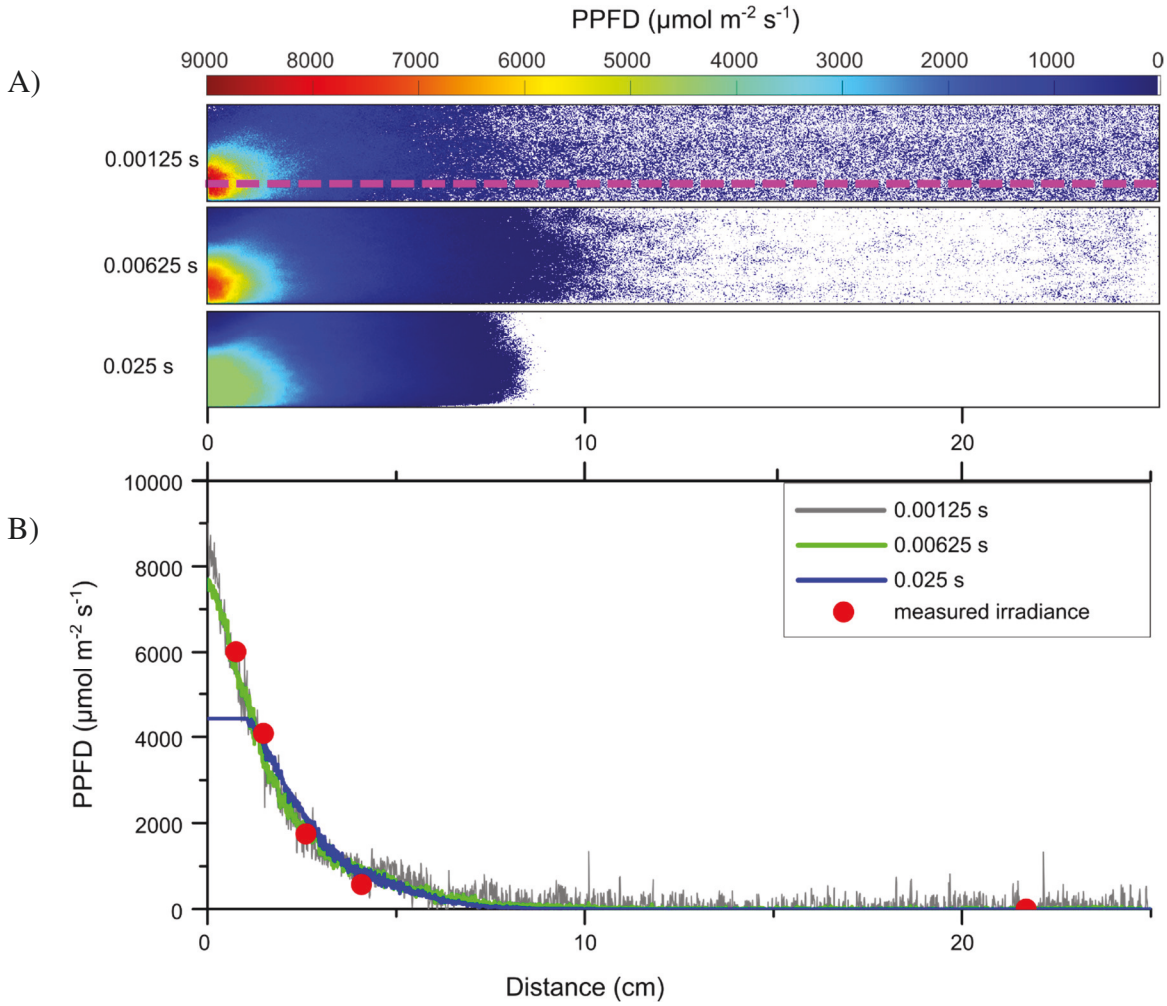

Figure 2-4: Comparison of light map conversions at different shutter speeds. A) Shows light maps (side view) based on the conversion of fluorescence images captured with three shutter speeds. The colourmap highlights different irradiance intensities with values below 15 µmol m^{-2} s^{-1} in white. B) The different light maps were analysed with a line profile (representative line shown in violet) and plotted as PPFD over the distance to the light source. The line plots show the different shutter speeds (grey, green, blue) with the corresponding irradiance measurements of the PAR sensor (red dots). The maps are based on fluorescence images of *P. tricornutum* (2.18×10^6 cells/mL) with a blue LED.

2.3.2 B-value

A correlation of the b-value (trend line slope, Eqn 1) with the cell density was observed for the different experimental settings (species and LED). With a constant shutter speed, the increase of cell density led to a constant increase of the b-value. Figure 2-5 A shows the datasets of the three LEDs in *P. tricornutum* and the correlation between the b-value and cell density. There appears to be a trend between the b-value and the cell density, although further data are required to confirm this. Additionally, the a-value and b-value of the trend line formula are linearly related, enabling an estimation of the values by knowing one (Figure 2-5 B). This trend was consistent for all conducted experiments. Considering that the c-value (trend line intercept) is set to zero, the conversion formula could potentially be applied to the uncalibrated fluorescence image of any cell density. As such, the conversion process of fluorescence images into light maps could be further reduced by excluding the PAR sensor calibration (calibration image) since the b-value can be estimated for each cell density. The relation of b-value to cell concentration is specific for species and light colour, therefore measurements with different cell concentrations for each of these configurations would still be needed to create a solid database on which this ultimate conversion formula is based. Another interesting aspect of this relationship is the behaviour of the b-value to the shutter speed. It was observed that b-value correlated with the shutter speed of the camera (Figure S 1). This correlation should be further analysed in future work, as it might be utilized to enhance the usage of the ultimate trendline and could be applied as an optical on-line cell density measurement [174].

A)

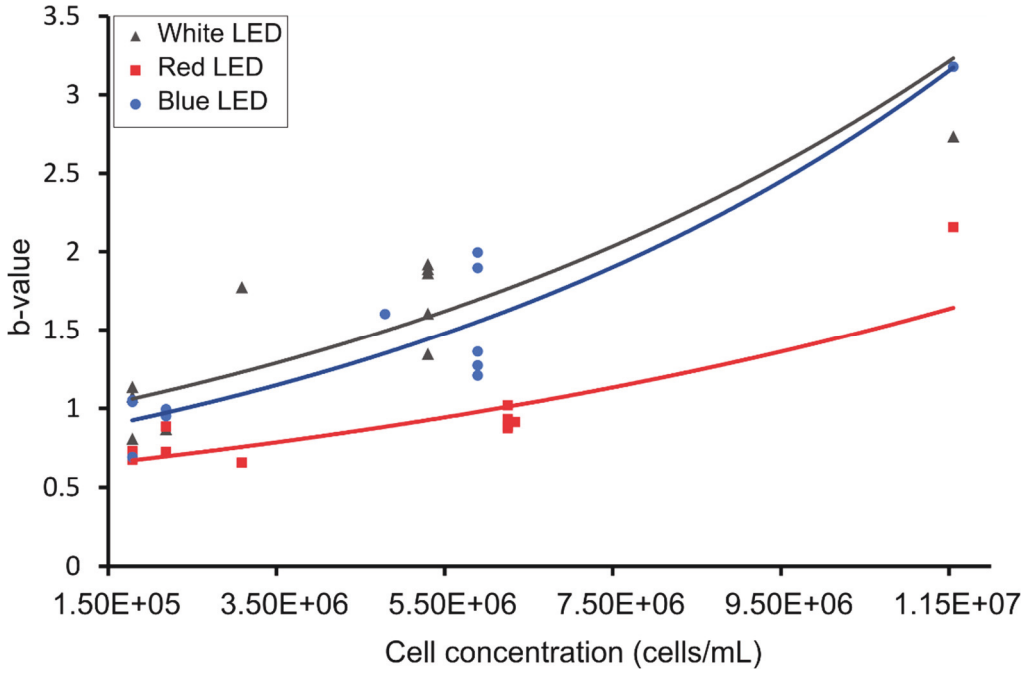

B)

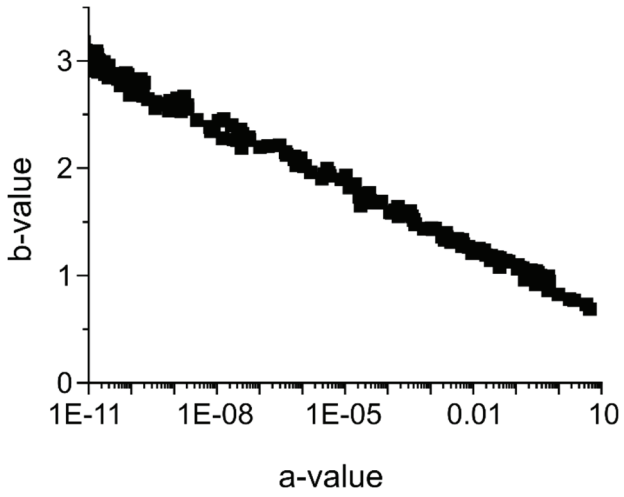

Figure 2-5: Correlation of the cell concentration with values of the conversion formula. A) The impact of the cell concentration on the b-value. Figure highlights the potential trend of b-value increasing with cell concentration, showing a representative trendline ($y = a*e^{(b*x)}$). Displayed are b-values of the three LEDs with *P. tricornutum*. B) Representative relation of the b-value and the a-value for the relationship of the blue LED with *P. tricornutum* for datapoints obtained from different shutter speeds

2.3.3 Light map analysis

The light maps facilitate a detailed overview of the actual shape of the LED light profile and reveals the light attenuation within the PBR. Resolutions of the images for top and side view reached 84 and 135 pixels per cm, respectively. To highlight certain regions of the LED light contour, certain light intensity regions were digitally coloured (MATLAB). The ranges and upper limits for light stress and light-limitation depend on species and wavelength. Therefore, three light regions were defined: dark, saturated, and high-light zones. The saturated light intensity was defined as between 15-400 µmol m^{-2} s^{-1}, a theoretical area with enough photons for most microalgae to grow, yet without photon-induced light inhibition ("sweet spot"). The

region below 15 µmol m^{-2} s^{-1} was considered as dark zones [175], areas in which the photon supply is not sufficient to grow. Values above 400 µmol m^{-2} s^{-1} were defined as high-light zones [134], the regions with photon emission potentially high enough to reduce growth due to light stress (photoinhibition). These modified light maps are displayed in Figure 2-6 A, B (*C. vulgaris*) and Figure 2-6 C, D (*P. tricornutum*) for a low and a high cell concentration. The figures visualize the high light regions, close to the LED, the "sweet spot" region, and the light-limited region at the far end of the bioreactor. The different LEDs are not directly comparable with each other, since the light intensities of the LEDs were not equalized for these light maps. The predominant focus of this study was the mapping of the artificial light sources and their capabilities to illuminate a bag reactor. Future experiments measuring the efficiency of light penetration of different wavelengths should consider adjusting the light intensity to be equal for comparison. For both species and concentrations, the blue and red LEDs have a dominant high light region, owing to the higher initial light intensity of the blue and red LEDs (max. 13,000 µmol m^{-2} s^{-1}, and 6,000 µmol m^{-2} s^{-1}, respectively). The white LED (max. 1,000 µmol m^{-2} s^{-1}) rarely exceeds the 400 µmol m^{-2} s^{-1} limit, creating an evenly distributed "sweet spot "region and shows practically no high-light zones. Although the high-light zone of blue and red are similar, the red LED overall penetrates deeper into the culture than the blue light, and has a better ratio of saturated light zone to high-light zone. This could be explained by the broad absorption peak in the blue wavelength spectra of microalgae [138]. Interestingly, while the white LED had the weakest initial intensity, its penetration depth into the culture is similar to the blue LED. The green wavelength band, contained within the white light spectra, might be the cause for the deeper penetration. Green light is inferior in its absorption by this algae allowing for a deeper penetration into the culture, before it finally gets absorbed [176][177].

The species were primarily chosen for their differences in cell size and cellular composition. *C. vulgaris* shows a greenish reflectance spectrum with a lower absorption of in green wavelengths [163], whereas *P. tricornutum* has a brownish reflectance spectrum (Figure 2-2). Different morphology and cell compositions of the selected species limit the direct comparability of the light penetration between species; however, the light cone shape and the distribution of the different light zones can be compared with each other. Furthermore, the light maps allow for the comparison of the absorption ratio of the three LED for the individual species. In *C. vulgaris,* blue and white light penetrate equally deep, whereas for *P. tricornutum* blue light appears to reach further into the culture. This might be caused by differences in pigment content of the species [178]. *C. vulgaris* has a stronger absorption around 480 nm, supporting the argument for a higher blue light absorption (Figure 2-2). On the other hand, *C.*

vulgaris cannot effectively utilize the green light spectrum (500 – 575 nm), while the carotenoid (fucoxanthin) content in *P. tricornutum* enables an extended absorption into the green spectrum [139]. Increased absorption around 550 nm with *P. tricornutum* might explain the stronger absorption of white light, yet the higher absorption of blue light in *C. vulgaris* could also cause this phenomenon. The shape of the white LED profile in *P. tricornutum* shows a clean transition between the light saturated and light limited zone, while the transition zone of *C. vulgaris* was more fragmented. This discrepancy in the shape between the LED profiles could be further explained by the differences in light absorption between the species or could be described by a distinct photon scattering profile of the microalgae. Typically, light approaching a microalgae cell is scattered in the forward direction, seemingly independent from wavelength and intensity [179][180], which supports the undefined fringes of all LEDs in the *C. vulgaris* culture. The clearer contours of *P. tricornutum* could then be explained by a different scattering characteristic related either to the cell morphology or the cell composition (silica content).

Future work could focus on the enhancement of light map with information about the electron transport rate (ETR). This would allow the light maps to be converted into ETR maps that highlight potential photo-inhibiting areas [160]. This could allow for a more precise adjustment of the light quality and quantity of the LED in order to reduce light stress. However, this would require additional calibration steps (e.g., PAM measurements for each wavelength and light intensity).

A)

C. vulgaris with low cell concentration

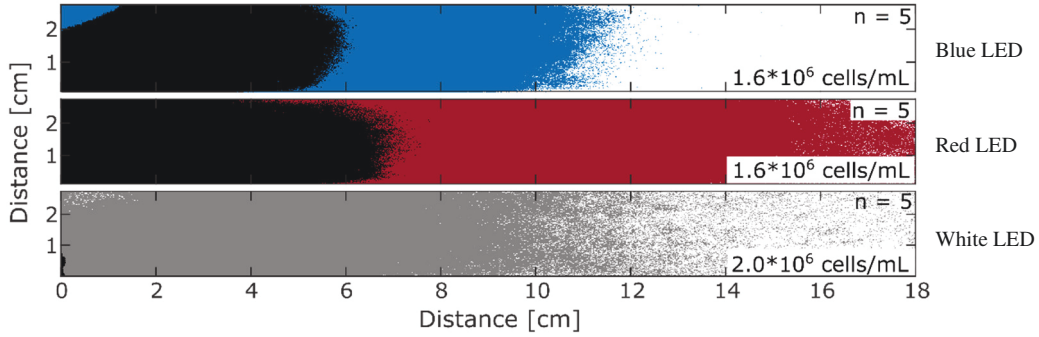

B)

C. vulgaris with high cell concentration

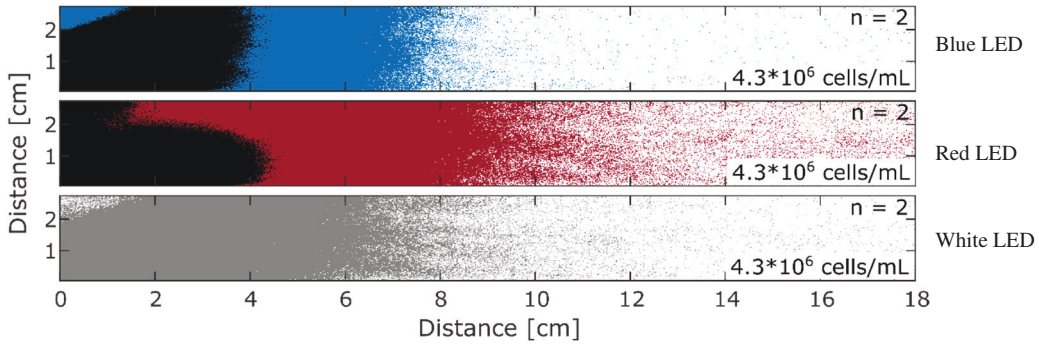

C)

P. tricornutum with low cell concentration

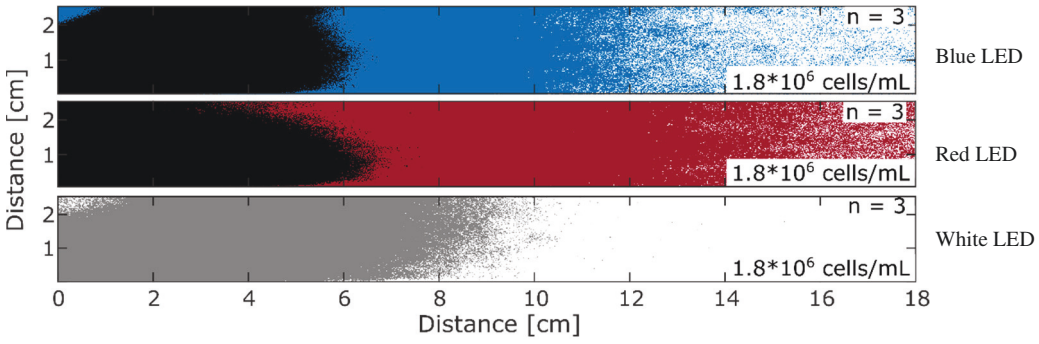

D)

P. tricornutum with high cell concentration

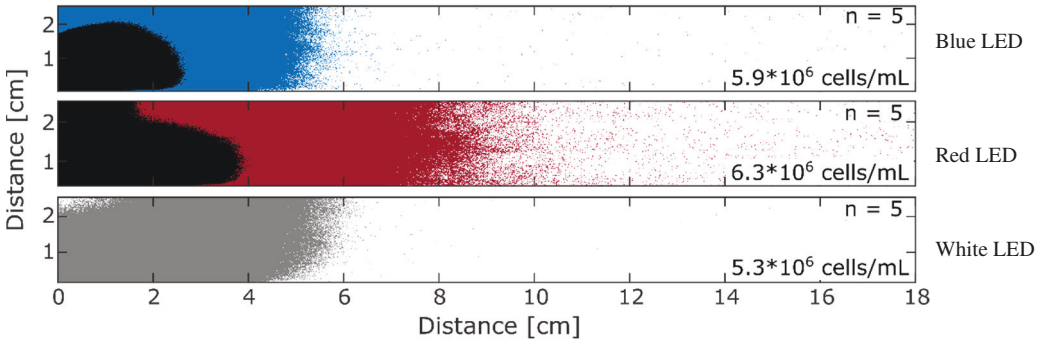

Figure 2-6: Averaged light maps (side view) for different LEDs (blue, red, white) for low (A,C) and high (B,D) cell density of *C. vulgaris* (A,B) and *P. tricornutum* (C,D). The light maps are organized by blue, red and white LEDs for each species and cell density. Artificial colours were used to display certain areas of the light maps for each LED: Black areas correlate to high light zones (>400 µmol m^{-2} s^{-1}), blue, red, and grey (coloured for the corresponding LED, with the white LED in grey) highlight the saturated zone (15-400 µmol m^{-2} s^{-1}), and low light zones are displayed in white (<15 µmol m^{-2} s^{-1}).

The light maps can be further used to analyse the light attenuation in the PBR by applying a line profile (3 mm width) to the light maps and extracting the irradiance values. The light penetration depths were calculated for light attenuation of 50% (D_{50}) and 90% (D_{90}). Figure 2-7 shows the result of *C. vulgaris* and *P. tricornutum* at high and low cell concentration with three different LED colours. The overall light attenuation of the D_{50} is of similar depth when compared between both species, which is due to the severe decrease in PPFD in the first few centimetres into the culture. This effect was observed in the representative line plot (Figure 2-4) and also found in previous studies, which showed a sharp light attenuation in the first few centimetres for *C. vulgaris* independent from the light intensity [133]. Statistical analysis showed clear differences in light penetration for the different LEDs and the cell concentration in the *P. tricornutum*. The D_{90} emphasize the strong absorbance of the blue wavelength. For both cell concentrations the blue wavelength has a reduced light penetration of around 50 % compared to the red wavelength. This suggests that the red LED is more efficient in achieving improved light penetration even with a lower initial light intensity emitted by LED. For the D_{50} and the D_{90}, low cell concentration showed a deeper light penetration for the red and blue light. In the case of the D_{90}, the higher cell density reduced the light penetration for all LEDs by ~50%, whereas the D_{50} exhibits only a minor decrease in penetration. This indicates that the light distribution of lower light intensities (deeper in the PBR) decreases more strongly with increased cell densities, while the distribution of higher light intensities close to the light source only slightly decreases in size. The *C. vulgaris* culture results are more difficult to compare since the difference between the high and the low cell concentration are less clear. The penetration depth for D_{50} and D_{90} showed no statistically significant difference, though slight trends in declining penetration depth are noticeable that show similar patterns observed in *P. tricornutum*. This might in part be explained by the chosen cell densities that were too similar, hence had only a slight impact on the light attenuation. Another explanation is the potential impact of background fluorescence from the culture in the PBR. Emitted fluorescence behind the focal plane of the camera can contribute to the observed fluorescence and thereby cause artifacts in the converted light map. Future work will focus on the evaluation of this background fluorescence and its effect on the light maps.

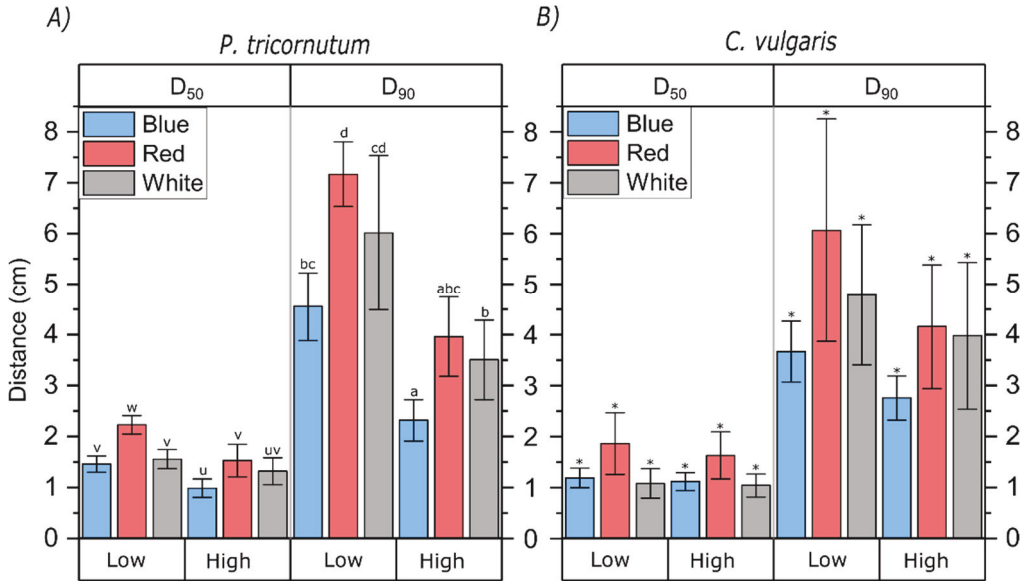

Figure 2-7: Light penetration depth of 50% and 90% irradiance attenuation for *P. tricornutum* (A) and *C. vulgaris* (B) at high and low cell density. The mean penetration depth for cell density range for *P. tricornutum* at low cell density (1.80×10^6 – 2.20×10^6 cells/mL), high cell density (4.80×10^6 – 6.25×10^6 cells/mL), and *C. vulgaris* at low (1.27×10^6 – 2.00×10^6 cells/mL) and high (4.30×10^6 -5.23×10^6 cells/mL) cell density. The three LEDs are shown in their corresponding colours (blue, red and white in grey). The letters above the columns indicate the statistical differences of the results as grouping (Pairwise Wilcoxon Rank Sum test), no statistical difference in groups are indicated with '*'. Statistical tests were done individually for species as well as D_{50} and D_{90}. The line profiles applied on the image had a width of 40 pixel (~3 mm). Data are mean ± SD (n≥4).

2.4 Conclusion and Future work

This chapter introduced the novel method termed DCFI, which was developed to create high resolution light intensity images (light maps) by recording the fluorescence of the algae. Two species with distinct morphologies and cell compositions were analysed in order to assess the robustness of the methodology. The resulting light maps emphasize the complex light contours of the chosen LEDs which enabled the separation of the PBR into distinct light regimes, while the light attenuation as a function of the radial position to the light source can be conveniently analysed digitally. It was shown that this method can be easily applied to bioreactors, without the need for expensive equipment. The resulting light maps reached a resolution of about 135 pixels/cm (side view), a value that could be further improved with advanced camera features (i.e., higher image resolution) or by positioning the camera closer to the fluorescence region of interest. In this case, special care has to be taken to exclude optical lens distortion with specific distortion free lenses or by applying digital lens distortion methods during image processing. The light maps can be used to optimize illumination systems by calculating the best positioning of the light sources, thereby enhancing light saturated areas and reducing high light zones.

Further research should focus on the creation of more datasets to verify the usability of the ultimate trendline, by building a library of different light sources and species. The current LED setup allowed a method benchmark over a diverse wavelength spectrum, however, depending on the microalgae species other wavelength might be more beneficial for cultivation or allow for deeper light penetration. Since the morphology and cell composition of the species potentially interact differently with changing light qualities, the trendline would be specific for each algae species and light setup. Further work would be needed to investigate if certain morphologies have consistent effects on light scattering, or if the analysis is unique to every species. However, it would enable a rapid production of light maps for new PBR designs without the need of additional calibrations. Additionally, the method can be applied to different PBR designs and should, in the future, include the effect of aeration on the light attenuation into the validated measurement system, in order to create a more realistic measurement platform. The enhanced system would give insight into the actual scattering and light attenuation, including the influence of bubbles, within a PBR.

Chapter 3
Methodology for the validation of the physical optimization system

Author contributions

Julian R. Kofler designed and performed all experiments and wrote the manuscript. Leen Labeeuw advised, supported the experiments, and assisted in writing. Peter J. Ralph advised, materially supported the experiments, and assisted in writing.

3.1 Introduction

Microalgae are photoautotrophic microorganisms and therefore need light and CO_2 for the synthesis of essential molecular components. Increasing cell densities in cultures increases the overall uptake of CO_2 from the media, leading to CO_2 depletion, substrate limitation, and ultimately to diminished growth [181]. As such, transfer of the CO_2 (most commonly in gas phase) is crucial for increased growth. The diffusion of this gas into the liquid media is concentration-driven and begins in a highly concentrated gas bubble which is introduced into the liquid, and ultimately diffuses from the liquid into the cell. The molecule has to pass through several boundary layers, located at the transition of the different phases each with different resistances (Figure 3-1). Although the diffusion of the CO_2 molecule through different phases (gas-liquid and liquid-solid) would seem to offer the highest resistance for mass transfer, the liquid film surrounding the bubble actually controls the gas transfer [182]. The mass transfer rate describes this diffusion and can be used as a measure of the efficiency of a bioreactor to supply CO_2. The mass transfer rate is highly dependent on environmental conditions, such as temperature, pressure, media composition, but can also be influenced by the design of the bioreactor [183].

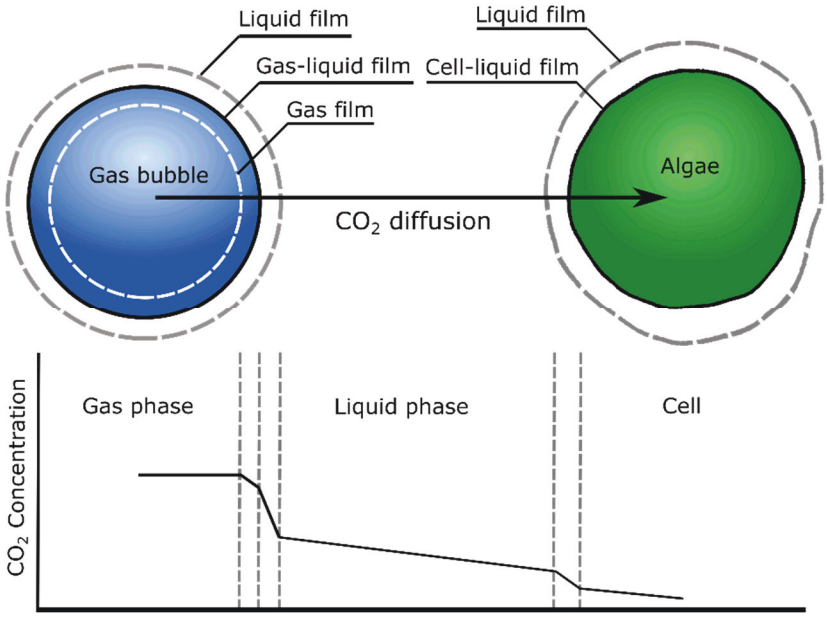

Figure 3-1: Overview of mass transfer resistance through different films in gas-liquid-cell system [184], highlighting the migration of a CO_2 molecule from gas phase to the cell with its different film and diffusion resistances.

Ideally, optimization of the mass transfer rate attempts to enhance the gas-liquid surface area, the retention time of the gas bubble in the media, or to increase the concentration of the required gas in the intake mix. The latter approach will raise the dissolved gas concentration in the culture, but since the culture medium is only able to absorb a certain quantity of gas molecules before the bubble collapses at the surface, larger quantities of the CO_2 gas will be wasted as exhausted gas [185].

In order to increase the gas-liquid surface area, the bubble size can be reduced, while keeping the aeration flow constant. Bubbles are classified by diameter: macro bubbles (10^4 – 10^2 µm), micro bubbles (10^2 – 10^1 µm), sub-micro bubbles (10^1 – 10^0 µm), and nano / ultra-fine bubbles (10^0 – 10^{-3} µm) [186]. The smaller size increases the surface to volume ratio of the bubbles, hence the mass transfer rate increases, provided the aeration rate stays constant. Reducing the bubble diameter also decreases the rising velocity [187], thereby extending the residence time of the bubble in the culture medium. The downsides of reducing the bubble size are the higher energy cost to achieve the reduced diameter and the increased bursting energy smaller bubbles possess [187]. When the bubble ruptures, the rapid retraction of the liquid can create shear stress of up to 95 N/m^2 which is strong enough to destroy cells in the immediate vicinity, an effect that can be utilized for liquid disinfection [188]; clearly, this effect should be avoided for algae cultivations. The negative impact on microalgae growth was observed in a bubble column that showed a correlation between an increase in cell death with a decrease in bubble diameter (< 2 mm) [189][190]. Another limitation of smaller bubble size is the ability to remove gas from the culture medium. During the microalgae cultivation, the culture medium absorbs the expelled O_2 produced by the cells that can be toxic at higher concentrations [191]. Dissolved oxygen concentrations over 30 g/m^3 where found to reduce biomass productivity in *C. vulgaris* by 30% [192].This O_2 has to be removed in order for the cells to reach optimal growth; this can be achieved with mixing or aeration of the culture [193][85]. This degassing effect might not be sufficient with sub- micro- and nano bubbles aeration, where bubbles can stay for minutes in the liquid and collapse in the culture instead of rising to the culture surface [186]. As such, the need for gas removal and reduction of the cellular death rate must be balanced against the increased mass transfer rate when optimizing bubble size.

While mechanical mixers such as an impeller further reduces bubble size by atomizing the bubbles, they also increase the turbulent flow in the PBR, thereby extending the retention time of the bubbles in the media [194]. The bubbles are dragged by the turbulent forces and have a prolonged travelling time within the bioreactor before they collapse at the surface. This effect

can be further improved with baffle systems that introduce additional turbulences in the PBR [195]. Agitating the culture has the additional effect of increasing the concentration-driven diffusion by homogenising the culture [83]. Usually in a PBR, the CO_2 concentration is highest close to the initial aeration region (e.g. sparger) [196]. This locally elevated concentration reduces the concentration driven diffusion of CO_2 into the culture in these areas. Moreover, while these regions are saturated with CO_2, other regions in the bioreactor might be CO_2 limited. Optimized mixing is therefore essential in order to homogenise CO_2 concentration within the bioreactor. Another important consideration of mixing is its impact on the hydrodynamical flow pattern of the culture. The flow pattern is relevant for the exposure of the microalgae to the light source. The PBR can be separated into three illumination regions: the light-inhibited, light-saturated, and light-limited regions [197]. The liquid flow drags algal cells through different regions of the PBR, which exposes the cell to the various light intensities for distinct retention times [197]; optimizing this flow could improve the photon distribution to the cells by keeping the microalgae longer in the light-saturated areas and exposing them only briefly to high-light areas that would induce light-damage. Adjusting the aeration rate or utilizing an impeller are the common approaches to control these flow rates and create a turbulent flow pattern. Higher impeller speeds increase liquid flow, but also increases shear stress applied to the cells. Shear stress in a bioreactor is defined as a hydrodynamic stress forced through mechanical agitation of liquid on the cells. It is associated with essential mixing and aeration of the culture, yet high rates of shear stress can cause cell damage or even cell death [198]. Microalgae are rather resistant to shear stress; however, shear stress sensitivity varies amongst species [199]. In order to achieve optimal growth conditions, a balance between mixing and cell protection must be found. A system has to supply sufficient CO_2 and light in a manner that does not induce light- or shear stress, yet also does not leave the cell substrate limited.

Process or design optimization on established bioreactor systems can be rather time consuming and expensive [200]. Typically, design changes are applied to simplified physical or digital models of a bioreactor. These models allow for an easier method of testing modifications before transferring them to the actual physical system. The scale-down approach is an effective method to increase optimization efficiency by reducing operational material and testing time [201]. In this concept the commercial bioreactor is volumetrically scaled down and the cultivation process is analysed in small scale. The results of these studies can support the identification of operation conditions that can be extrapolated across multiple scales. The utilization of small scale processes is a suggested method in guidelines such as the ICH Q11

[202]. The approach can be defined in several steps [203]: i) analysing the commercial bioreactor, ii) mimicking the commercial bioreactor conditions in a scaled-down system, iii) trial of modifications and optimization in the scale-down system, iv) translating the findings to the large-scale bioreactor, and v) implementing the improvement to the industrial scale bioreactor. When a bioreactor is scaled down, the focus should be on maintaining the linear relation of a particular parameter (e.g. mixing time or mass transfer) [204]. The correlation of bioreactor parameters have to be considered while scaling: for example, to ensure equivalent mixing time at larger scales, the impeller speed must be increased, thereby raising the power uptake and shear forces at the impeller. Maintaining a few relevant physical parameters as constant during the scale-down ensures that modifications tested on the scaled-down version are transferable to the up-scaled industrial system. Preserving the mixing time is a common approach, as it controls the mass transfer and the homogeneity of the culture [205]. In regards to the photo-bioreactor, the relationship between the illuminated area and culture volume is an important parameter to consider in order to keep the light distribution for all scales comparable.

The project aims to convert an industrially used bioreactor into a PBR system. As such, an optimization platform was designed to ensure rapid and flexible testing of design modifications. The proposed bioreactor system is the GE Xcellerex system [206], a single-use bioreactor that can be categorized as a stirred-tank reactor, and is commonly used to cultivate mammalian and bacteria cells (Figure 3-2 A). The system consists of a single-use bag that is contained in a cooling jacket, and is supported by a controlling unit that monitors impeller revolutions and aeration rates. The adaptable single use bags include a sparging and impeller system which are interchangeable for different impeller types and aeration systems to achieve low shear stress cultivation conditions, typically for mammalian cells.

In order to retrofit and optimize this bioreactor to suit microalgae cultivation, a streamlined optimization platform was designed that mimics the original bioreactor characteristics. Modifications on the design were tested in these systems before they can be applied to the Xcellerex. The 200 L PBR (Figure 3-2 B) was designed according to the dimensions of the Xcellerex 200 L system. Mixing and mass transfer were found to be crucial parameters for algal cultivation [207], therefore these parameters were used as benchmarks to prove similarity between the optimization platform and the Xcellerex system. In anticipation of the elevated shear stress potentially inflicted by an impeller [199] and the economic implication of the additional power consumption, the 200 L PBR was only agitated with a sparging system.

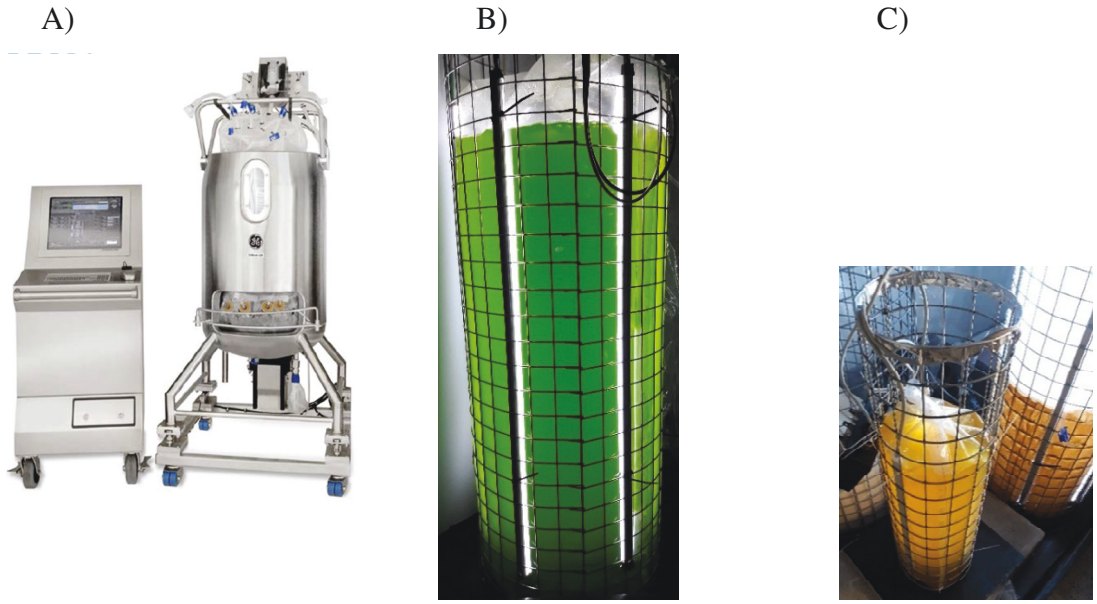

Figure 3-2: Overview of the A) industrial single-use GE Xcellerex 200 L bioreactor system, and the physical components of the optimization platform with B) the 200 L PBR (part 1) and C) the 20 L PBR (part 2).

By using a scaled-down version of the PBR, it is possible to reduce material costs, further ease the manual handling, and allow rapid cultivation experiments. The scale-down approach was based on the 200 L PBR system by keeping the dimensional ratio of surface to volume constant (Figure 3-2 C), thereby maintaining the relation of illumination area to volume. The scaling focused on mass transfer and mixing behaviour; therefore scale-down evaluation revolved around these parameters. Furthermore, the hydrodynamical flow behaviour of the scaled and the full-scale PBRs were compared. Similar flow patterns in both scales should ensure a comparable light exposure of the cells by exposing them to same dark-light oscillation. The flow pattern in the 200 L and 20 L PBR were measured by particle tracing, which characterised the hydrodynamic flow regime of both PBRs.

This chapter will present the mass transfer rate, mixing time and hydrodynamic flow data of the 200 L PBR and the 20 L PBR. These data will partly be assessed against the characteristics of the Xcellerex system [206], in order to create a comparable, and robust system, that will be used as the foundation for the optimization platform.

3.2 Method

3.2.1 Photo-bioreactor system

The physical optimization platform consists of a 200 L and three 20 L PBRs, where the 200 L system was designed to mimic the original Xcellerex model (height: 80 cm, diameter: 56 cm), while the 20 L PBRs dimensions were modified to keep the height / diameter ratio constant during scale-down (height: 38 cm, diameter: 26 cm). Calculation of the down scaling were based on the diameter of the 20 L PBR (D_{20L}) as followed:

$$D_{20L} = \sqrt[3]{\frac{V_{20L} \times 4}{\pi \times \left({}^{H_{200L}}/_{D_{200L}}\right)}} \qquad 2)$$

with V_{20L} as the expected Volume, and the ratio of height (H_{200L}) and diameter (D_{200L}) of the 200 L PBR. These PBRs were crafted from a wire frame to support the single layered polyethylene (PE) bags (Figure 3-2). Aeration used PE tubing and was controlled by a mass flow controller (FMA5400/5500, OMEGA). The 200 L system was fitted with a sparging disk obtained from a commercial Xcellerex bag (GE Healthcare). The plastic disc containing 8 sparging stones (pore size: 20 µm, Ø=25 mm) which was centred in the bioreactor. The 20 L system contained a single sparging stone (pore size: 20 µm, Ø=25 mm) positioned close to the side wall of the PBR.

3.2.2 Mass transfer coefficient – gassing-in method

The dynamic gas stripping method [208] was used to define the mass transfer coefficient (k_La) in the bioreactor system. Pure nitrogen (BOC Australia) was used for the aeration system to strip oxygen out of the solution, after which the increase of the dissolved oxygen (dO_2) concentration was measured under normal aeration conditions (FireStingO2 (FSO2-4), Pyroscience GmbH). All evaluations of the mass transfer coefficient were based on O_2 measurements; however, the mass transfer rates of O_2 and CO_2 can be correlated by the penetration theory [209] and can be converted if necessary in the future [210]. The k_La calculation was based on the static gassing out method as described by van't Riet [208]. using the absorption of oxygen [182] where:

$$\ln\left(1 - \frac{C_L}{C^*}\right) = -k_l a \cdot t \qquad 3)$$

C^* = concentration in the gas-phase

C_L = concentration of the gas in the liquid at the end

k_La = mass transfer coefficient

t = time of aeration

Mass transfer measurements to define the cultivation performance have to consider cell density and the composition of the growth media, as these parameters can impact the mass transfer coefficient [211]. However, since the aim of this study is the validation of the optimization platform and the scale-down process, tap water (23°C) was used to different fill volumes and aerated with air at various flow rates (Table 3-1).

Table 3-1: Experimental configuration of gassing-in method. The fill volume of the PBR with the different aerations, the effective travelling length of the bubble in the bioreactor, and the sparger system.

PBR	Fill Volume (L)	Aeration (L/min)	Water level (cm)	Height of sparger to water surface (cm)	Sparger system
200 L	200	8.4	80	76	8 sparging stones
	120	8.4	48	44	8 sparging stones
20 L	20	2.1	39	32	1 sparging stone
	10	2.1	23	16	1 sparging stone

3.2.3 Mixing time

The mixing capability of the platform was measured with two methods: pH-method and dye method. The pH-method monitored the pH shift in the media after injecting acids or bases into the reactor, while the dye-method recorded the optical colour change of the media with cameras after a soluble colour was injected.

3.2.3.1 pH mixing time

For the pH-method, the mixing time was calculated for the pH step to reach 95% (t_{95}) of its final concentration. The experimental setup was similarly designed as the method previously used in measurements with the original Xcellerex bioreactor system [206]. The configuration of the experiment can be found in Table 3-2. In order to combine the pH-measurement data from multiple sensors, a microcontroller board (Uno R3, Arduino) was used, extended by a

shield board (Tentacle shield, ®Whitebox Labs) and 4 pH sensors (vers.1, Atlas scientific). Sensor placement in the PBR with different fill volumes are outlined in Figure 3-3. Tap water (23°C) was used as media, while the pH-change was induced by HCl (0.5M) and NaOH (0.5M) in a 1:1000 volume ratio [206]. Statistical analysis of data were done with the Shapiro-Wilk to test normality, non-parametric Kruskal–Wallis test and Pairwise Wilcoxon Rank Sum Tests for pairwise comparison between group levels. Correction for multiple testing was performed using Benjamini & Hochberg method. Variation withing groups were considered significant at $p<0.05$. All statistical analyses were done with R (Version 1.2.5033) [173].

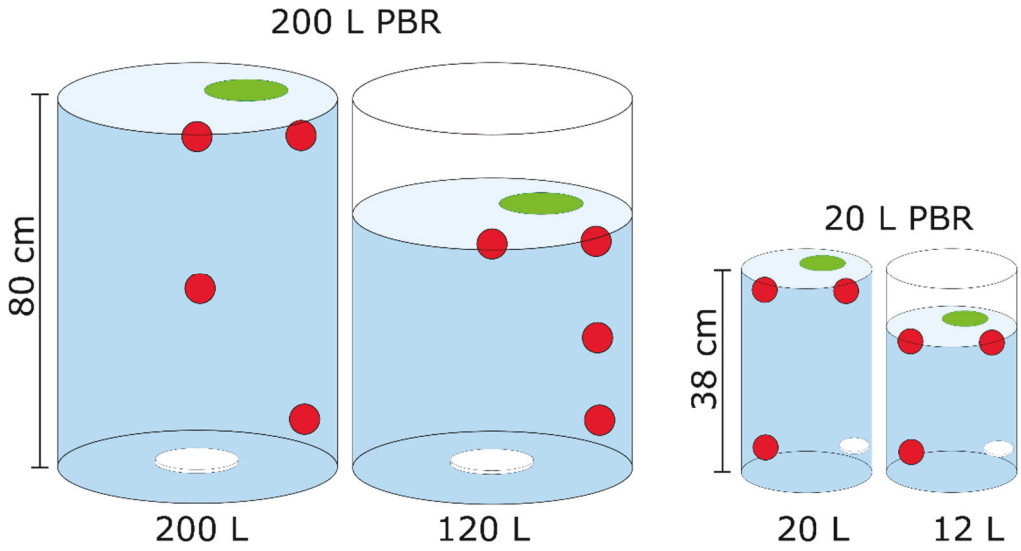

Figure 3-3: Sensor positioning of the pH-methods. The 200 L PBR (fill volume of 200 L and 120 L) and the 20 L PBR (fill volume: 20 L and 12 L) are shown. Red points mark the sensor positions of pH-sensors inside the PBR. Green highlights the injection position of HCl, NaOH, and dye (colorimetric-method). White discs represent the sparger position inside the PBR.

3.2.3.2 Colorimetric mixing time

This colorimetric method measures the time required to change the colour of the media after a dye injection. The mixing time was estimated by measuring the time from dye injection till the media colour change reaches 95% across the bioreactor. The dye-method used 5 mL food colour (blue, yellow, Dr. Oetker Queen) per injection, to induce a colour change in the media. The injection points were similar to the pH-method, shown in Figure 3-3. The optical change was recorded with two cameras (Canon EOS 1500D, EOS 1200D, with EFS 18-55 mm Macro 0.25 m/0.8 ft lens) and digitally analysed with Blender video editor (2.90.1, Blender Foundation). Measurements were conducted for the two PBRs at different aeration rates on fill volumes (Table 3-2).

Table 3-2: Experimental configurations for the mixing time (pH- and colorimetric measurement) and particle tracing. The fill volume of the PBR with the aeration rates, the effective travelling length of the bubble in the bioreactor, and the sparger system

PBR	Fill Volume [L]	Aeration [L/min]	Water level [cm]	Bubble raising length [cm]
200 L	200	8, 7, 6, 5, 4	80	76
	120	8, 7, 6, 5, 4	48	44
20 L	20	2, 1.5, 1	39	32
	12	2, 1.5, 1	23	16

3.2.4 Particle movement

3.2.4.1 Particle tracing method

In order to visualize the flow pattern within the bioreactor, the movement pattern of a floating particle was tracked. This approach was based on an existing method [153] with the following alterations. For the particle, an alginate sphere was created of 0.5% w/v alginate (Sigma-Aldrich) mixed with a 0.05% v/v liquid fluorescence marker (yellow, Schwan-Stabilo). The alginate solution was injected into 2% w/v $CaCl_2$ solution, thereby creating polymerised spheres (Ø=0.5 cm). The spheres were washed in deionised water and transferred into the PBR. The average density of the alginate spheres was 1.013 g/L (referenced with NaCl solution at 20˚C). The particle motion was recorded with two cameras (Canon EOS 1500D, EOS 1200D, EFS 18-55 mm Macro 0.25 m/0.8 ft lens, Olympus E-M10II, Olympus M.Zuiko Digital 14-42 mm f/3.5-5.6 II R Lens). The cameras were positioned perpendicular to each other, facing the front and side of the cylindrical PBR. Dark, low reflecting plates were positioned behind the PBR to create a contrasting background. Distortion of the camera lenses were corrected according to the MATLAB (R2019a, Update5, The MathWorks) Camera Calibration plugin.

A calibration step was carried out first, where the PBR was mapped with a fluorescence marker that was placed at various heights and locations inside the PBR. Each of these positions were captured with both cameras, and the recordings digitally analysed for the pixel coordinates (x, y) of the marker (Blender video editor). Since the real and digital coordinates of the marker are known, the particle position can be converted into real PBR dimensions. For the particle tracing measurements, each frame of the recording was analysed in MATLAB by filtering the colour threshold of the unique colour emitted by the alginate sphere. The resulting image was binarized and the region of interest (ROI) was classified with the 'regionprops' command. The ROI list were filtered for ROI size, shape and centroid position to refine the identification criteria and to match the alginate sphere and exclude interfering reflections. By combining the front and side coordinates, the three-dimensional position (x, y and z) of the

particle in the bioreactor was reconstructed. The fluorescence of the alginate sphere was tracked in the two PBRs with different fill volumes and aeration rates (Table 3-2). The alginate sphere was not always visible for all cameras, as reflections or optical distortions caused by the PBR obscured the camera view. This can create situations where only one or no camera at all had a visual of the sphere. These missing positions were interpolated from contiguous data points. Three cases of particle detection were defined: sphere position observed with both cameras (case one), coordinate set of one camera and an interpolated data set (case two), neither camera had visual on the sphere and both coordinate sets were interpolated (case three). The interpolations (linear) were done in MATLAB starting at the point where the camera lost the sphere to the position the camera regained visual identification of the sphere.

3.2.4.2 Particle and speed map

Once the three-dimensional particle positions were identified, the datasets were used to analyse the trajectory and the velocity of the particle in the PBR volume. Flow path visualisation can be used to reveal the particle path and gives insight on eddies and turbulences within the PBR. Furthermore, particle and speed maps can be created and used to highlight regions with high particle presence and velocity, thereby identifying laminar and turbulent zones within the PBR. The maps were created by slicing the digital PBR into cube volumes with side lengths of 4 and 3 cm for the 200 L and 20 L PBR respectively. For the particle maps, these cube volumes contained a number of detected particles. In these maps, particle detection of case one and two were used (without using the completely interpolated data, case 3). Case two datasets were used due to the synchronized height (Y-axis) of both cameras, which allowed for a relatively interpolated positioning of the missing datapoints. The cube volumes of the speed maps contain the average velocity of a particular area. The calculation was done only for complete datasets with both cameras (case one). Velocity was calculated by determining the distance travelled by the particle for each recorded frame (1/50 s). For the average velocity calculation, potential outliers were removed with the statistical generalized extreme studentized deviate (GESD) method. The influence of height on the velocity and particle presence was analysed by creating horizontal cross sections of the PBR, resulting in cylindrical disc volumes of 4 and 3 cm height for the 200 L and 20 L PBR respectively. Particle presence in these slices were normalized with the maximum particle occurrence, whereas the velocity was calculated as described earlier.

3.3 Results and discussion

The experimental setup was designed to compare the optimization platform with the GE Xcellerex bioreactor in regards to mixing time and mass transfer. Comparison was done by assessing the experimental results of the optimization platform with previously obtained data from the Xcellerex bioreactor (provided by the manufacturer [206]).

In industrial-scale cultivations, it is not uncommon to reduce the maximum fill volume in order to improve certain parameters, such as mixing time or mass transfer, or simply to reduce the production volume [212]. As such, the measurements of the optimization platform were likewise conducted with different fill volumes based on a previous study of the industrial bioreactor [206]. The Xcellerex system was optimized for mammalian (and bacterial) cell cultures, which have different operating requirements. Mass transfer measurements on the Xcellerex were conducted with aeration rates adequate for mammalian and bacterial cell cultivation (0.5, 2.75, 5 L/min air flow). Additionally, an impeller was used to support the mass transfer (30, 110, 190 rpm) [206]. The 200 L and 20 L PBR were operated at higher aeration rate (Table 3-1) to ensure sufficient supply of CO_2 for algal cultivation, while not relying on an impeller for agitation. Typically bubble columns achieve sufficient algae growth without additional impeller agitation [207]. As such, while impellers may be a future option for the PBR, initial trials were conducted with only aeration as mixing.

3.3.1 Mass transfer coefficient

The 200 L and 20 L PBR both had a mass transfer coefficient of around 25 – 30 h^{-1} (Figure 3-4). This demonstrates the effectiveness of scale-down for the 20 L PBR. It should be noted however that unlike the applied dimensional scale-down of 1:10, the aeration rate of the scaled-down PBR had a ratio of 1:4. As such, the 20 L PBR needs proportionally higher aeration rates compared to the 200 L PBR to reach an equivalent mass transfer. Clearly, the mass transfer is correlated with the aeration rates. This dependency can be observed for settings with lower aeration rates, in which the reduced bubble numbers (and therefore smaller gas-liquid surface area), result in a reduced mass transfer. As such, higher k_La with improved CO_2 supply are subject to higher aeration rates. A slightly improved k_La can be achieved by decreasing the fill volume, which can be due to the improved ratio of volume to aeration [213]. The constant aeration increases the volumetric power input in the smaller volume which directly influences the mass transfer [214]. However, decreasing the fill volume also reduces the retention time of the gas phase in the liquid, and therefore decreases the surface area of the bubbles (gas holdup)

[212]. This should be further considered for cultivations with reduced production volumes, as there has to be a balance between increasing the volumetric power input and decreasing the surface area in order to achieve an optimal mass transfer. Compared to the Xcellerex system (Figure 3-4) which reaches a k_La of 25 h^{-1} (200 L fill volume) and 30 h^{-1} (120 L fill volume), similar values were achieved with the PBR systems.

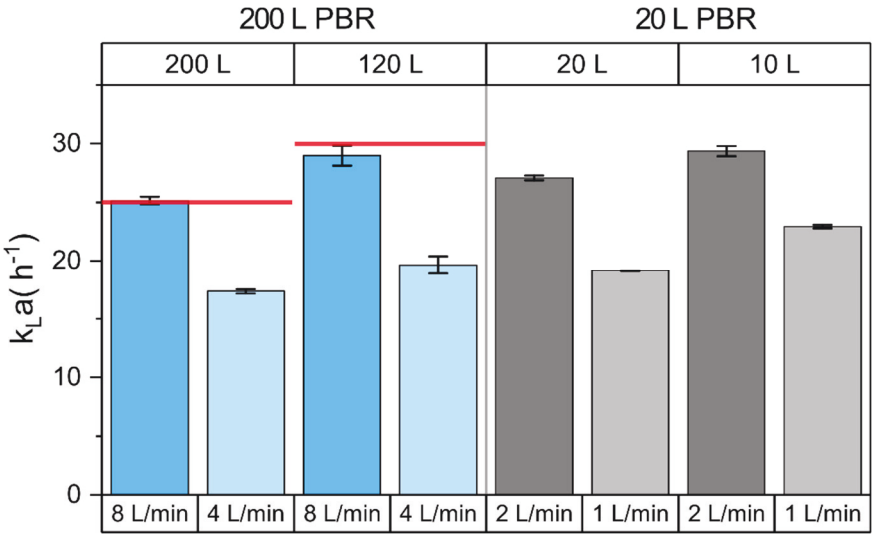

Figure 3-4: Comparison of gas transfer coefficient (k_La) of different PBR setups to the Xcellerex system. 200 L PBR (blue) with fill volumes of 200 L and 120 L and different aeration rates. 20 L PBR (grey) with fill volumes of 20 L and 12 L and different aeration rates. Red lines show the Xcellerex setup with an impeller speed of 190 rpm and airflow of 5 L/min for the two fill volumes of the 200 L PBR. Data are mean ± SD ($n \geq 3$).

3.3.2 Mixing time

Mixing time can be defined as the time the reactor needs to reach a certain degree of homogeneity after a substrate impulse [83]. In order to measure the mixing time, two methods based on different principles were employed: the pH-method and the dye-method.

Results for the mixing time using the pH-method (Figure 3-5) are rather inconclusive. The readings of the 200 L PBR with different fill volumes and aeration rates show no significant difference due to large standard deviations relative to the mixing time. A similar trend can be seen for the 20 L PBR with equally high standard deviations. No significant difference between the operational parameters can be observed, although a mixing time of approximately 60 s for the 200 L PBR and 40 s for the 20 L PBR can be estimated. These values are within the tested range for the impeller-only mixed Xcellerex system with 200 L fill volume that achieved mixing times of 160 and 30 s for an impeller speed of 30 and 190 rpm, respectively.

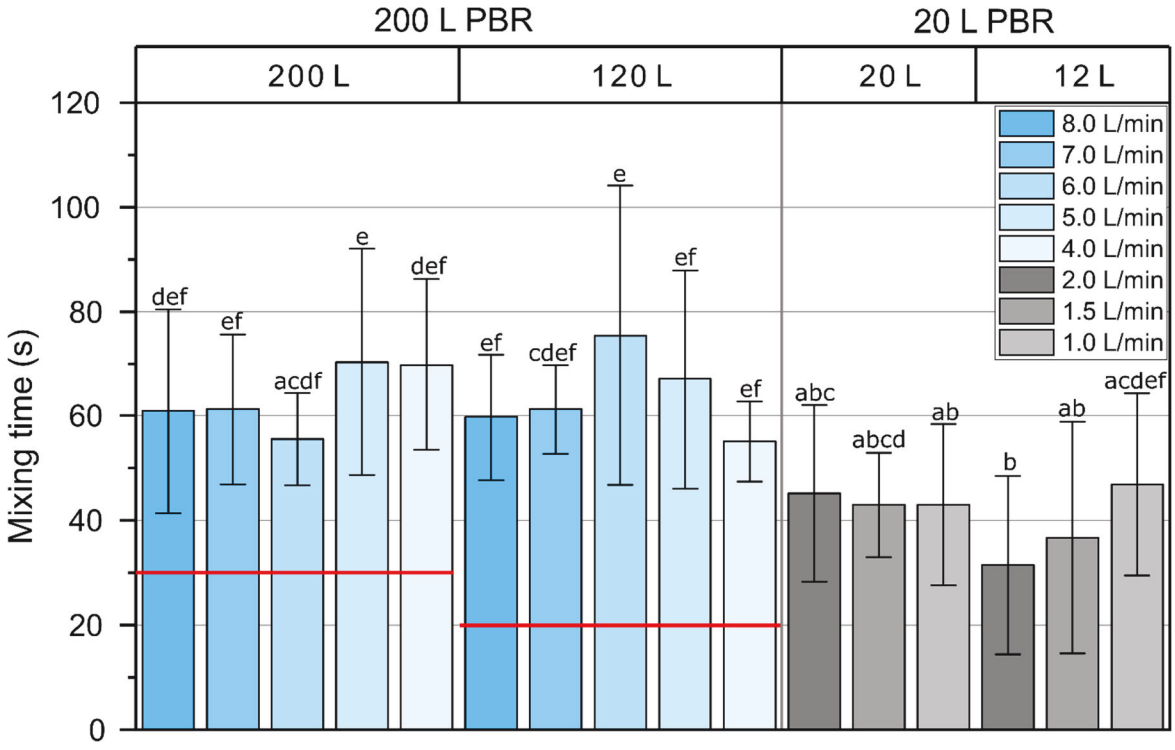

Figure 3-5: Mixing time measured with the pH-method for PBR. 200 L PBR in blue with fill volumes of 200 L and 120 L and different aeration rates. 20 L PBR in grey with fill volumes of 20 L and 12 L and different aeration rates. Red lines show the Xcellerex setup with impeller speed of 190 rpm for comparison. Data are mean ± SD (n = 4). The letters in columns indicate the statistical differences of the results as a grouping, statistical comparison was done for the 200 L PBR with both fill volume together with the 20 L PBR with both fill volumes.

This large variability could be due to several factors. One issue could be the Arduino system which was custom-built for this experimental setup. The pH-sensors had a reaction time of 2-3 s, (referenced with pH-meter (inoLab® Level 2, WTW)), which should be sufficient to determine the mixing time. However, the measurements were recorded with the Arduino extension board in order to synchronise the reading of the 4 sensors. Technical constraints of this setup restricted the sensor readout to a 4 s interval. This slow sensor refresh rate had a considerable impact on the measurements, but does not fully explain the high standard deviations. Another plausible issue could be the inferior liquid mixing of certain regions in the PBR. The pulse technique was designed to record the time lapse of the bioreactor to reach a certain degree of homogenisation. As such, all sensor positions have to reach the final equilibrium, which makes this method strongly dependent on the slowest sensor. Sensors positioned in a laminar flow or poorly mixed region could then suggest an overall global slow mixing time. In order to verify this possibility, the time period from substrate injection till pH equilibrium (t_{95}) for the sensors were compared. Figure 3-6 depicts the positions of the sensors

that reached t_{95} last. It can be observed for the 20 L and 200 L PBR setups that the sensors closer to the bottom had a longer delay in detection (the acid/base was added at the top of the water level). In a well mixed system, it could be assumed that the substrate has a certain travelling time with a constant hydrodynamic flow, resulting in the delay at that position consistent with the travel length. However, the sensor delay for the lower pH-probes does not seem to be related with the normal travelling time, since it took up to 70 % longer for these sensors to stabilize compared to the fastest sensor (data not shown). This insight suggests that the PBR could have inconsistent mixing. The lower regions of both reactors are potentially not as well mixed as the upper part, leading to a faster response in the upper part and delayed detection in the lower part. This highlights how zonal mixing patterns within a bioreactor are important considerations, rather than just looking at the overall mixing time [215].

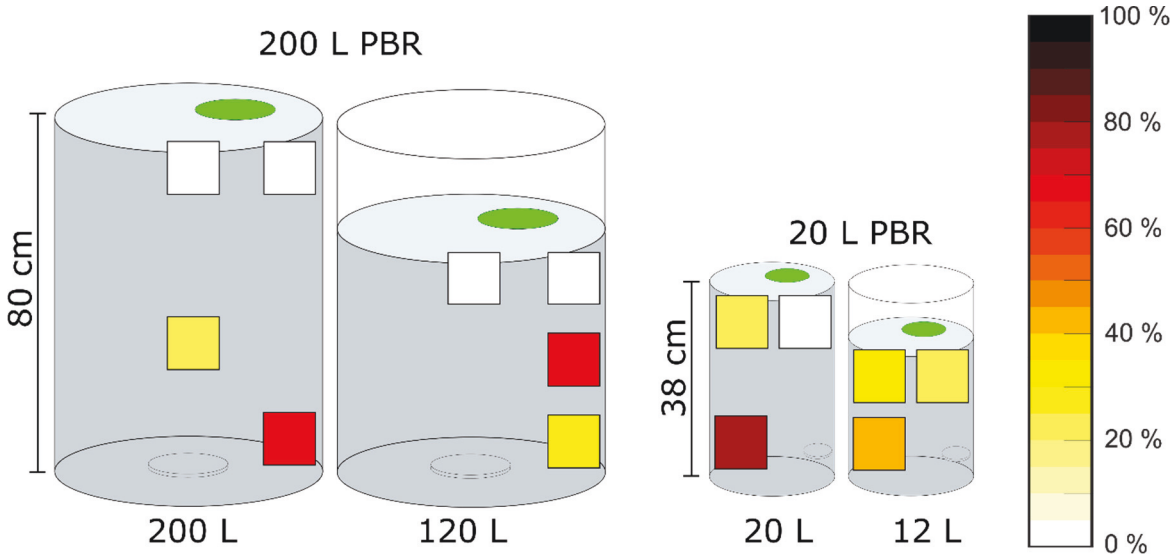

Figure 3-6: Heat map of the sensor position highlighting how often sensors measure a delayed equilibrium, shown for the 200 L and 20 LPBR with different fill volumes. Squares represent the sensor positions with colouring that represent the percentage of delayed sensor reads for all tested aeration rates (normalized with the maximum sample size 200 L PBR n = 33, and 20 L PBR n=18). Injection position displayed as green circle.

The dye method showed higher precision than the pH-method, reflected in the smaller standard deviation (Figure 3-7). The 200 L fill volume demonstrated an increased mixing time for the reduced aeration rates. This effect can be explained with the changing ratio of volume to pneumatic power input [83], a phenomenon also observed with the mass transfer measurements. When the aeration input was reduced, liquid velocity decreases which extends the mixing time [216]. This also explains the improved mixing time for lower aeration rates of the 120 L, compared to the 200 L fill volume. While the aeration input stays constant, the overall

liquid volume is reduced, hence liquid velocity increases. The mixing time of the 120 L does increase only with the lowest aeration rate, which could imply that the mixing time reached the maximum possible for that sparger system and size, and the increase of aeration rate above 6 L/min can not improve the mixing time. The 20 L PBR exhibited a mixing time of 10 s, around twice as fast as the 200 L PBR. This could be caused by the asymmetrical positioning of the sparger system that supports a more stable flow pattern of rising and down-coming zones (similar to an airlift system). Another explanation could be the higher exhaust velocity of the sparger. While the 200 L PBR uses 8 sparger units that inject, in the best case, 1 L/min air per unit, the 20 L PBR depends on a single sparger that injects 2 L/min. Measurements with the dye-method found a mixing time of approximately 10 - 20 s for the 200 L PBR which is similar to the mixing time achieved with 350 rpm impeller in the Xcellerex. The results of the pH- and dye methods suggest that the optimization platform realizes similar mixing times under aerated-only operation than the industrial Xcellerex system.

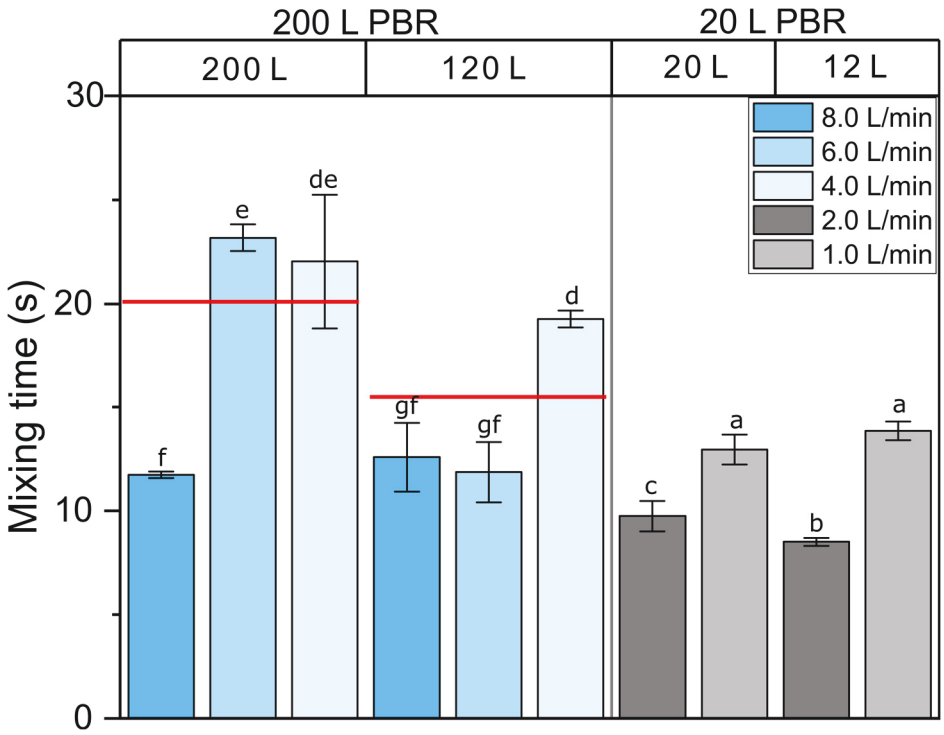

Figure 3-7: Mixing time measured with the dye-method for PBR. 200 L PBR in blue with fill volumes of 200 L and 120 L and different aerations. 20 L PBR in grey with fill volumes of 20 L and 12 L and different aerations. Red lines show the Xcellerex setup, impeller speed 350 rpm for comparison. Data are mean ± SD ($n \geq 3$). The letters in columns indicate the statistical differences of the results as a grouping, statistical comparison was done for the 200 L PBR with both fill volume together with the 20 L PBR with both fill volumes.

Both methods yielded different results, a consequence that was discussed by Ascanio (2015) and relates to the different operational modes of the two methods [217]. The pH-measurement is of an intrusive nature; the introduced pH-probes can interfere with the initial hydrodynamic flow and thereby create flow patterns that do not reflect the real circumstances of the PBR [218]. This effect particularly applies to smaller volumes (e.g., 20 L PBR), in which the interference is magnified. Another influence on the measurements might be the interaction of the probe with the media. The pH-method is an indirect measurement technique of the mixing time since it depends on probes that experience reaction delays due to physical or chemical reaction steps. These effects can negatively impact the precision of the measurement. On the other hand, the dye-method is a non-intrinsic method so, unlike the pH-method, the hydrodynamic flow is not influenced. Moreover, this method can directly observe the mixing induced colour change in the PBR, and coupled with a camera system, the colouring progress can be digitally analysed, potentially explaining the more precise measurements found with this method. Interestingly, the pH method gives insights into potential laminar flow regimes of the PBR, that will be further examined in the hydrodynamic flow pattern analysis (section 3.3.3). The dye-method can potentially also be used to identify laminar regions in the PBR, however, to precisely observe the colour changes in the reactor vessel several cameras would need to be utilized covering the front, side and top of the PBR.

3.3.3 Particle tracing

Mixing time provides an overview of the total mixing capability of the bioreactor, but does not give detailed information about the hydrodynamic flow patterns. As the mixing time experiments indicated, there might be different flow regimes within the two bioreactors. A particle tracing method was employed in order to further analyse these zones. Information about the flow patterns are valuable in order to identify laminar flow regions, in which the low fluid velocity could potentially promote substrate limitation or cell accumulation. Additionally, flow pattern obtained with the particle tracing method can be combined with light maps of the bioreactor - heat maps for PAR intensity - to estimate the light history (light exposure) of microalgae cells [153] (Chapter 4).

The principle of the method is simple: a buoyant particle (alginate sphere) is carried by the current in the liquid media of the bioreactor, while cameras record the movement of the particle from different angles. The recordings are synchronised and reconstructed into a three-dimensional particle movement. The data are presented in different ways, highlighting specific

characteristics of the PBR. The three-dimensional visualization of the trajectory, particle and speed maps are each useful for the optimization of design changes of the PBR.

The trajectory map (Figure 3-8) draws a travelling path within the bioreactor, allowing for the identification of the overall flow pattern and estimations about the circulation time. Riser and downcomer zones, as well as consistent flow patterns in the PBR can be identified. This visualization method additionally enabled the management of the underlying particle tracing data to screen for potential errors; recurring reflections can be identified and adjustments in the particle identification can be made in order to exclude them. Figure 3-8 shows a representative travelling path within the bioreactor for 44s duration (although it should be noted that the displayed time lapse is not sufficient to make estimations about the overall particle trajectory). Analysis of longer periods showed that for the 200 L PBR, with its central sparging disk on the bottom, the particle is carried with the rising bubbles in the centre of the PBR and then travels down along the side walls (data not shown). The 20 L PBR with its sparging stone closer to the wall, demonstrates a similar behaviour, where the sphere is agitated by the rising bubbles and then moves down along the opposing walls. This flow pattern is more distinct than in the 200 L PBR, as it has a more clearly riser (sparging unit) and downcomer (opposing side wall) region that creates a clear vertically circulating flow path for the liquid. The downcomer regions of the 200 L PBR at the side walls are more chaotic, with more random movement along the side and radial into the PBR, which can affect the particle velocity and will be further analysed in the speed maps.

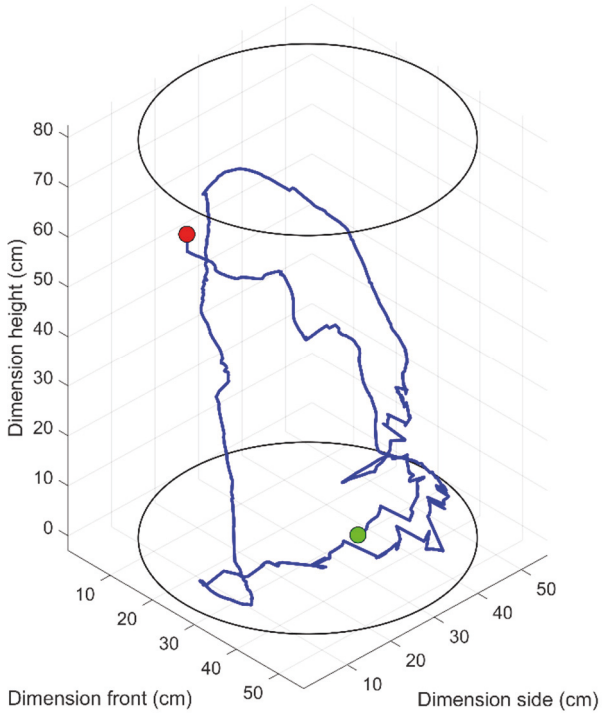

Figure 3-8: Three-dimensional visualization of the particle trajectory for the 200 L PBR with an aeration rate of 8 L/min, with a tracing duration of 44 s. Blue trace marks movement of the particle. Circles at the top and the bottom recreate the perimeter of the PBR. Green dot marks the start of the particle movement, while red indicates the end.

3.3.3.1 3D particle and speed maps

Three-dimensional particle and speed maps allow for the visual analysis of various hydrodynamic zones within the PBR. These maps ignore the particle trajectory, but instead cluster particle position and velocity in order to highlight certain areas with high particle presence or increased velocity. High particle presence in a certain areas can indicate areas of frequent particle flow or low hydrodynamic flow areas in which the particle remains longer. When related to the speed maps, these areas can be characterized, where reduced particle occurrence with high velocity can indicate a turbulent area, whereas high particle occurrence with low velocity imply a laminar flow area. For visualization purposes, Figure 3-9 A shows such a representative three-dimensional particle map of the 200 L PBR, while Figure 3-9 B shows the correlated velocity map. Comparing both maps, the bottom area shows higher particle occurrence, but not a high velocity, which could imply a laminar flow zone at the bottom region of the PBR. In contrast, the upper part of the PBR shows higher velocity and low particle presence, indicating it as a turbulent area.

A) B)

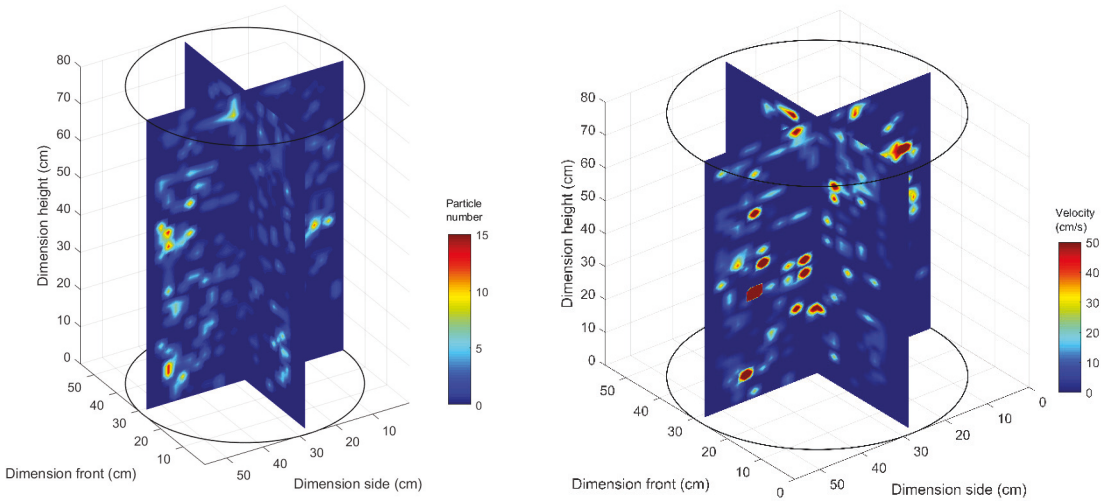

Figure 3-9: Three-dimensional visualization of A) the particle presence and B) the particle velocity in the 200 L PBR with an 8L/min aeration rate. Cross sections were created in the particle volume at the front and at the side at 28 cm (vessel centre) which highlight high particle densities and velocity. Circles at the top and the bottom recreate the perimeter of the PBR. Data represents 10 minutes sampling time.

3.3.3.2 Statistical analysis of different PBR heights

Particle and speed maps allow for the statistical analysis of data, in order to compare different experimental setups and their impact on the flow patterns within the PBRs. This analysis was done with different fill volumes within the PBR as the observed laminar flow area in the lower part of the PBR might change with different experimental settings. One approach is to look at the different layers of the PBR according to the axial position (height). Figure 3-10 shows the normalized particle occurrence in the different height layers of the 200 L PBR. The lowest aeration rate (4 L/min) for the 200 L PBR with 200 L fill volume did not yield usable results, as the sphere tended to sediment in the bottom area of the PBR. This would suggest that this aeration rate was not sufficient to keep the sphere constantly in motion. The setup with 120 L fill volume could be operated with 4 L /min aeration, implying that the lower volume supports the flow pattern by reducing the travelling time and thereby the velocity of the liquid. This effect was already observed in the mixing time experiments, where the reduced fill volume led to an improved mixing time. Both fill volumes showed an even distribution of the particle across all heights with higher aeration rates; however, the lowest aeration rates for both fill volumes (5 L/min for 200 L and 4 L/min for 120 L) exhibit an increased occurrence of particles in the lower part of the PBR. These aeration rates could indicate a threshold at which the mixing

flow is not strong enough to move the particle efficiently out of the lower PBR regions, which potentially signifies an increase of the laminar flow areas at the bottom with reduced mixing.

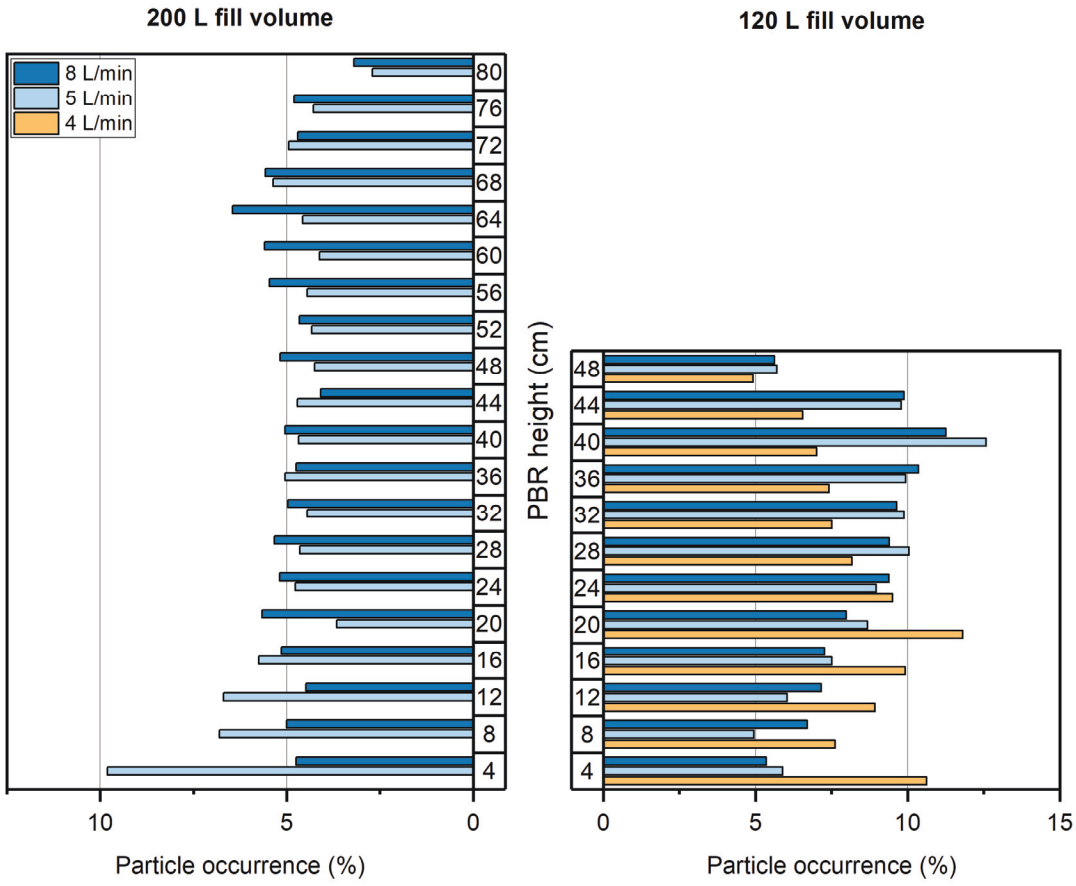

Figure 3-10: Particle presence of different height layers in the 200 L PBR with fill volumes of 200 L and 120 L. Height layer thickness is 4 cm. Shown are the particle occurrence normalized with the maximum particle presence for aeration rates of 5 and 8 L/min for both fill volumes and additionally the 4 L/min for 120 L fill volume (lowest measured aeration). Results based on at least 30 min of recording.

From the velocity analysis (Figure 3-11), an overall lower particle velocity can be observed in the lower zones of the PBR for all setups, which indicates a laminar flow area in that region. This confirms the observations made with the pH-measurements, that showed a delayed reaction of sensors close to the bottom (Figure 3-6). Regions further up in the PBR experience a gradual increase in velocity and can reach an average speed of 18 cm/s (0.18 m/s). The aeration rate seemingly does not greatly impact the velocity, as median and mean for the aeration rate are mostly similar in each layer. These results correlate with the mixing time observations that did not show distinct differences with changes in aeration. This could indicate that high circulation times could be reached with low aeration rates, which could enable a reactor

operating with a lower power input. However, the mass transfer is highly dependent on the aeration rate, and cultivation with high cell density might suffer from CO_2 limitation with lower aeration rates. As such the aeration rate would need to be dynamically adjusted in accordance to the CO_2 requirements of the culture in order sufficiently supply CO_2.

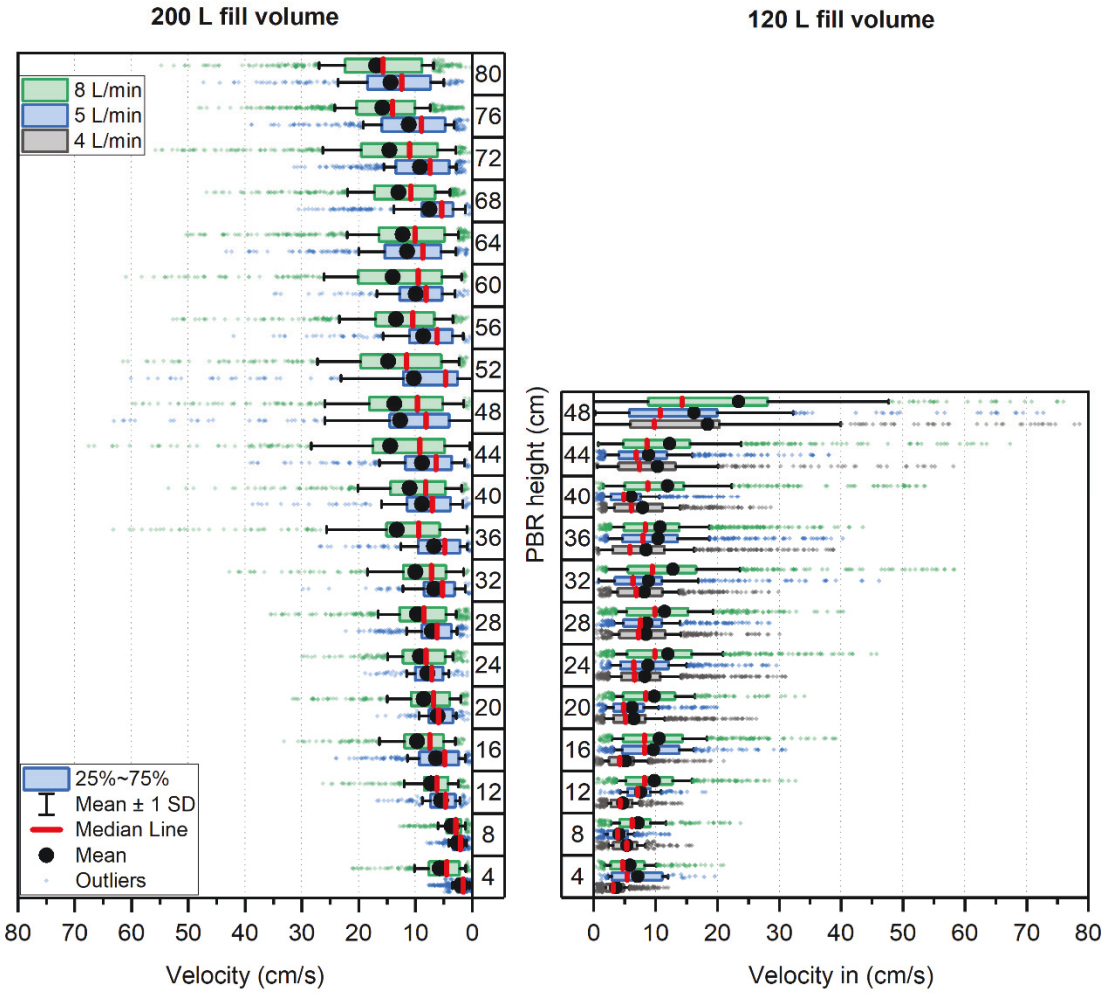

Figure 3-11: Particle velocity of different height layers in the 200 L PBR with fill volumes of 200 L and 120 L. Height layer thickness is 4 cm. Shown are the mean particle velocity (black dot) of 5 and 8 L/min aeration rate for each height layer, and sample distribution in form of median (red) and the interquartile range (25% - 75%). Additionally, the 4 L/min for 120 L fill volume (lowest measured aeration) is displayed. Error bars show the standard deviation with outliers marked as dots beyond the error bars. Results based on at least 30 min of recording.

Particle distribution within the 20 L PBR (Figure 3-12) shows an increased occurrence of the particle in higher regions of the PBR; however, the impact of the aeration rate seems to be minor for this setup, as the distribution is similar of all aeration rates. Unlike the 200 L system,

the three aeration rates (1, 1.5, 2 L/min) applied in the 20 L created a similar particle distribution in the PBR (data of 1.5 L/min not shown). The lack of particles found in the lowest region of the PBR for lower aeration rates could be explained with the vertical circulation of the liquid, induced by the sparging position on the side wall of the PBR. This sparger position could create a more clear riser and downcomer section, as seen in other airlift PBRs [219], a theory supported by the enhanced mixing time measurements of the 20 L PBR. Other reasons for the minor impact of aeration on zonal distribution could be the relatively high aeration rate to begin with, as it was 2.5 times higher than the 200 L PBR aeration, as well as the physical differences in the sparging systems. A single sparging unit reaches the aeration rate of 1 L/min in the 200 L PBR, while the 20 L PBR operates with an aeration rate of 2 L/min with the single sparging unit. This results in a higher aeration velocity in the 20 L PBR, which translates into a higher liquid velocity [220]. This could suffice to induce a turbulent flow even for the lowest tested aeration rates, while the flow with the lowest aeration within the 200 L PBR creates local laminar flow zones.

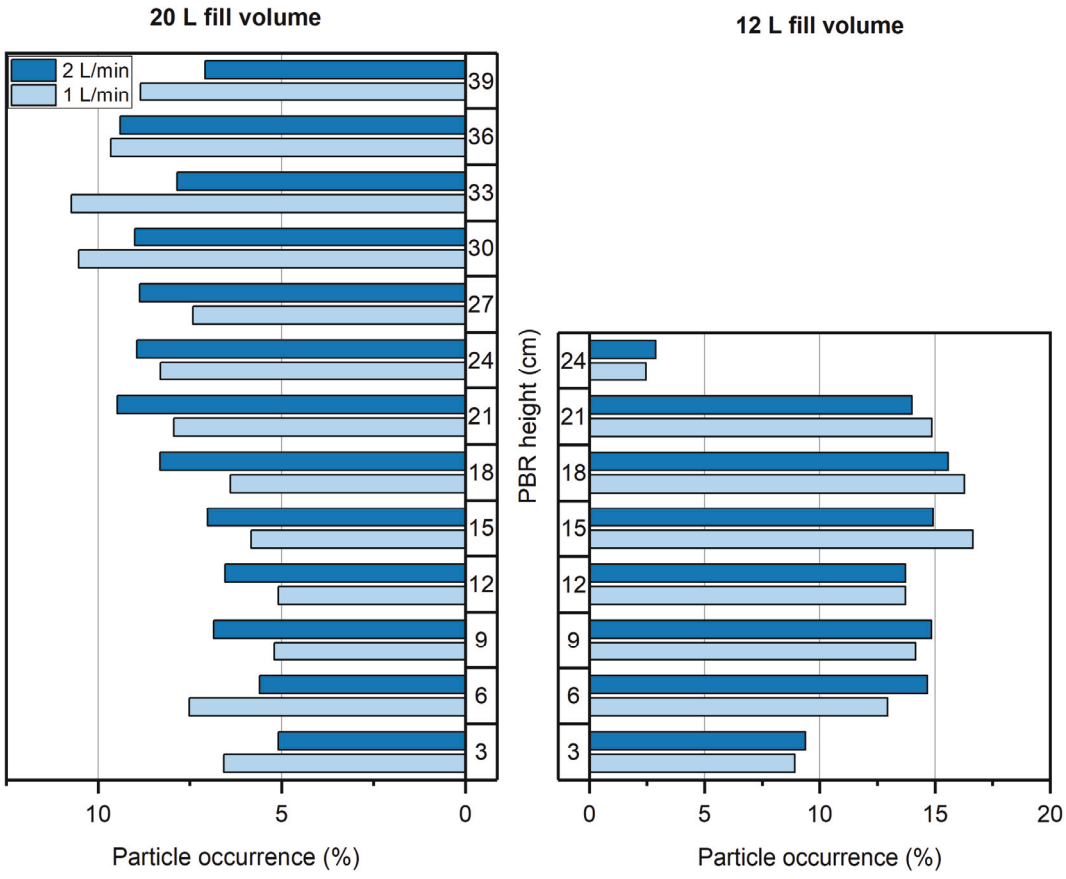

Figure 3-12: Particle presence of different height layers in the 20 L PBR with fill volumes of 20 L and 12 L. Height layer thickness is 3 cm. Shown are the particle occurrence normalized with the maximum particle presence for aeration rates of 1 and 2 L/min in both fill volumes. Results based on at least 30 min of recording.

Velocity measurements in the 20 L PBR (Figure 3-13) support the suggestion of the improved hydrodynamic flow in the scaled bioreactor. The maximum velocity in all horizontal slices, except the top slice, are comparable, suggesting a relatively consistent flow velocity. The top slice demonstrates a rise in velocity, that is correlated with the aeration rate. It is unclear if an actual increase of velocity at the surface was present, and if it can be related to the higher gas velocity, or if it is due to reflections of the bubbles that are misinterpreted as particle movement. With increased aeration, these artifacts could accumulate with bubble number and seemingly increase the average velocity. However, potential interactions of the bubbles with the surface, such as bursting and the spreading along the surface, could also lead to locally high velocities. The different fill volumes seemingly have no large impact on the particle distribution or the velocity in the PBR. In contrast to the 200 L PBR, the 20 L PBR setup creates a better flow pattern. As such, additional adjustments to the sparging system are needed, with the sparging system centred in the PBR and an enlarged sparging area (reduction of gas velocity). This might increase the mixing time and could produce a more equivalent mixing pattern in the scaled-down system.

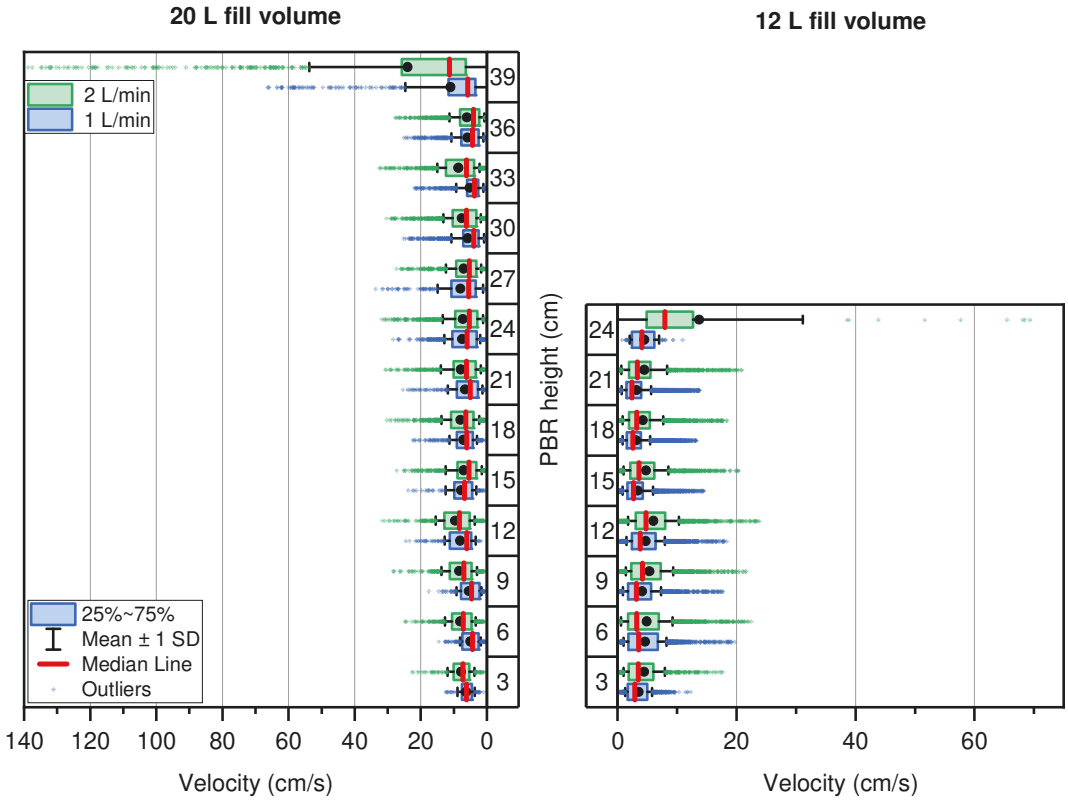

Figure 3-13: Particle velocity of different height layers in the 20 L PBR with fill volumes of 20 L and 12 L. Height layer thickness is 3 cm. Shown are the mean particle velocity (black dot) of 1 and 2 L/min aeration rate for each height layer, and sample distribution in form of median (red) and the interquartile range (25% - 75%). Error bars show the standard deviation with outliers marked as dots beyond the error bars. Results based on at least 30 min of recording.

3.3.3.3 Method evaluation

In order to evaluate the performance of the particle tracing method, the occurrence of three particle detection cases were compared, with: 1), sphere visualised with both cameras, 2) visualised with only one camera, and 3), no visual with either camera. Ideally, mainly case 1 and case 2 should be observed. Figure 3-14 shows that the detection rate for at least one camera is around 50% with the 200 L PBR experiments and around 60% for the 20 L PBR. The 200 L PBR shows a lower rate for case 1 (~10%), which can be explained by the limited coverage of the PBR with two cameras, while the detection rate of the sphere with both cameras for the 20 L PBR is around twice that than observed with the 200L. However, the complete disappearance of the particle for longer than 0.5 s contributes only 5% to the overall recording, which means that around 90% of case 3 instances are shorter than 0.5 s. As such, the method can be used to recreate the flow part of the alginate sphere.

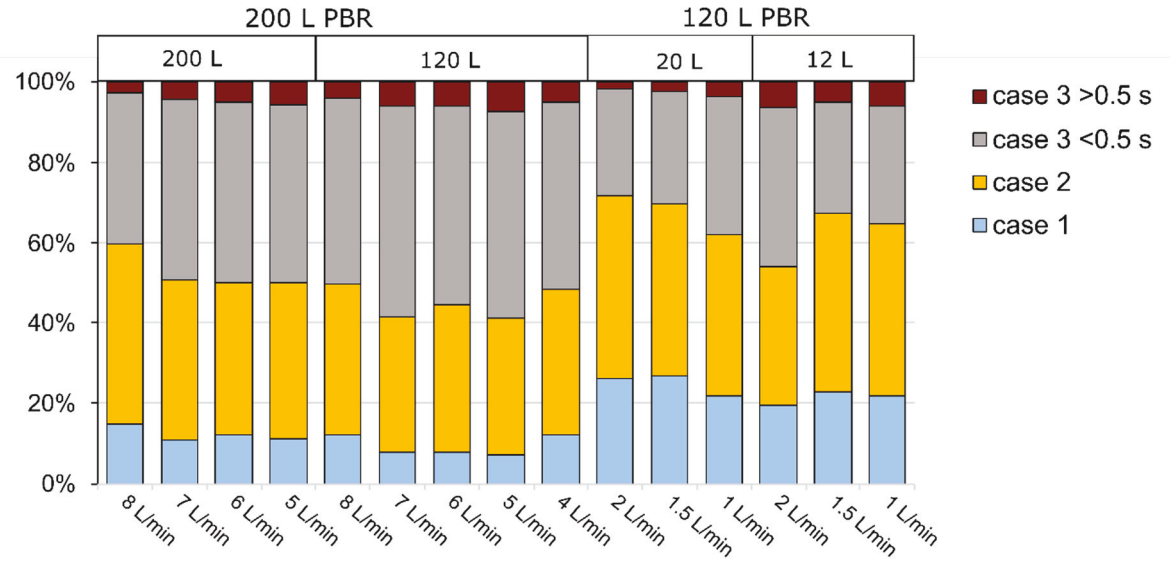

Figure 3-14: Method evaluation of the particle tracing method. Comparison of the occurrence of the three cases. Case 1, both cameras detect the particle. Case 2, only one camera detects the particle. Case 3, neither camera detects the particle. Case 3 were analysed for the duration of particle disappearance and were separately displayed (shorter than 0.5 s and longer than 0.5 s). Data shown was normalized by maximum recording duration for different PBRs, fill volumes, and aeration rate.

3.3.3.4 Method challenges and further improvements

The method has been demonstrated in laboratory-scale [153] with a 3.7 L airlift PBR, though in order to apply the method on the 200 L PBR and 20 L PBR, several challenges had to be overcome. One challenge was posed by the external wire frame of the PBR. This frame is necessary to provide support to the bag, but the plastic bag within it curved under the water pressures and formed lens like shapes with unfavourable optical distortions. These distortions led to reflections, and generated an effect where the alginate sphere seemingly disappeared. The impact of the bag deformation could have been minimized by using a transparent hard plastic layer between the PBR metal frame and the bag or by replacing the wire frame with a glass or plastic cylinder entirely. However, these approaches were not applied due to their impact on the geometry and the corresponding hydrodynamic properties. The bending of the bag generates a unique flow pattern that can also be found within the original single-use Xcellerex system. The size of the 200 L PBR provided an additional challenge, as there was limited visual coverage of the alginate sphere with just two cameras. For alginate spheres travelling close to the wall, the anticipated two camera setup – positioned frontal and lateral to the PBR – occasionally resulted in the loss of the particle from view. However, these tracing difficulties can potentially be reduced for future applications by including additional cameras, covering more angles of the bioreactor.

Another potential improvement is the conversion step of pixel dimension into physical dimensions. These are currently done for each camera perspective individually (two-dimensional), which ignores the effect of the common perspective distortion of the camera lens [221]. This simplification introduced a certain error depending on the position of the fluorescence marker. Positions further from the image centre suffer a stronger distortion, which is especially true for enlarged objects such as the 200 L PBR in which the furthermost positions reached deviations of up to 3 cm. A more precise approach would be a calibration step with three-dimensional coordinates. Both cameras would need to be synchronised for each calibration position in order to obtain the three-dimensional coordinates of the calibration marker. Thereby the position of the marker could be more precisely identified, even in positions further away from the cameras.

The method also has certain limitations related to the physical properties of the alginate sphere. The alginate sphere does not have the same characteristics as a microalgal cell and could exhibit stronger sedimentation effects in these laminar zones. The density of the sphere was slightly higher than the surrounding liquid, which promotes sedimentation. Increased dimensions of the particle, which are magnitudes higher in size and mass than microalgae, also impact the inertia and the friction forces of the sphere. This makes vector changes imposed by the current more sluggish, and smaller currents suffer from interference by the sphere while travelling through them. These differences in flow behaviour can impact the flow path reconstruction of eddies in the laminar flow areas; however, strong currents in the turbulent (riser and downcomer) areas of the PBR are profiled accurately with the sphere (Figure 3-8). Adjustments on the sphere dimensions can improve this flow behaviour; however, reduction in size also hinders the detectability of the sphere for the cameras. Therefore, a balance for the fluorescence marker was found at with 0.5 cm diameter. This data can therefore give the general path and flow within the PBR, but further refinement may be necessary, e.g. through computational fluid dynamics (CFD) models. These models can easily trace the particle movements of a digital reactor system, yet empirical hydrodynamic flow measurements are still needed to validate the system [222].

3.4 Conclusion

The applicability of the optimization platform depends on the similarity of certain characteristics to the industrial bioreactor. CO_2 and light are of utmost importance for micro-algae to grow. Hence, mass transfer and cell exposure to light are of considerable relevance for the PBR design and optimization.

The results of the mass transfer and the mixing time measurements indicate that similar operational conditions to the Xcellerex were achieved. Mixing was achieved exclusively via aeration (compared to the Xcellerex impeller), therefore the current setup is more energy efficient and should create less shear stress on the cells. However, the observed laminar zones at the bottom of the PBR shows that mixing supported by an impeller might be needed. The down-scaling part of the optimization platform works as intended with mostly similar results for mass transfer and mixing time. Future growth experiments with various algae species using the 200 L and the 20 L PBR will show if the growth behaviour are reproducible in both scales.

The pH-method for the mixing time proved to be challenging due to technical limitations of the methodology; however, it gives an approximate view of the flow behaviour within the reactor vessel. The optical dye method presents a valuable addition to the pH-method, as it seems to be more precise by using direct measurements, and also shares the same overall hard-ware setup as the particle tracing measurements. The particle tracing method was successfully adapted to fit the 200 L PBR. The method proved to be an excellent tool to describe and analyse the flow current in the PBR. It is possible to see high particle residence areas and collect velocity readings for different areas in the PBRs. Future work should focus on optimizing the alginate sphere by reducing the diameter and increasing the quality of the fluorescence material. This would improve the flow behaviour of the particle in laminar zones and increase the emitted fluorescence, thus improved detectability. Additional cameras in the setup will also provide a better coverage of the PBRs and thereby improve the tracing. This particle history in the PBRs can be used to calculate the light exposure of the culture, and thereby facilitate the optimization of the light system and the mixing pattern (Chapter 4). With the given methodology, it was possible to verify the optimization platform while additionally collecting flow data that will enable the calculation of light exposure. Changes in the PBR setup can be tested easily and the impact on CO_2 supply, mixing and hydrodynamic flow can be validated.

Chapter 4
Calculation of optimal LED arrangement for the photo-bioreactor illumination

Author Contributions

Julian R. Kofler designed and performed all experiments and wrote the manuscript. Leen Labeeuw advised, supported the experiments, and assisted in writing. Peter J. Ralph advised, materially supported experiments, and assisted in writing.

4.1 Introduction

Photons are an essential source of energy for phototropic organisms; in order to achieve unrestricted growth of algae in a photo-bioreactors (PBR) systems, a suitable and sufficient light supply has to be provided. The adequate supply of light can be challenging as light attenuation dramatically increases with increasing depth into the bioreactor vessel [133], especially when operated at high cell concentrations. As such, the distribution of light is a crucial factor in determining the performance of a PBR. The illumination source of a PBR should not be quantified simply by its capacity to introduce photons into the culture, but by the actual irradiance it provides to the cells. For example, PBRs with intense light input and insufficient mixing will expose cells that are close to the light source with high photon intensities for an extended time; algae cells in these regions might suffer from photoinhibition, while cells further from the light sources experience photon starvation [223]. Photoinhibition occurs when photon intensity reaches a harmful level for the cell, which is revealed by reduced cell growth and can even lead to cell death. On the other hand, photon starvation can occur after extended periods in light undersaturated regions of the PBR, which equally diminishes growth. Irradiance values used in laboratory scale cultivation systems vary wildly and depend on the algae species and the cultivation condition. Typically, the photosynthetic photon flux density (PPFD) range for algae can be defined between 15 and 400 µmol m^{-2} s^{-1} [224][134][175] – yet clearly these values are exceeded (up to 2000 µmol m^{-2} s^{-1} [225]) with outdoor cultivations recieving direct irradiation by sunlight [226]. There is no consistent value at which photoinhibition limits culture growth, as it is dependent upon numerous factors, such as algal species, wavelength, exposure time and culture conditions, e.g. temperature and media composition [227]. As such, preventing photoinhibition has to be evaluated based on the individual cultivation system and growth conditions.

Optimized PBR systems should minimize light stress to the cells, for instance by applying adequate mixing in order to transport algal cells with a higher frequency through the different light zones in the PBR, thereby creating temporal variation of PPFD exposure; this effect also distributes the photons across a greater volume of the culture. This optimized flow design could additionally improve growth by inducing the “flashing light effect” to the cells [228][229]. In this phenomenon, the cell is exposed to a high frequency of dark and light (D/L) intervals. In the illuminated phase, the photosynthetic apparatus is saturated with photons, while the dark phase provides time to process the photons and repair photodamage to the cell [230]. The frequency of the dark and light phases offers a range of beneficial effects. The duration of these

dark and light periods vary for different species [228][134], whilst some species do not show a positive impact from D/L frequency at all [231]. The ability of pneumatic mixing to create a flashing light effect remaining a topic of debate [232][233]. A beneficial impact on growth was observed for *Chlorella vulgaris* in a flat panel PBR designed to maximize the flashing light effect on the culture [234]. Vertical baffles redirected rising bubbles which created turbulences that moved the algae cells in front of the illuminated surface and then subsequently further back into the darker areas of the PBR. This created a D/L frequency of around 1 Hz. In comparison, another study could not observe a positive influence of the flashing light effect while mixing *Chlamydomonas reinhardtii* in a bubble column PBR (1 L) [233], but noted an improved growth with artificially induced D/L frequency that was higher than 50 Hz using flashing LEDs. This suggests that the mixing capability of that particular PBR did not reach a sufficiently high frequency D/L cycle to create a beneficial effect. This highlights the difficulty in achieving this effect solely by mixing, as it is highly dependent on the PBR design, type of mixing and the illumination setup. Using mixing alone, D/L frequencies range from 0.1 Hz in airlift PBRs (100 mL) [235] to 5 Hz for flat-panel PBR (2.5 L) [236], and were even calculated up to 4-22 Hz in a static mixer unit of a tubular bioreactor [237]. However, all these described cases operated with a homogenously illuminated surface (e.g., illumination along the entire surface of the PBR), hence with a photic volume close to the PBR wall and a clearly separated dark zone further inside the PBR. This uniform light attenuation across the illuminated surface (i.e., side walls) means that the culture is constantly exposed to light, while travelling close to the side walls and is in the dark when further from the walls. In the case of an airlift PBR, this light profile can create a D/L cycle of 1 – 100 s, as the culture circles from the dark drafting tube (riser area) through the illuminated peripheral regions (downcomer section) of the PBR [85]. This does not reflect the actual light profile of an artificially illuminated PBR system, in which light is emitted by small point sources with a conical shape (e.g., LEDs). This complex light pattern establishes an illuminated surface with high and low photosynthetic photon flux (PPF) zones close to the illuminated surface, leading to distinct fluctuations in PPFD for cells migrating through these various zones. This specific light pattern could enhance the D/L frequency of cells moving through these zones. Additionally, the utilization of artificial illumination could allow for the application of the flashing light effect by manipulating the operational mode of the light sources [238]. In knowing the retention time and the flow pattern of the cells, the PPFD experienced by cells travelling through the light profile of the PBR can be adjusted by controlling the light intensity and frequency of the light source. This allows for

the adjustment of the illumination setup and the creation of a defined PPFD via light pulses in certain PBR regions.

In recent decades, computer simulations have been increasingly used in the design and optimization of PBRs. Moving optimization steps from real PBRs to simulated ones can save time and effort [239]. Structural changes can rapidly be simulated, and the most promising results can be transferred onto the physical test system. However, for the simulation to be precise, the model depends on accurate input data to build upon [240]. This input can be calculated, based on formulas that describe a physical phenomenon, or from experimentally derived data, and enables the simulation of certain parameters such as mass transfer, hydrodynamics and light exposure; even biological parameters such as growth rate can be predicted with sufficient data [241][242][225].

Light exposure simulations are usually based on two datasets: the fluid dynamics, and the light attenuation, both obtained either numerically or empirically. An *in-silico* approach was used to evaluate the light exposure of a helical tube mixer for a tubular PBR [237]. In this study, a hydrodynamical single-phase (liquid only, so no gas phase present) simulation contributed the data of particle/cell trajectory, while the light attenuation was calculated with a hyperbolic light model (light intensity as a function of cell concentration and light path [243]), which enabled the calculation of the theoretical light history of a cell. Once established and proven, the model can be used to easily calculate physical parameters (e.g., light attenuation), enabling the rapid generation of data in various scenarios, thereby replacing the need for extensive real-world experiments. However, there are currently limitations in the complexity available in simulated PBR systems. This can include complex PBR geometry and the variable biological elements, such as the microalgae and their light absorbing properties that are dependent on culture health, culture conditions, and acclimatisation to various light intensities and wavelengths [157]. Simplifications such as homogenously illuminated surfaces can be applied in order to reduce the complexity of the simulation; however, these might reduce the accuracy of models [242]. An empirical approach to the light exposure was reported with a 3.7 L airlift PBR [153]. The hydrodynamic flow pattern of this PBR was mapped by tracing an alginate sphere with a camera setup, thereby revealing the particle trajectory. The light distribution in the PBR was mapped manually by measuring the PPFD (using spherical PAR sensors) at different locations inside the vessel. This method calculated the PPFD entirely based on empirical data, yielding more realistic results. However, using this approach, measurements of light attenuation have to be conducted for each species, each cell concentration, each

illumination settings, and with each PBR scale independently, rendering this approach more labour-intensive and impractical.

As part of a project to convert a bioreactor into a PBR, this chapter focuses on the optimal LED configuration for the efficient light supply into the PBR. As such, an algorithm was developed to model the LED light distribution across the PBR and identify the optimal positioning, based on the ideal PPFD and the D/L frequency. This computer aided design (CAD) relies on empirical data for light distribution (light maps, Chapter 2) and hydrodynamic flow (particle trajectory, Chapter 3). The light maps are a more accurate approach than the mathematical model and are easier to generate than most empirical methods, especially for complex optical PBR geometries and illumination systems. The Direct Chlorophyll Fluorescence Imaging (DCFI) method was designed to generate high resolution irradiance maps that can contour the light attenuation profile of artificial light sources such as LEDs. In this chapter, these light maps are converted into three dimensional volumes replicating the volumetric PPFD in the culture media. These LED volumes are arranged to maximize the PPFD supply of a defined intensity range. This arrangement was performed using two approaches: the static representation, by maximizing the PPFD area in the PBR (without accounting for how the particle moves), and the dynamic version, by calculating the optimal LED distance based on light history experienced by the particle as it moves through the PBR volume. Both approaches created an optimal LED configuration. The static approach started by creating the optimal LED configuration based on the ideal photic volume, and then using the particle trajectory data to calculate the light history of the particle (e.g., D/L frequency, time in illuminated zones). The dynamic approach used the particle trajectory and light history of the particle to then calculate the optimal LED configuration. This chapter established a versatile CAD process to optimize LED distribution based on the analysis of dynamic light characteristics. As such, the CAD can be utilized to design individually fitted LED configuration for a variety of PBR systems.

4.2 Method

4.2.1 Source of data

4.2.1.1 Experimental particle tracing

Empirical particle tracing data from Chapter 3 were used for the 200 L PBR with aeration rates of 4 and 8 L/min and the 20 L PBR with aeration rates of 1 and 2 L/min. The data were generated by tracing an alginate sphere with a two-camera setup. Missing particle coordinates

of one camera were interpolated to provide a complete dataset, so data obtained by both or a single camera were used for the light exposure calculation (case 1 and 2). As such, there were instances when the particle was not visible to either camera (case 3), which resulted in a partially reconstructed particle trajectory.

4.2.1.2 Light maps

Light maps generated with the DCFI method (Chapter 2), reflect the light behaviour of different coloured LEDs with *Phaeodactylum tricornutum* and *Chlorella vulgaris* at different cell concentrations (Table 4-1). The light maps show the complex light profile of the LEDs, including potential reflections of the PBR, as PPFD values for each image pixel. Light maps based on the top view were used as they show the distinct shape of the light profile of the LED penetration into the culture. Since the light maps have a high resolution (84 pixel/cm for the top view), digital processing of them presented a challenge, as the size of the generated map would severely prolong the calculation time in MATLAB (R2019a, Update5, The MathWorks). As such, the light map resolution was reduced (bicubic) by the factor of ten. Details of the algal species can be found in section 2.2.2. Two cell concentrations from each species were analysed, which will be referred to as high and low cell concentration.

Table 4-1: List of light maps for different species and cell concentrations.

Species	Low cell concentration [cells/mL]	High cell concentration [cells/mL]	LEDs
P. tricornutum	2.02×10^6	5.87×10^6	Blue (450 nm), Red (670 nm), White (3997 K)
C. vulgaris	1.56×10^6	4.10×10^6	Blue (450 nm), Red (670 nm), White (3997 K)

4.2.2 Processing of particle exposure

4.2.2.1 Light map processing and LED arrangement

In the first step, the light maps showing the complete light profile of the LED were cropped along the centre line of the LED, leaving a bisected light profile (Figure 4-1 A). In order to use these maps for digital calculations they had to be converted into three-dimensional light volumes that contained the light intensity information of the LED. Therefore, the halved profile was extrapolated (nearest-neighbour) by revolving the two-dimensional image around the

central axis (MATLAB) (Figure 4-1 B). These steps were repeated for each light map with the different LED colours, cell densities and species (Table 4-1).

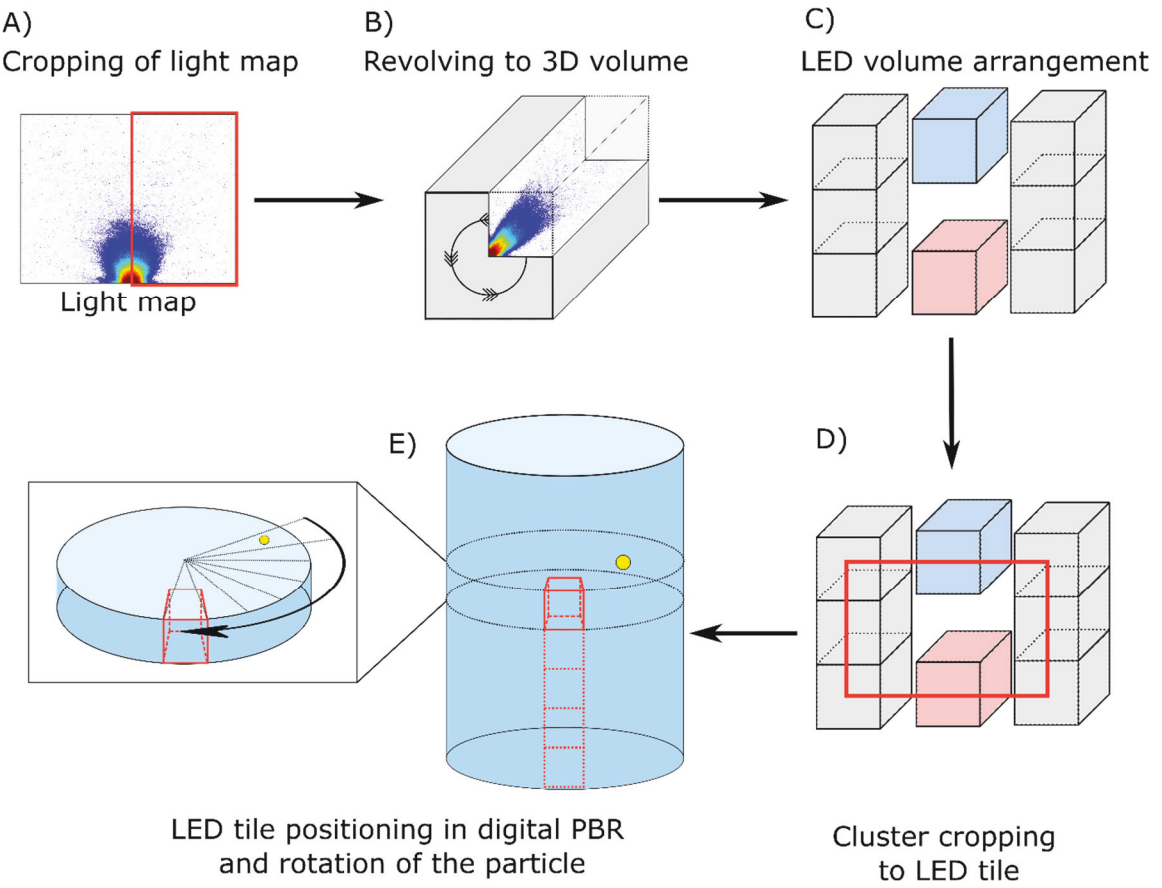

Figure 4-1: Flow diagram of the data processing for the particle exposure. A) Light map with the full cone of a single LED highlighting the cropped area, B) revolution of the cone around the central axis, C) shuffling of the LED volumes (white, red, and blue) and creation of a LED cluster, D) cropping of the LED cluster in order to create LED tile, and E) digital placement of a single LED tile in the PBR and rotation of the particle (yellow dot) to fit the illumination profile of the LED tile.

The LED volumes were then digitally arranged (Figure 4-1 C) by gradually moving them according to the spatial requirements of the static or the dynamic approach. Shuffling was initiated by stacking the LED volumes at the same initial position from which the volumes were pixelwise repositioning. The PPFD volumes contained the light intensity values, as such superimposed volumes contributed to the overall photon flux in that area and were summarized. For each LED position, the static and dynamic light parameter were calculated, based on these parameters the ideal LED configuration were determined. The digital LED arrangement followed a specific pattern, considering that the LEDs are commercially available in the form of LED strips – LED chips are mounted on a flexible circuit board. In order to comply with

these design requirements, two different strips were assumed for the digital volume arrangement (Figure 4-2): a white LED strip, consisting of only white LEDs and a blue/red LED strip, consisting of an alternating red and blue LED pattern. The white LEDs moved stepwise along the theoretical strip away from each other. This movement was restricted to have an equal distancing between each LED. The blue and red LEDs were moved unrestricted along the blue/red LED strip, so the LEDs were freely relocated on the strip. Both strips were placed vertically along the side wall of the cylindrical PBR system. While the white LED strip was locked at the initial position, the blue/red strip was stepwise moved along the theorical periphery of the bioreactor away from the white LED strip. To account for the circular geometry of the PBR, the blue/red LED strip was additionally rotated according to the curvature of the reactor side walls. The stepwise movement of the white LEDs and the blue/red strip were synchronised, so any increase of white LED distancing led to the relocation of the blue/red strip. For each relocation of the blue/red strip, the blue and red LEDs were moved independently along their strip. The stepwise movement was conducted for the distancing between both strips, the white LEDs and the blue and red LEDs, independently.

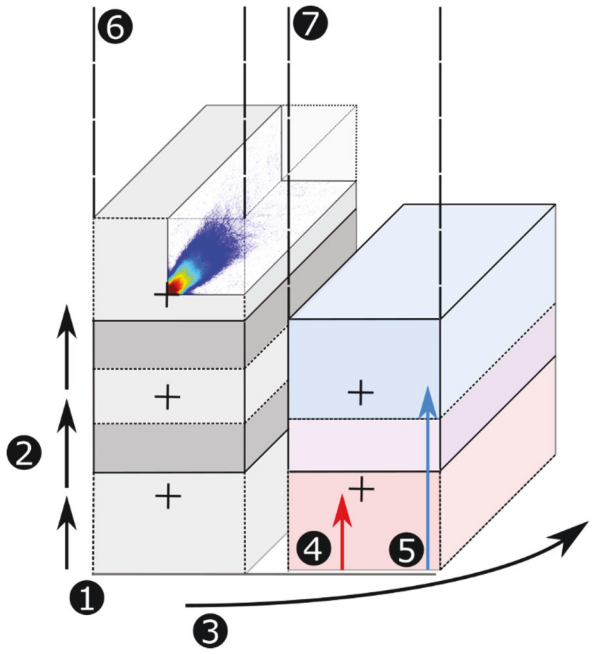

Figure 4-2: Arrangement pattern of LED volumes. Grey, blue and red cubes represent white, blue and red LEDs, respectively. Overlapping areas of the cubes are highlighted in darker colours and represent areas in which PPFD of the LEDs were summarized. The movement is shown, where there is the 1) initial position of the LED arrangement, 2) stepwise movement of the white LED volumes, 3) stepwise horizontal movement of the blue/red LED strip away from the initial position (synchronized with the white LED steps), additionally the LED volumes were rotated according to the curvature of the PBR geometry 4) movement of the red LED volume along the blue/red strip, and 5) movement of the blue LED volume along the blue/red strip, with the 6) theoretical white LED strip, and 7) theoretical blue/red LED strip.

4.2.2.2 Creating LED clusters and calculating particle exposure

In order to reduce computational requirements of the analysis, only a small representative set of LEDs were used in the arrangement process (< 16 LEDs). This LED cluster contained the PPFD values of the LED volumes and were further processed into what will be called LED tiles. These tiles were needed for the calculations of particle light exposure and frequency. To create these LED tiles, the LED cluster was symmetrically cropped in order to create a representative volume of the LED colours (Figure 4-1D). These tiles were created to be stackable, much like a mosaic, so arranging these tiles across the PBR could theoretically recreate the defined LED pattern. However, this would require the placing of numerous LED tiles with subsequent interpolation steps for the necessary rotations in order to fit the LED tiles according to the curvature of the digital PBR, which would require significant computing power. As such, computational requirements were kept to a minimum by using the lowest viable number of tiles that could still accurately be extrapolated to represent the entire PBR.

Different ways of calculating the light exposure of a particle were explored. Initial trials focused on the horizontal slicing of the PBR at the height at which the particle was positioned. These slices contained the correlated light profile of LEDs across the PBR side walls together with the particle position (Cartesian coordinates), thereby allowing for the identification of the estimated PPFD intensity at the particle position. However, this approach strongly relied on the rotation of the LED tiles in order to arrange them around the circular shape of the digital PBR, which introduced some imprecision due to the necessary interpolation and the need to correctly position the rotated light profile in the PBR matrix. Therefore, another approach was chosen to calculate the particle exposure. This method rotated the particle around the central axis of the cylindrical PBR and positioned it inside a single LED tile, which enabled the calculation of the particle exposure at this position (Figure 4-1E). This was done by converting the Cartesian system (x, y, z) of the particle position into polar coordinates (*rho*, *theta, z*) and adjusting the angle (*theta*) and the height (*z*) to fit the LED mosaic at this position. The adjusted polar positions were then re-transformed into Cartesian units and superimposed on the light intensity of LED tile. By placing only one tile in the PBR matrix, interpolation and complex digital volume alignments could be avoided.

4.2.3 Photic volume

Photic volume was calculated as an estimate of the illuminated liquid volume for the 20 and 200 L PBR. The photic volume was derived from the PPFD values of the LED tiles and the

total reactor volume. PPFD values above 15 µmol m^{-2} s^{-1} were defined as illuminated. Photic volume calculations were performed in MATLAB.

4.2.4 Calculation of D/L frequency

D/L Frequency was analysed using two methods: the calculation of the binary distribution [237][244], and the transformation of the light exposure using fast Fourier transformation (FFT) [237]. Both methods were evaluated for their ability to describe the D/L frequency induced by mixing and changing LED setup. Calculations were conducted using MATLAB.

4.2.4.1 Binary distribution

The binary distribution assessed the duration of the D/L cycle that the particle experienced. The particle light exposures were binarized such that light intensities below 15 µmol m^{-2} s^{-1} were assumed to be dark and given a value of zero, and intensities above that were defined as light and given a value of one. The durations of these flashing cycles (dark and light phases) were calculated and averaged. The mean D/L frequency was derived from the resulting time periods.

4.2.4.2 Fast Fourier Transformation

The oscillating light exposure (PPFD) of the moving particle were converted into a frequency spectrum using the FFT, an algorithm to compute the discrete Fourier transformant A_k of the signal sequence a_n [245]:

$$A_k = \sum_{n=0}^{N-1} e^{-i\frac{2\pi}{N}kn} a_n \qquad 4)$$

where k = 0…N-1 as the N_{th} roots of unity, N is the number of samples and n the time index. The FFT was calculated in MATLAB with a sampling interval of 50 samples per second.

4.2.5 Static and dynamic light exposure

The LED arrangement were validated by two different approaches. The static light exposure was utilized to maximise the distribution of a PPFD range between 15 and 400 µmol m^{-2} s^{-1}. PPFD below 15 µmol m^{-2} s^{-1} was considered as light limited [175] and values above 400 µmol m^{-2} s^{-1} as photo-inhibited [134]. The light distribution of the PPFD range was calcu-

lated for each LED configuration in order to find the configuration with the highest light characteristics (i.e. highest distribution of the PPFD range into the PBR). Different light intensity ranges were tested for a wider variety of irradiance maxima (200, 300 and 500 µmol m^{-2} s^{-1}), yet these threshold adjustments changed the distancing of the LED merely by a millimetre. As such the initial irradiance range of 15 - 400 µmol m^{-2} s^{-1} was used for all subsequent analysis.

The dynamic light exposure directly combined the LED arrangement with the particle trajectory to compute the particle light exposure. The LEDs were similarly shuffled as described for static light exposure (Figure 4-1 C), yet for the identification the optimal LED configuration, values of the mean D/L frequency (binary-method), the total PPFD experienced by the particle within the defined PPFD region, and the retention time of the particle in the defined PPFD region (15 - 400 µmol m^{-2} s^{-1}) were compared. The LED distancing which yielded the highest result for all three parameters was defined as the optimal LED positioning. Computational requirements of this step were reduced by running various iterations of the dynamic light exposure calculations. The first iteration started with larger spacing between the LEDs to find regions with high frequency and light exposure and then, based on these results, smaller regions were selected in order to analyse in detail by gradually decreasing the LED spacing in these areas. The first computation was done using 11.9 mm steps between each LED, which yielded a region of interest close to the optimal LED configuration (i.e., highest parameter values). Based on this configuration the distances above and below were analysed in 1.19 mm steps (minimum resolution of resized light map) in that defined range of 11.9 mm.

4.3 Results and Discussion

4.3.1 Static LED configuration

The LEDs were arranged in a manner to maximise the distribution of the light intensity across the range of 15 - 400 µmol m^{-2} s^{-1}. The resulting distance between the LEDs, together with the theoretical number of LEDs necessary to equip the PBR for different cell concentrations, are shown in Table 4-2 for the 200 L PBR and in Table 4-3 for the 20 L PBR. For the blue/red LED strip, with consecutively placed blue and red LEDs along the strip, it was found that for all LED configuration, the red LED was always located at its initial position (position zero). As such, the pattern of blue and red LED always started with the red LED at the beginning of the strip. Therefore, the positioning of the red LED is not additionally listed in the results. Both PBR sizes show decreasing distance between LEDs with the increasing cell density, which can be explained by the increase in light attenuation with denser cultures. With

high cell densities, the LEDs have to be positioned closer to each other in order to maximize the defined light intensity area. This also highlights the possible benefit of adjusting the LED operation according to the cell density, i.e., the cultivation stages. In the first stages of inoculation and exponential growth, parts of the LED strips could remain off, and as cell density increases, LEDs could be successively switched on. This could potentially improve the growth rate due to the reduction of light stress, while additionally reducing the power consumption of the illumination system [137]. It is noticeable that the LED distancing for *P. tricornutum* is more strongly affected by the cell density, while for *C. vulgaris*, the increase of cell concentration requires only a minor change in LED placement. This can be explained by the lower impact of cell concentration on the attenuation of the lightmaps for *C. vulgaris* in the same setup which was discussed previously (Figure 2-7).

Table 4-2: LED distances of the 200 L PBR and the number of LED for complete illumination of the PBR. The distance between the white LEDs furthermore defines the distance between the white and the blue/red LED strip.

Species	Cell concentration	Distance between white LEDs [cm]	Distance between blue to red LEDs [cm]	Total amount of LED strips (white and blue/red) *	LEDs per strip (strip length 80 cm)	
					White *	Blue and red *
P. tricornutum	Low	6.31	12.62	8	12	10
P. tricornutum	High	3.93	7.50	12	18	18
C. vulgaris	Low	6.31	12.62	8	12	10
C. vulgaris	High	5.71	10.48	9	13	12

*result rounded to fit PBR dimensions

Table 4-3: LED distances of the 20 L PBR and the number of LED for complete illumination of the PBR. The distance between the white LEDs furthermore defines the distance between the white and the blue/red LED strip.

Species	Cell concentration	Distance between white LED [cm]	Distance between blue to red LED [cm]	Total amount of LED strips (white and blue/red) *	LEDs per strip (strip length 38 cm)	
					White *	Blue and red *
P. tricornutum	Low	5.95	11.79	5	5	4
P. tricornutum	High	3.45	6.79	6	9	8
C. vulgaris	Low	6.31	12.50	5	5	4
C. vulgaris	High	5.11	10.12	5	5	4

*result rounded to fit PBR dimensions

Although the smaller dimensions of the 20 L PBR reduced the overall number of LEDs placed on the PBR surface, a nearly identical LED distancing between the LED was found for

both scales. Clearly, the smaller diameter combined with similar LED configuration created an improved light distribution within the culture. This can be roughly seen by comparing the total photic volume of the PBRs. In the scenario of a high cell density of *P. tricornutum*, the static light configuration of the 200 L PBR would illuminate only 38.8 % of the culture volume, whereas the 20 L PBR reached a photic volume of 90.1%. This highlights the unfavourable ratio of illumination surface area to cultivation volume of the 200 L PBR. Improvement in the photic volume at the 200 L scale can only be further achieved by reducing the diameter for the bioreactor, which would require a drastic redesign of the existing system. Alternatively, increasing the illuminated surface area could be achieved by internal lighting, although this would affect the hydrodynamic flow within the PBR [246].

The 20 L bioreactor as such could not accurately reflect the larger scale system and the dark/light zones, unless the light intensity of the individual lights were decreased. However, while this may be useful for scale-down experiments in the future, it is of less interest when looking at the interaction between mixing pattern and light sources. As such, the 20 L system was not considered for further analyses with the dynamic light exposure.

The calculated optimal illumination system consists of 216 white and 216 blue/red LEDs for the 200 L PBR and 54 white and 48 blue/red LEDs for the 20 L PBR. However, these calculations represent the configuration of LEDs for a static volume, which are based solely on the results of the light maps and do not consider the mixing and the correlated particle flow. As such additional iterations were done to adjust the LED spacing according to the hydrodynamic mixing pattern in order to improve the light history of the microalgae cells. Figure 4-3 visualizes the illumination configuration in a part of the PBR system as a two-dimensional cross section. The image overlays the hydrodynamic velocity fields (Figure 3-9) with the theoretical LED distribution across the PBR surface. The displayed LED setup is based on the white LED strip in high cell density culture of *P. tricornutum* and highlights the shape of the light cone of PPFD above 15 µmol m^{-2} s^{-1}. The light maps were trimmed to display the complete shape of the LED profile, including areas with low PPFD further away from the LED centre. As such the subsequent LED volumes had extended zones of low PPFD that are not visible in this illustration as they are below 15 µmol m^{-2} s^{-1}. The current calculation of the LED positioning was restricted by the PBR dimensions, in a way that the LED volumes could not exceed the boundaries of the PBR height. Future improvements on the CAD process will address this and adapt the shuffling steps by allowing additional LED placement at the top and bottom of the PBR. Enlarging the view of the LEDs enables the detailed examination of the

dark and light zones distributed between the LEDs along the side wall. These irradiance gaps might induce an enhanced D/L cycle on the cells.

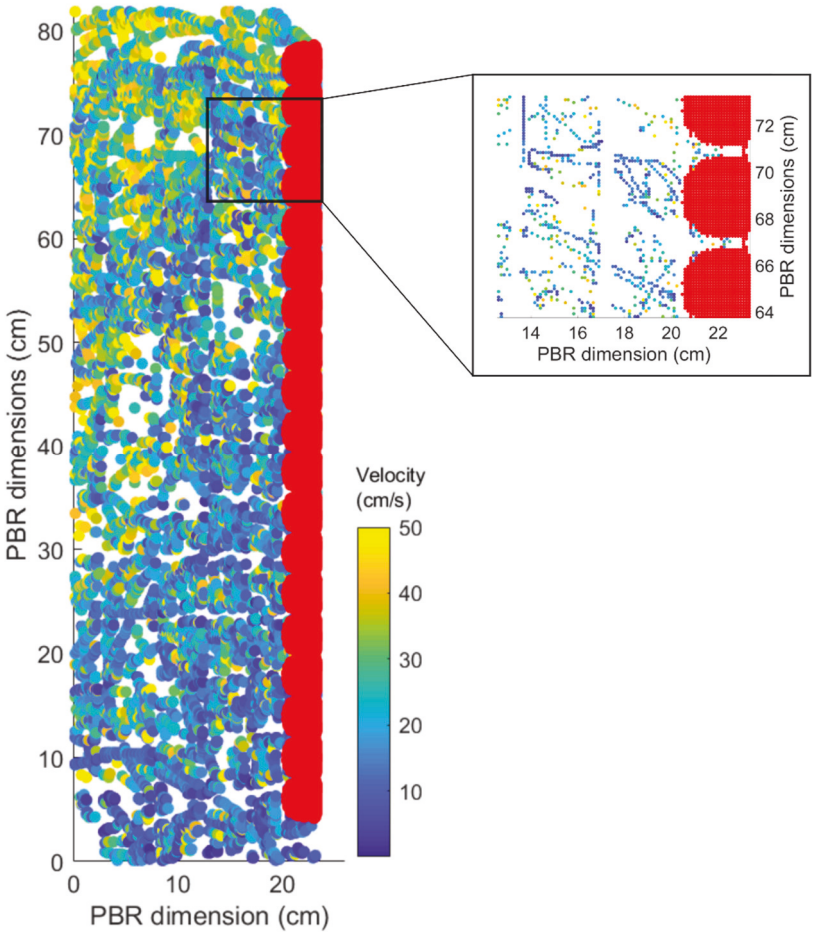

Figure 4-3: Vertical cross section from middle to side of the 200 L PBR visualising the particle velocity map with related colour bar (blue to yellow) and the overlapping theoretical LED configuration (red) on the PBR side wall. Velocity map is based on data with an aeration rate of 8 L/min. Overlapping LED configuration is a cross section of the white LED strip based on the results of the static approach for *P. tricornutum* with high cell concentration. LED coverage represents PPFD values above 15 µmol m^{-2} s^{-1}. The zoomed in area shows the LED illumination gaps between the LED light cones. Changes in spacing at the bottom and the top of the PBR are due to the cropping of light maps.

The velocity map shows the particle speed within the PBR, with higher velocity areas in the upper regions and reduced velocity in the lower regions of the vessel (detailed in Chapter 3). In visualising the result of the static LED arrangement, it becomes clear that a uniform distribution along the PBR height might not result in the best possible light experience for the cells, since the particle velocity is not constant throughout the PBR and correlated D/L fluctuation

might differ depending on the region. Future investigations with the CAD process will include an individual LED placing that accounts for variations in velocity across the illuminated zones.

4.3.2 Analysis of LED configuration

A CAD process was designed that combined the LED spacing with the particle trajectory data and analysed the light characteristics. Three parameters were considered for the optimization of the light distribution in the PBR: the total PPFD experienced by the particle within the defined PPFD region (15 - 400 µmol m^{-2} s^{-1}), the retention time of the particle in the defined PPFD region (15 - 400 µmol m^{-2} s^{-1}), and the mean D/L frequency. Data of the experimental particle tracing were used to calculate the light exposure of the algae cells within the PBR, which can then be used to compare the impact of cell density and aeration rate on light exposure. These calculations were done to validate the characteristics of the LED configuration of the static light exposure.

4.3.2.1 Particle light exposure

Particles migrating through the PBR encounter different PPFD for fluctuating time periods: this experience can change depending on the light profile and the mixing pattern. Figure 4-4 shows a representative image that demonstrates the impact of cell density with *P. tricornutum* culture on the light exposure of the particle for a random 10 s period. The plot shows PPFD for high and low cell densities together with the radial distance of the particle to the illuminated side wall. For high cell density conditions, the particle experienced a reduced PPFD in comparison to the low cell density, which can be explained by the deeper penetration of light in lower cell densities due to the reduced photon absorption and scattering by microalgae cells (Figure 2-6), which allows for deeper illumination into the culture volume. The total PPFD experienced by the particle was found to be around 60% lower in the case of high cell concentrations, compared to the lower cell density for both species. Detailed analysis of Figure 4-4 highlights cases in which the particle experienced different irradiance at similar radial distances to the periphery. This phenomenon can be observed at around 6 s (Figure 4-4), where the particle is close to the LED (6 cm), but experiences no irradiance whatsoever. This is due to the non-uniform light region created by the point source LEDs, with dark areas closely situated to the light source (Figure 4-3). As such, particles migrating with a constant radial distance through regions close to the PBR side walls pass through different light regimes and exhibit fluctuations in photon flux density. Radial positioning is commonly used to highlight

the travelling path of the particle through different light zones of a homogeneous light distribution and therefore allow the calculation of the PPFD, since light attenuation is a function of distance [247]. This approach cannot be applied for the particular light regime of these LEDs as it is too complex to visualize two-dimensionally. Light exposure depends not only on the distance to the illuminated surface, but also on the relative horizontal and vertical position of the different LEDs.

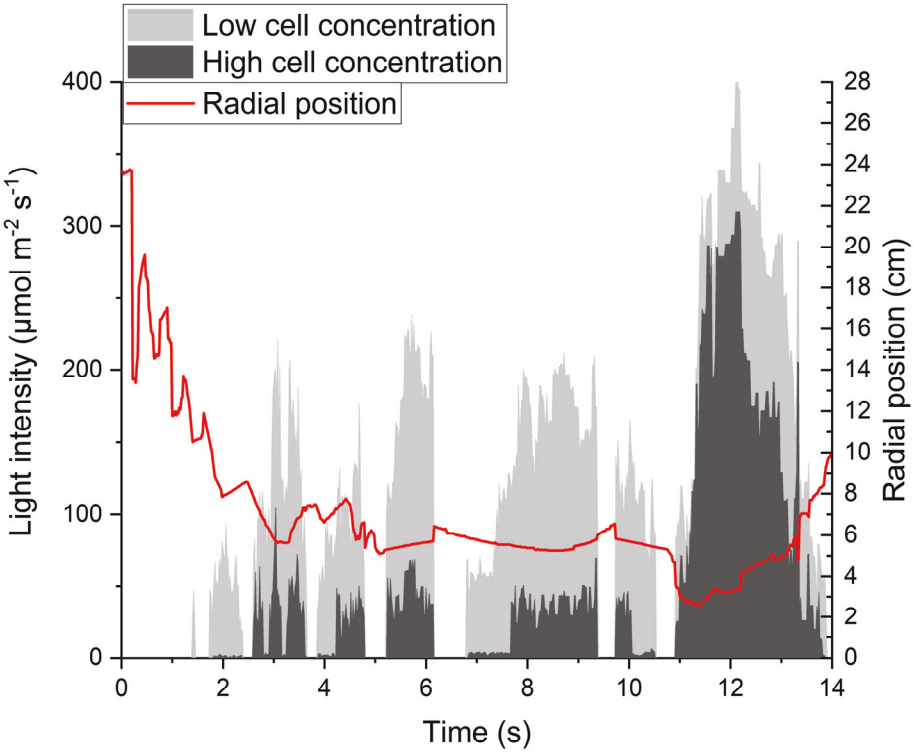

Figure 4-4: Light exposure in *P. tricornutum* for high cell concentration (black), and low cell concentration (grey) and radial position of the particle (red) based on the experimental particle tracing data of the 200 L PBR. In red the radial positioning of the particle. Scale of 14 seconds for 8 L/min aeration rate, based on LED configuration of the static light exposure.

4.3.2.2 Retention time

The impact of hydrodynamics and the LED configuration on the light experience of the particle was analysed by calculating the particle retention time (total) in different PPFD regimes. High retention times in PPFD ranges of 15 - 400 µmol m^{-2} s^{-1} were defined as favourable. Hence, increased total duration in this region can signify an improved light exposure of the cell. The light ranges can be further adjusted to fit different algal species requirements, but this range was chosen as a proxy for this current setup. Figure 4-5 shows a histogram of the

total particle retention time in the various light regimes of the 200 L PBR for different aeration rates. Lower aeration rates will slightly improve the light distribution by reducing the residence time of the particle in the dark zones. This indicates that using this particular LED configuration, a lower aeration rate of 5 L/min is seemingly better suited to provide sufficient photons to the culture. However, higher aeration rates improve the mass transfer coefficient (Figure 3-4) and thereby ensure sufficient CO_2 supply, another essential parameter that has to be considered for unrestricted growth. Further work would be needed to establish the appropriate mixing in order to combine the optimal photon supply and mass transfer for the dynamic demand of microalgae throughout the cultivation cycle.

Cell density also affected the PPFD distribution experienced by the particle, as the lower culture densities had increased retention times in the favourable light intensity range. This pattern can be observed for both species, though the impact of cell concentration for *C. vulgaris* is less distinct. This can be explained by the reduced influence of the chosen cell concentrations on the light maps for this species (as described in Chapter 2), or by a LED configuration that equally serves both cell concentrations. One thing that is of interest is that the particle does not spend long in high irradiance zones, which would apply for particle occurrences close to the PBR side wall. While this might be linked to a slight decrease in measurement precision close to the PBR frame by the tracing method (section 3.3.3.3), it does indicate that the particle is not often in the high light intensity zone, so decreasing the dark zone seems to be of greater importance when optimizing the PBR.

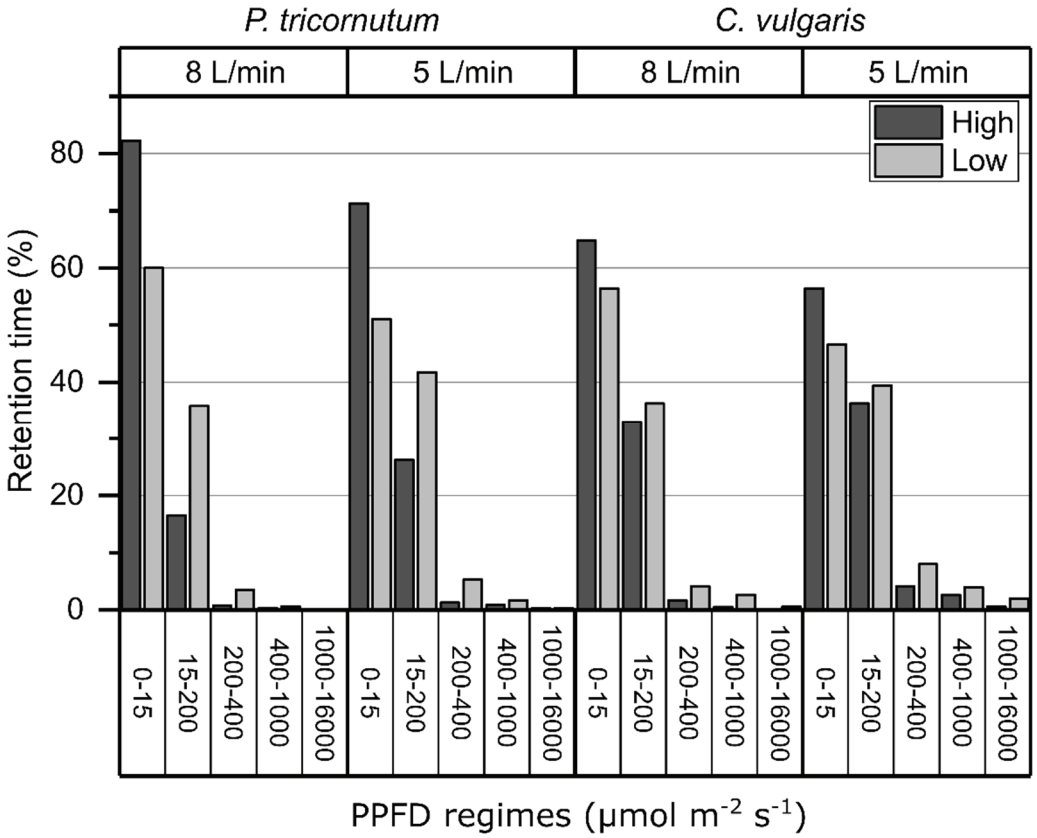

Figure 4-5: Histogram of particle retention time in PPFD regimes for *P. tricornutum* and *C. vulgaris* at aeration rates of 5 and 8 L/min and different cell densities, based on particle tracing of at least 10 minutes. Retention time was normalized to the maximum value to allow comparison of the different setups.

4.3.2.3 D/L Frequency analysis

The analysis of the particle retention time in certain light regions facilitates the direct comparison of the light exposure for different light and mixing configurations, yet it does not account for the frequency by which the particle moves between these zones. This D/L frequency was another parameter that was considered for the validation of the LED configuration, as it is shown that intermittent light has an effect on microalgal growth rate [228]. Variations of the binary exposure method are commonly utilized to calculate the mean D/L frequency [237][244]. Figure 4-6 A shows a representative binary distribution of the particle light exposure for a 20 s time lapse of the *P. tricornutum* culture (8 L/min aeration rate, high cell density). The particle spent an average of 0.3 s (3.3 Hz) in the light phase and in the dark phase, approximately 1 s (1 Hz). A broad diversity in frequencies was observed in the analysed data, which is characterized by high standard deviation (see Supplemental materials). This variety of frequencies could be due to turbulent eddies in the liquid flow that create fluctuating velocity fields within the PBR, as observed with the particle tracing method (Figure 3-11).

Another possible explanation is that the LED configuration creates a complex dark and light pattern. Particles travelling through the illuminated volume can experience light oscillation due to the inhomogeneous illumination, as shown in Figure 4-4. Mixing is an important parameter for improved D/L frequency; however, comparison of the aeration of 5 and 8 L/min revealed no significant variation between them. This could imply that mixing with these aeration rates does not have a significant effect on improving the D/L frequency. Similar results were observed in a simulated plate PBR (1 L) in which the commonly used aeration rates (0.25 and 0.75 L/min) did not affect the dominant D/L frequency [156].

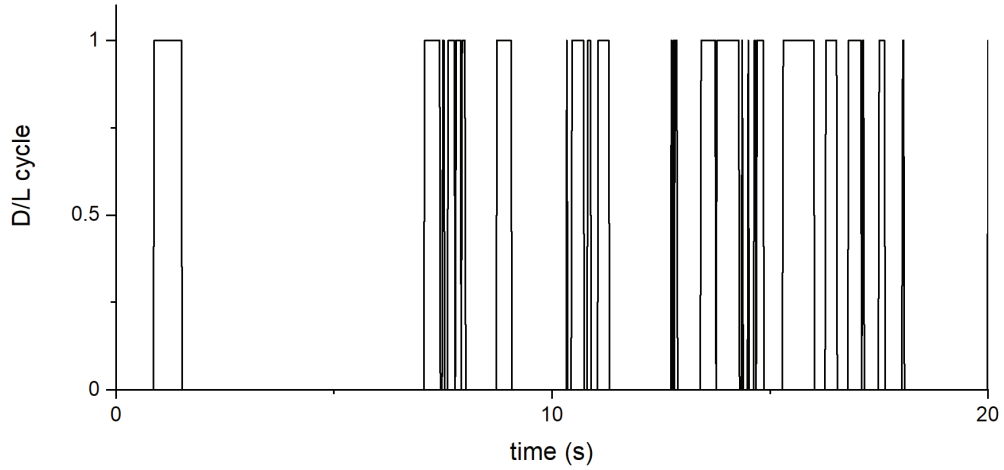

Figure 4-6: Representative data of the binary distribution used to calculate the mean D/L frequency. Data shown is based on the 200 L PBR with aeration rates of 8 L/min and light maps of *P. tricornutum* at high cell density (20 s time lapse). Values of 1 indicates the exposure to light intensities above 15 µmol m^{-2} s^{-1}, while 0 indicates particle is in the dark. Time represents travelling time of a particle through the PBR.

The Fast Fourier transformation algorithm was used to convert the dark/light fluctuations of the particle into a frequency spectrum [237]. The FFT was applied to the light exposure of the different species, cell concentrations and aeration rates. Figure 4-7 plots a representative frequency spectrum of different aeration rates for *P. tricornutum* at high and low cell concentrations. Peaks in magnitude mark light intensity changes of the particle when moving from dark to light. This method gave a similarly broad range of frequencies for the various configurations as the binary distribution, meaning comparison between configurations did not have the resolution to be fully utilized in the optimize of the system. However, results of all configurations showed dominant frequency amplitudes below 5 Hz (data not shown), which supports the results of the binary method. Therefore, the binary distribution was utilized for the further

analysis of the LED configurations, as the resulting mean D/L frequency could be compared between the different setups and the calculation could be easily incorporated into the algorithm.

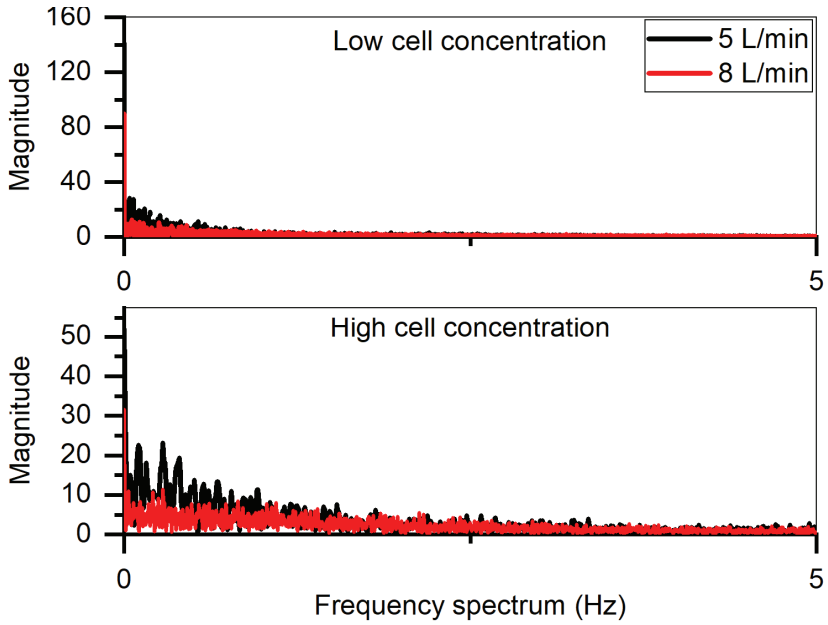

Figure 4-7: Frequency spectrum of the fast Fourier transformation for the 200 L PBR at aeration rates of 5 and 8 L/min. The figures show the frequency spectrums based on light maps of high and low concentration in *P. tricornutum.* Dominant amplitudes were only observed in the lower frequency spectrum.

Both analytical methods yielded similar frequency results for the measured scenarios between 0 – 5 Hz, which agrees with findings in literature about the mixing induced D/L frequencies. The simulations of a tubular bioreactor with a helical baffle system on its side walls achieved theoretical D/L frequencies of 2.28 Hz [244]. A more similar PBR geometry to the one described here – an airlift PBR with a lantern-shaped draft tube (~8 L culture volume) – reached a simulated frequency of 0.475 Hz [248], while in another study a frequency of 0.14 Hz was found in an simulated airlift PBR (18 L) [249]. Compared to these simulated values, the D/L frequencies observed for our system seems rather high, especially considering the high volume of the 200 L PBR. One major difference however is that these studies had a homogenous illuminated surface, instead of point source LEDs. This could indicate an enhancing effect of the LED pattern on the D/L frequency by creating a distinct dark light pattern for particles migrating through the illuminated regions. As such, high D/L frequencies could be realized without increasing the mixing, with its correlated shear stress and higher energy consumption, by simply adjusting the LED pattern. Metabolic stimulation has been mainly found for frequencies around 50 Hz and higher; however, lower frequencies (1-10 Hz)

were also proven to have beneficial effects on microalgae [235][250]. These frequency ranges are feasible in the PBR system and could even be further optimized by modulating the LEDs in order to create PPF pulses. These artificially induced light fluctuations could achieve higher D/L frequencies and potentially enable a more economical operation of the illumination system by reducing overall power costs of the LEDs [251].

4.3.3 Optimization of the LED distribution – dynamic model

So far, the ideal LED arrangement was based on the optimal light distribution calculation for a specific light intensity range in a static system, which did not include the mixing pattern as a parameter in the LED configuration. A more dynamic approach for the calculation of the LED arrangement is to combine LED distancing directly with the particle trajectory. In this case, the identification of the ideal LED positioning focuses on the light characteristics that the particle experiences rather than the ideal illumination of a static volume. This approach enabled the detailed analysis and comparison of different LED positions for their effect on the mean D/L frequency, the total PPFD experienced by the particle in the defined PPFD range (15 – 400 µmol m^{-2} s^{-1}), and the retention time of the particle in the defined PPFD range (15 – 400 µmol m^{-2} s^{-1}). The optimal LED alignment chosen in this study was done by giving equal importance to each of the three parameters. Changing the rating, or importance, for certain parameter would facilitate the identification of LED setups that enhance specific illumination characteristics; for instance, a higher frequencies or increased particle exposure.

Representative heatmaps visualize the impact of LED distancing (white and blue LED) on these three parameters for the 200 L PBR with an aeration rate of 8 L/min (Figure 4-8). The three plots show different patterns as the LEDs are moved away from each other, which highlights the different optimal LED positioning based on each individual parameter. The particle retention time increases with increased distance between white and blue LEDs, with a peak retention time for the distancing around 3.5 cm (Figure 4-8 A). The total light exposure shows a similar behaviour (Figure 4-8 B), but indicates a potential maximum in light exposure outside the analysed LED positions, meaning that the optimal LED setup for maximising the light exposure can only be found with greater distancing. On the other hand, the mean D/L frequency displays a nearly linear dependency on the distance between both LEDs (Figure 4-8 C). Higher D/L frequencies are found with consistently increased blue and white LED spacing, which signifies an enhancing effect of higher LED spacing on the dark/light cycle.

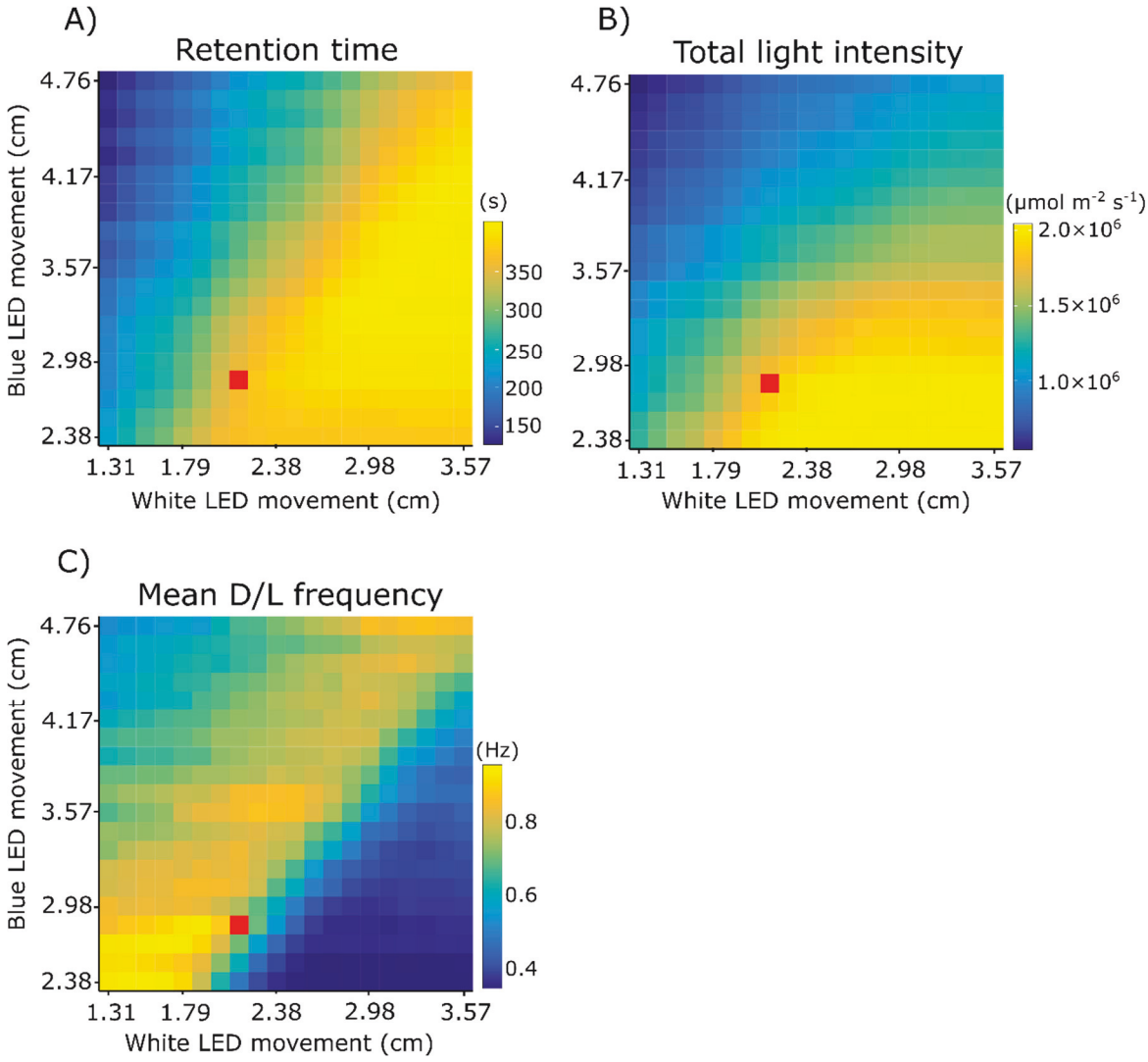

Figure 4-8: Representative heatmaps of A) retention time of the particle in the defined light region (15 - 400 µmol m^{-2} s^{-1}), B) total light intensity experienced by the particle in the defined light region (15 - 400 µmol m^{-2} s^{-1}), and C) mean D/L frequency. The maps show the positioning of white LEDs and blue LEDs. Distancing of the white LED and blue/red LED strip are synchronised. Red marks the optimal LED distancing for this setup (200 L PBR, 8 L/min, *P. tricornutum* with high cell concentration). The colour bar highlights high values for the three parameters in yellow.

Compared to the static light exposure (Table 4-2), the number of LEDs increased by using the dynamic approach due to a more compact LED configuration (Table 4-4). The different aeration rates only had a minimal impact on the LED distribution, which concurs with the observed minor influence of mixing on D/L frequency and the retention time of the particle. The high cell density setup for *P. tricornutum* requires a total LED number of 341 white LEDs, and 506 red and blue LEDs, which is double the number compared to the static calculation. There is a trade-off however, as this increase should balance the gain in algal biomass due to

the increased light availability with the cost of the illumination system and the increased power consumption. The current CAD process optimizes the LED configuration solely on the optimal light conditions for the culture: by additionally including the number of LEDs as a parameter, the algorithm would place value on the economic criteria of a reduced LED usage in the identification of the optimal LED distribution.

Table 4-4: List of adjusted LED distances based on the dynamic light exposure of the particle for different aeration rates in the 200 L PBR. The distance between the white LEDs furthermore defines the distance between the white and the blue/red LED strip.

Species	Aeration rate [L/min]	Cell concentration	Distance between white LEDs [cm]	Distance between blue to red LEDs [cm]	Total amount of LED strips (white and blue/red) *	LEDs per strip	
						White *	Blue and red*
P. tricornutum	8	Low	2.74	4.29	11	25	16
P. tricornutum	8	High	2.14	2.86	11	32	23
C. vulgaris	8	Low	7.26	8.57	8	10	8
C. vulgaris	8	High	2.62	3.69	11	27	18
P. tricornutum	5	Low	2.98	4.29	11	25	16
P. tricornutum	5	High	2.14	2.86	11	32	23
C. vulgaris	5	Low	7.38	8.33	8	10	8
C. vulgaris	5	High	2.98	3.93	11	27	18

*result rounded to fit PBR dimensions

The drastic difference between the dynamic and static method is outlined in Table 4-5. The dynamic LED setup enhances at least two parameters and has a consistently beneficial effect on the total light exposure. This is interesting to note, as the static light exposure setup maximised the ideal light distribution (15 – 400 µmol m^{-2} s^{-1}) throughout the PBR, therefore a high light exposure of the migrating particle would initially be assumed. However, reshuffling the LED volumes with the dynamic approach magnified the ideal light exposure of the particle by up to 298.2% (*P. tricornutum* at high cell density), which is curious as the ideal light distribution established in the static approach decreased by 50% in the dynamic LED setup, meaning that overall less PPFD of 15 – 400 µmol m^{-2} s^{-1} is present in the PBR. This shows the importance of LED positioning tailored for the specific hydrodynamic flow within the PBR, so the cells can optimally harness light. The results highlight the strong impact of hydrodynamic flow on the PPFD experienced by the cells which should be considered in the illumination design, especially in the case of non-uniformly light distribution.

Table 4-5: Difference between the static and dynamic light exposure of the 200 L PBR with aeration rates of 5 and 8 L/min. Defined light region of 15 – 400 µmol m^{-2} s^{-1}. Detailed results shown in supplemental materials.

Species	Aeration rate [L/min]	Cell concentration	Changes in mean D/L frequency [%]	Changes total exposure in defined light regime [%]	Changes in retention time in defined light regime [%]
P. tricornutum	8	Low	6.1	290.4	40.9
P. tricornutum	8	High	23.5	298.2	103.9
C. vulgaris	8	Low	-12.8	78.8	44.1
C. vulgaris	8	High	-44.1	285.8	48.6
P. tricornutum	5	Low	-11.9	278.2	41.8
P. tricornutum	5	High	19.7	245.0	66.9
C. vulgaris	5	Low	-8.7	50.8	33.8
C. vulgaris	5	High	-71.7	254.7	37.6

Further improvements for this optimization methodology could include the rearrangement of the LED strips. These are currently assumed to be vertically aligned to the PBR walls; by rotating them horizontally it might be possible to further increase the dark/light circulation of the particle. The hydrodynamic trajectory for the PBR demonstrated a clear pattern whereby a particle moved vertically more than horizontally; as such horizontal LED layers could create a higher intersection rate of the particle as it moves through these light "belts". The overall light distribution to the cells could be further improved by applying lenses on the LED chips (e.g., collimator lenses) and thereby manipulate the light path of the LED. This could allow for different LED configurations with advantageous light distribution compared to the currently used LED light profiles.

Another factor to consider for future improvement is that the current calculation assumes an even LED distribution across the PBR (e.g., same at the top and the bottom). This approach does not account for potential high or low velocity zones in the PBR which would benefit from further optimized LED configuration. Adjusting the algorithm could enable the calculation of this optimized configuration for the different zones of the PBR using the dynamic light exposure to truly create a customized LED configuration that is optimally suited for the specific geometry of the PBR and the algal species.

4.4 Conclusion

This chapter introduced the third part of the optimization platform - the LED distribution CAD process. The algorithm used for this chapter computes the optimal static light intensity distribution as a starting point, and then refines this by combining the light profiles with the particle trajectory data to create the dynamic light exposure. The LED configuration was

evaluated with equal importance to three parameters: mean D/L frequency, the retention time of the particle in a defined PPFD range, and the total PPFD experienced by the particle in the defined PPFD range.

For the static and dynamic approach, the D/L frequencies induced by mixing and the LED pattern with the specific dark and light zones along the illuminated surface were found to be below 5 Hz. This indicates that mixing alone might not induce a beneficial flashing light effect on the cells. However, an increase in LED spacing demonstrated a shortening of the D/L cycle time (i.e., higher frequency), which can be further optimized together with modulation of the artificial light source (pulsing) to achieve higher frequencies. There is also the potential for improved economic operation by reducing the LED activity depending on the state of the cultivation. Low cell densities require less LEDs than higher cell densities, while not impacting growth. The optimal LED configuration for two algal species, *P. tricornutum* and *C. vulgaris,* at both high and low cell concentration were defined (Table 4-4), which emphasized the importance of fine-tuning the LED arrangement based on the algal species. The next step for this illumination setup would be to implement it into the 200 L PBR of the optimization platform or directly into the industrial bioreactor system and measure the growth rates.

This chapter was based on experimentally obtained data of the particle trajectory; however, the methodology can similarly be applied to simulated particle tracing data. Hydrodynamic simulation would simplify the testing of new PBR geometries and furthermore allow the implementation of a complex internal illumination system *in silico*, before the need to build the real-world system. The current model forms the starting point for a more complex simulation system, which will be successively enhanced by implementing models for other relevant physical parameters, such as flow dynamics, mass and heat transfer, shear stress, and eventually microalgal growth as a function of the light they experience. This would enable the detailed prediction of the microalgae growth behaviour and the impact of light arrangement and mixing pattern within a bioreactor of various geometries or operational conditions. This model will provide the foundation for ongoing optimization efforts on the converted PBR.

Chapter 5
Synthesis of findings

Author Contribution

Julian R. Kofler wrote the manuscript. Leen Labeeuw assisted in editing. Peter J. Ralph assisted in editing.

5.1 General conclusions

Microalgae are an emerging new platform for the production of biopharmaceuticals. Production of recombinant proteins in algae is predicted to be lower in cost compared to commonly used host systems, which makes this technology attractive for industry [131]. New photo-bioreactor systems are needed to satisfy the high quality requirements of these products within the pharmaceutical market. As such this project developed an optimization platform that can facilitate the conversion of an industrially established bioreactor system to become a PBR equipped with an optimized illumination system for algal cultivation. While this approach can eventually be used for any bioreactor in principle, this optimization platform was focused on the conversion of the GE Xcellerex, an existing bioreactor used in GMP facilities.

Through this thesis, I: i) designed a practical and versatile method to create high-resolution light maps of the PBR (**Chapter 2**), ii) tested physical properties of the optimization platform with regards to mass transfer, mixing time and flow pattern (**Chapter 3**), and iii) created a computer aided design (CAD) process to calculate the light exposure and the optimal light configuration by combining the light maps with empirically obtained particle trajectory data (**Chapter 4**).

5.1.1 Optimization platform

The optimization platform consists of a physical component (200 L PBR and 20 L PBR that recreate the conditions of the GE Xcellerex bioreactor) and a computer aided design process (LED distribution algorithm). The physical part of the optimization platform was designed to mimic the operational parameters (mass transfer and mixing) of the industrial bioreactor system; therefore, reproducibility between the PBR systems needed to be established (**Chapter 3**). Operational conditions of the PBR system were tested with different methods, such as the gassing-in method (mass transfer), pH- and dye-method (mixing time) and optical particle tracing (hydrodynamic flow). Similar rates were demonstrated for mass transfer and mixing time compared to the industrial counterpart, and the successful down-scaling of the bioreactor from 200L to 20 L PBR system was shown to be effective for certain key parameters. While these methods have been used previously, little work has been done to directly compare them for suitability. Interestingly, the different methods yielded additional insight into the bioreactor characteristics. For example, the pH-method revealed zonal flow differences in the PBR, indicating zones of laminar flow. It was found that the bottom of the 200 L PBR encountered inconsistent mixing created by the aeration system of the reactor. In order to analyse the

hydrodynamic flow inside the PBR systems, I utilized a particle tracing method [153]. The original method was designed for laboratory-scale PBRs (<10 L), thus adaptions of the method were necessary to fit the requirements of the 200 L PBR system. I re-engineered the image processing and data analysis to improve the detection rate for the particle in the PBR setups. However, the optical properties of the PBR geometry remained a challenge and future work will need to apply further improvements. This could include additional cameras to cover a wider angle of the PBR surface, which would improve the particle detectability of the alginate sphere and thereby aid in the reconstruction of the particle path. The generated particle trajectories enabled the analysis of different parameters, such as flow path, the particle presence, and the liquid velocity within the PBR. Analysing these data confirmed the slower particle movement closer to the bottom of the 200 L PBR. This design was only tested with a PBR that was mixed by aeration alone. Given that the results indicated that there are areas of poor mixing, this indicates the need for additional mixing, or changes in how the system is aerated. The implementation of an impeller into the system should be considered as a possible improvement to overcome this slow velocity region, though the increase of shear stress on the cells [198] and the additional power consumption of the system would also have to be reviewed.

This chapter resulted in the development of a methodology that can be employed to characterize various bioreactor systems and scales. The techniques utilized have been used individually before, but this is the first time that they have been combined and performed at this scale. The methodology was designed such that it can be done without the need for expensive or specialized equipment, and was tailored to measure critical physical parameters of a bioreactor. In addition, the setup used for the optical measurements (dye-method and the particle tracing) allowed for the measurement of various parameters such as hydrodynamic flow, mixing time (**Chapter 3**), while at the same time it could be used for measuring the light distribution (**Chapter 2**) in a non-intrusive manner, based on a domestic camera system with some easy modifications.

5.1.2 Light attenuation

One of the primary objectives of this thesis was to design a system to easily find the optimal light configuration for use in a pre-existing bioreactor (Xcellerex), to turn it into a photo-bioreactor. The light system had to provide sufficient photons for unrestricted growth, while not overexposing the cells and inflicting damaging light inhibition. To achieve this, I first

identified the right LEDs to optimize the microalgae growth. This was done by fitting the LED wavelength with the specific absorption peaks of the algae of interest (*P. tricornutum* and *C. vulgaris*). In particular, I focused on blue (450 nm) and red wavelengths (670 nm) which are known to stimulate metabolic pathways and biochemical cell composition [230]. Additionally, a white light with comparatively lower light intensity was included to ensure the supply of a broad light spectrum and avoid potential growth limitations due to the supply of only certain narrow wavelengths. The next design step concerned the light distribution of the LEDs. As artificial point sources of light, LEDs allow for a flexible configuration on the surface of the PBR, yet care must be taken as inadequate configurations can create unfavourable light regimes within the PBR. However, the light distribution within a culture is not only dependent on the bioreactor geometry, but also on the algal species and density. As such, a clear understanding of the light profile for different species, cell concentration, and wavelengths are crucial.

Current methods used to obtain this light distribution, such as light attenuation calculations and measurements with light intensity probes, do not suffice for the given setup of a PBR and illumination system as they either require empirical collection of constants for each species at each density, or do not give sufficient information about the exact shape of the light cone within the bioreactor [153][154][155]. An artificial illumination system (e.g., using LEDs) creates a distinct non-homologous light profile depending on the positioning of the point light sources. This complex optical condition and the need for a versatile and streamlined measurement technique led to the development of a novel Direct Chlorophyll Fluorescence Imaging (DCFI) method for the creation of light map. I designed this method to be easy to use with a domestic camera system and a streamlined digital data processing method, that enables rapid measurement of different illumination systems and microalgae species (**Chapter 2**). This method builds upon previous methods that were designed for measurements within a leaf [159], or within a small scale cuvette ([160] unpublished). DCFI generates high resolution light maps with more than 100 pixels per cm (depending on the camera setup), that contour the light profile of artificial light sources in detail, including potential reflections, e. g., in case of the single-use bag system or the PBR shell. This provided an advantage to the calculated approach (e.g., Beer-Lambert), as it depicts the actual light conditions within the PBR.

The generated light maps show zones of high and low irradiance distribution and highlight potential zones of excess and insufficient light within the PBR. I assessed the irradiance profile and attenuation of *P. tricornutum* and *C. vulgaris* at different concentrations and found distinct absorption characteristics with the different LEDs. The light maps highlighted differences in the species-specific absorption characteristics as variations in light cone shape and penetration

depth. This differential utilisation of various wavelengths affects the design of an ideal illumination system as the metabolic impact of the wavelengths must be considered in order to support optimal cell growth. I found that the mathematical formula used to convert the raw fluorescence images into the light maps is correlated with the cell density of the algae culture. The 'b-value' in the conversion formula gradually increases with higher cell densities. Further work is needed to validate this across species, but it would mean that only a single calibration step is needed for each new species, which would then work across the whole growth cycle of the culture.

5.1.3 Light history

Bringing together the light maps with the hydrodynamic data allows for knowledge about the overall light exposure of the culture, a crucial parameter in the evaluation of a PBR system (**Chapter 4)**. As such, the ideal light distribution of the LEDs were calculated for the two PBR sizes. This was done firstly for the static light distribution (assuming no mixing) by maximising the area of a specific photosynthetic photon flux density (PPFD) range (15 - 400 µmol m^{-2} s^{-1}) of the LED arrangement. I designed a CAD process that converted the two-dimensional light maps into three-dimensional light volumes and aligned them in order to create the ideal light distribution within the PBR. These LED configurations did not include the hydrodynamic pattern induced by mixing, and as such were used as a starting point for further optimization. The range of the PPFD can be adjusted for different species as necessary, but there was minimal impact when looking at a variety of ranges (15 - 200, 300 and 500 µmol m^{-2} s^{-1}) on the final LED alignment. However, static light exposure does not reflect the actual photon flux density available to the cells in a mixed PBR.

The light exposure of cells is dynamic and depends on the retention time and flow pattern through different light regimes within the PBR. This dynamic light exposure was calculated by combining particle tracing data (**Chapter 3**) with the generated LED volumes. Three parameters were considered relevant for the optimal light exposure determination: the dark to light frequency, the retention time in a defined light range, and the overall exposure time in a defined light range experienced by the particle. The dark to light frequency is of interest, as this can allow cells to regenerate in the dark [228]. However, previous work has indicated that this requires frequencies >50 Hz, while the D/L frequency of this system was 0-5 Hz. Two different methods were used to extract the frequency from the light exposure data, and both yielded comparable results. Nevertheless, knowledge of this parameter can be used for further

optimization (e.g. operation of the lights or altering the mixing). Based on the highest values of all these parameters, the optimal light configuration was identified for the 200 L PBR system and can be configured based on different aeration rates or volumes as required. The dynamic light exposure calculation yielded a more dense LED configuration than the initial static light exposure, which highlights the necessity of incorporating all the components (flow pattern and light map) when designing an artificial light setup with non-homogeneous light distribution.

An interesting aspect that emerged from the analysis was that the aeration rate which provided the highest mass transfer (8 L/min) was not necessarily the best for providing the type of mixing that kept algal cells in the photic volume (5 L/min). This could be due to the specific flow pattern in the geometry of this PBR that forces algal cells towards the middle of the bioreactor, then along the illuminated PBR periphery. As such, while the higher aeration rate may have good mass transfer properties and keep the overall bioreactor mixed, it also establishes a flow pattern that keeps cells away from the light. That is an advantage of this digital platform, as it allows this type of fine-tuning that finds the balance between these various optimization components. Further work is required to find the differential effect of light vs mass transfer on the growth of the algae. For the highest aeration rate (8 L/min) and cell density (*P. tricornutum*), an illumination setup of 341 white LEDs, and 506 red and blue LEDs were identified for the 200 L PBR system. However, the 200 L bag at 8 L/min aeration rate with low cell concentrations of *P. tricornutum* achieved the ideal light exposure with a reduced operation of white LEDs (25%) compared to the high cell concentration. This knowledge allows for a reduced quantity of LED to be switched on during the early stages of the cultivation, followed by the successive initiation of the remaining LEDs throughout the cultivation cycle. The configuration of the final LEDs, along with the optimal mixing rates, can be found using the CAD algorithm I designed, and then applied to the physical 200 L PBR system for growth trials, or directly implemented into the Xcellerex system.

5.2 Future work of the complete platform

The platform designed in this thesis presents the methodological foundation to convert and optimize a commercial bioreactor into a photo-bioreactor. Currently, the optimization platform consists of a physical component and a computer aided design component. Promising findings from the computer aided design portion (e.g., the optimal light configuration) still have to be tested in the physical portion of the optimization platform. The light maps are a central part of

the optimization platform, with the method used to obtain these light maps being easily applicable to other light sources and PBR geometries. The current work focused on that the illumination of the PBR system being from the outer surface area. Future work can employ this technique to measure and analyse illumination sources of different designs, such as internal illumination.

The design of the physical component could be further enhanced to ensure a greater flexibility of the illumination system. The system must be controllable in a way that the LED activity and intensity can be manipulated seamlessly in order to adapt the photon flux and the emission of certain wavelengths. These adjustments in light quality and quantity for different cultivation stages potentially supports the algae growth and can increase the product yield [143]. Furthermore, the fully controllable LED system would facilitate the manipulation of the exposure frequency of the microalgae cells by oscillating the operational cycles of the lights. Ideally, the PBR system is homogeneously mixed, however, if slow velocity zones are unavoidable due to the PBR design, the algorithm for LED distribution can be adapted to treat different regions of the PBR independently. This would create a more diverse configuration of the light sources adjusted to the different dynamic light exposures of the cells in the differently mixed zones of the bioreactor.

One limitation of the current system is that the flow pattern is still determined empirically. Any change in PBR geometry would need additional particle tracing measurements to confirm the modified hydrodynamic flow. This requires the presence of a physical system on which to test this. One option for the future is to have a simulated bioreactor, whereby various designs can be tested, and then further refined and validated with a physical model (Figure 5-1). The simulation, consisting of computational fluid dynamics (CFD) and particle simulation, would allow for the rapid impact-validation of modifications on the liquid flow pattern, while also understanding the effect on the dynamic light distribution, since the simulated particle trajectory data can be easily implemented into the established algorithm for light optimization. Furthermore, for a comprehensive bioreactor model, other parameters such as the bubble size, CO_2 or heat transfer rate has to be further considered. Heat transfer is another parameter that should be examined, as it can have large implications for the growth of microalgae. In this scenario of an industrial Xcellerex system, cooling/heating of the culture is done by conductive energy transfer through a contact area between bag and the cooling jacket. As such the implementation of a LED system on the cooling shell will reduce the contact area between the culture and the cooling jacket, which can impact the cooling/heating of the culture. This should be further considered in the enhancement of the simulation, especially when utilized for PBR

designs without active cooling/heating. The comprehensive simulation with a mass transfer module would further allow for the identification of the most efficient aeration rates for different cultivation stages, and highlight potential substrate limitation zones of the PBR. The simulation would also enable the validation of changes in mixing or PBR design to address these limitations, and directly verify the corresponding impact on other characteristics (e.g., dynamic light distribution). These data can also be employed to identify certain thresholds for the physical cultivation system, such as ideal aeration rate and light intensities for specific cell densities.

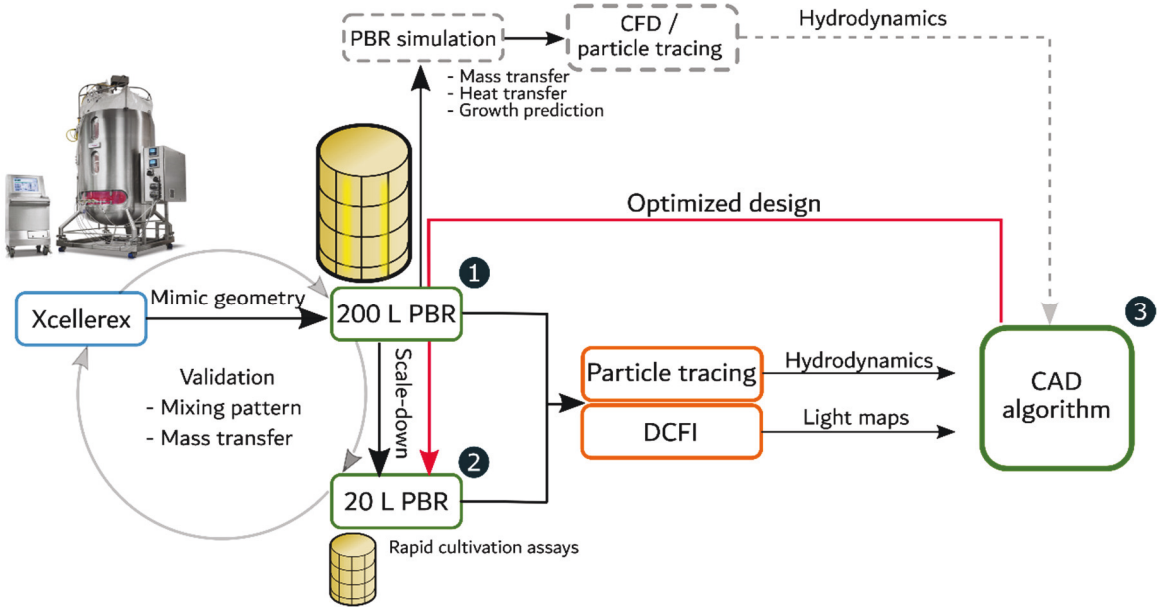

Figure 5-1: Future project overview. Augmentation of the existing system, consisting of the 20 and 200 L PBR (part 1 and 2) and the CAD algorithm (part 3), with the PBR simulation that will generate particle tracing data based on the CFD and particle tracing modules. The PBR simulation is further expandable for models of mass and heat transfer, and growth predictions.

Ultimately, the simulation module can be extended to predict the growth of microalgae, based on the amount of supplied substrates (e.g., photons, nutrients, CO_2) to the cells [252]. Further work is needed to measure or incorporate the growth of the algae in the different light conditions (e.g., through measuring how differing light wavelengths affect the photosystem, or by looking at the overall growth rate). With detailed knowledge about the impact the different conditions have on the algal metabolism, the light history and mass transfer rates can be directly related to the overall growth of algae, which would allow for the design of a PBR that maximizes algal productivity. This would allow for a true 'digital twin' that can be used to enhance the operation and design of a PBR.

5.3 Conclusion

The production process of biopharmaceuticals using microalgae must comply with the necessary regulatory guidelines to ensure the production procedures and the product quality. This can be done either by designing an entirely new system (which would then have to pass through multiple verification steps in order to achieve GMP compliance) or could be done by the conversion of an established cultivation system into a PBR. This would also allow for the new production platform to reach the market much faster. As the biopharmaceutical market is highly competitive, decreased production costs by improving productivity are crucial issues. Therefore, the constant optimization of the cultivation system is an essential and continuous part of production process, which is particularly true for an emerging system such as microalgae. The optimization platform highlighted in this thesis is the first step towards creating such a system.

Supplemental materials

Appendix Chapter 2

At low shutter speeds (short exposure times), the b-value shows a minimum value (valley), while at longer exposure times the b-value reaches a maximum (plateau). This is to be expected since the exposure time limits the quantity of photons captured by the camera sensor and the b-value is proportional to the fluorescence. Shorter exposure times result in a diminished fluorescence recording, to a point at which the image is undersaturated, whereas long exposure increases the number of captured photons, leading to an over-saturated image. Apparently, this pattern of valley, linear increase and plateau, is specific for each cell concentration, and shifts with changes of the cell density (Figure S 1). The figures display a representative data set of *P. tricornutum* for different LEDs in which the shutter speed and the b-value are plotted for different cell concentrations. It is possible to see a particular pattern in which higher cell concentrations reach the maximum plateau with faster shutter speeds, whereas the lower cell concentrations need longer exposure times to reach the maximum b-value. The three colours show an overall shift for the linear increase of the b-value. That seems to be due to the difference in initial light intensity of the LED. Lower light setups such as the white LED need longer exposure time to saturate the image sensor with photons, while high intensity LEDs reach saturation with lower exposure time.

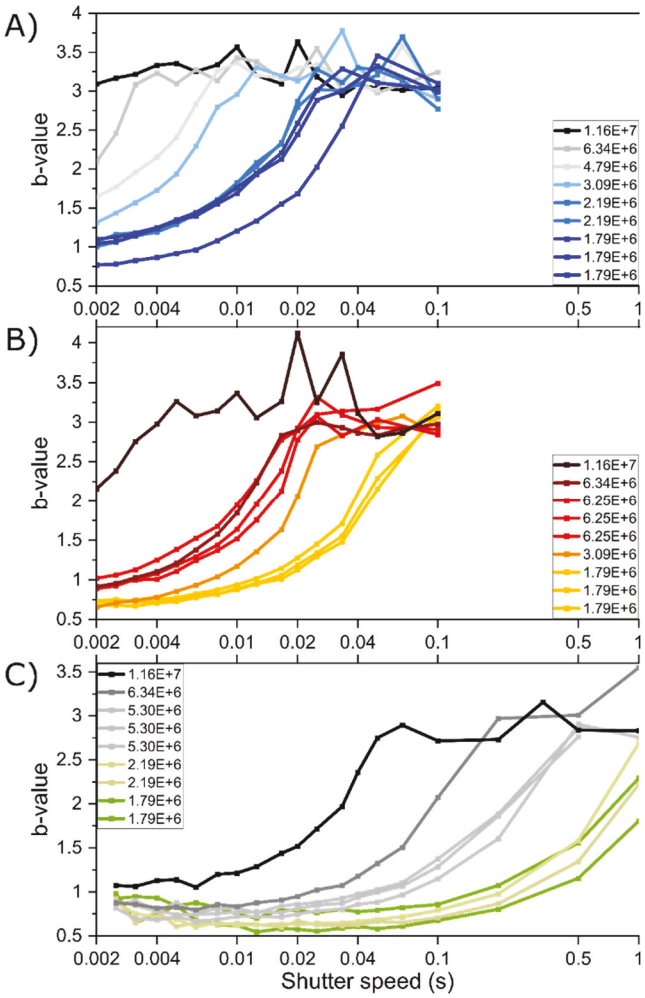

Figure S 1: Comparison of b-value with the shutter speed for three LED colours: (A) red, (B) blue, and (C) white. Each light colour shows measurements of the different cell concentration and the gradual increase of b-value with rising exposure time. Shutter speed is show in log-scale.

Appendix Chapter 4

Table S 1: Values from the static approach for the 200 L PBR with 8 L/min aeration rate.

Species	Cell conc.	Mean light interval [s]	Standard deviation light interval [s]	Mean dark interval [s]	Standard deviation dark interval [s]	mean D/L cycle [s]	Standard deviation D/L cycle [s]	Total exposure in defined light regime [µmol m^{-2} s^{-1}]	Retention time in defined light regime [s]
P. tricornutum	Low	0.41	0.59	0.81	1.61	1.22	1.78	908490.99	296.26
P. tricornutum	High	0.29	0.35	1.32	2.59	1.61	2.63	464961.90	155.82
C. vulgaris	Low	0.35	0.74	0.45	0.93	0.80	1.56	1670963.87	363.08
C. vulgaris	High	0.29	0.48	0.54	1.17	0.84	1.31	952828.91	311.28

Table S 2: Values from the dynamic approach for the 200 L PBR with 8 L/min aeration rate.

Species	Cell conc.	Mean light interval [s]	Standard deviation light interval [s]	Mean dark interval [s]	Standard deviation dark interval [s]	mean D/L cycle [s]	Standard deviation D/L cycle [s]	Total exposure in defined light regime [µmol m-2 s-1]	Retention time in defined light regime [s]
P. tricornutum	Low	0.59	0.70	0.55	1.20	1.14	1.45	3546762.49	417.30
P. tricornutum	High	0.47	0.60	0.76	1.86	1.23	2.01	1851319.54	317.76
C. vulgaris	Low	0.57	1.21	0.33	0.82	0.90	1.56	2987617.68	523.32
C. vulgaris	High	0.69	0.84	0.52	1.10	1.21	1.42	3675579.54	462.56

Table S 3: Values from the static approach for the 200 L PBR with 5 L/min aeration rate.

Species	Cell conc.	Mean light interval [s]	Standard deviation light interval [s]	Mean dark interval [s]	Standard deviation dark interval [s]	mean D/L cycle [s]	Standard deviation D/L cycle [s]	Total exposure in defined light regime [µmol m^{-2} s^{-1}]	Retention time in defined light regime [s]
P. tricornutum	Low	0.67	2.12	0.98	2.25	1.65	3.26	841840.84	236.48
P. tricornutum	High	0.59	2.17	1.44	2.52	2.03	3.28	511728.32	167.14
C. vulgaris	Low	0.60	2.12	0.53	1.13	1.13	1.56	1569114.21	287.68
C. vulgaris	High	0.49	1.77	0.62	1.48	1.11	2.33	911487.89	259.72

Table S 4: Values from the dynamic approach for the 200 L PBR with 5 L/min aeration rate.

Species	Cell conc.	Mean light interval [s]	Standard deviation light interval [s]	Mean dark interval [s]	Standard deviation dark interval [s]	mean D/L cycle [s]	Standard deviation D/L cycle [s]	Total exposure in defined light regime [µmol m^{-2} s^{-1}]	Retention time in defined light regime [s]
P. tricornutum	Low	1.17	2.41	0.68	1.38	1.85	2.85	3183844.23	335.30
P. tricornutum	High	0.85	2.09	0.78	1.85	1.63	2.82	1765305.91	278.94
C. vulgaris	Low	0.87	2.93	0.36	0.93	1.23	1.56	2366047.82	385.00
C. vulgaris	High	1.30	2.79	0.61	1.26	1.91	3.09	3233107.35	357.34

Since the total retention time and total light exposure are dependent from the sampling length of the particle tracing experiment, results of these parameters cannot be directly compared among different aeration rates, as both experiments have different durations.

References

[1] G. Walsh, "Biopharmaceutical benchmarks 2018," *Nat. Biotechnol.*, vol. 36, no. 12, pp. 1136–1145, 2018, doi: 10.1038/nbt.4305.

[2] P. market Research, "Global Market Study on Biopharmaceuticals: Asia to Witness Highest Growth by 2020," 2015. https://www.persistencemarketresearch.com/mediarelease/biopharmaceutical-market.asp (accessed Apr. 09, 2019).

[3] J. Seo and K. J. Lee, "Post-translational modifications and their biological functions: Proteomic analysis and systematic approaches," *J. Biochem. Mol. Biol.*, vol. 37, no. 1, pp. 35–44, 2004, doi: 10.5483/bmbrep.2004.37.1.035.

[4] T. Amann, V. Schmieder, H. Faustrup Kildegaard, N. Borth, and M. R. Andersen, "Genetic engineering approaches to improve posttranslational modification of biopharmaceuticals in different production platforms," *Biotechnol. Bioeng.*, vol. 116, no. 10, pp. 2778–2796, 2019, doi: 10.1002/bit.27101.

[5] T. Friedl, N. Rybalka, and A. Kryvenda, "2 Phylogeny and systematics of microalgae: An overview," in *Microalgal Biotechnology: Potential and Production*, C. Posten and C. Walter, Eds. Berlin, Boston: DE GRUYTER, 2012, pp. 11–38.

[6] F. Hempel and U. G. Maier, "An engineered diatom acting like a plasma cell secreting human IgG antibodies with high efficiency," *Microb. Cell Fact.*, vol. 11, pp. 2–7, 2012, doi: 10.1186/1475-2859-11-126.

[7] C. L. Cramer, J. G. Boothe, and K. K. Oishi, "Transgenic plants for therapeutic proteins: Linking upstream and downstream strategies," *Curr. Top. Microbiol. Immunol.*, vol. 240, pp. 95–118, 1999, doi: 10.1007/978-3-642-60234-4_5.

[8] S. P. Mayfield, S. E. Franklin, and R. A. Lerner, "Expression and assembly of a fully active antibody in algae," *Proc. Natl. Acad. Sci.*, vol. 100, no. 2, pp. 438–442, 2003, doi: 10.1073/pnas.0237108100.

[9] Y. Gong, H. Hu, Y. Gao, X. Xu, and H. Gao, "Microalgae as platforms for production of recombinant proteins and valuable compounds: Progress and prospects," *J. Ind. Microbiol. Biotechnol.*, vol. 38, no. 12, pp. 1879–1890, 2011, doi: 10.1007/s10295-011-1032-6.

[10] D. Jha, V. Jain, B. Sharma, A. Kant, and V. K. Garlapati, "Microalgae-based Pharmaceuticals

and Nutraceuticals: An Emerging Field with Immense Market Potential," *ChemBioEng Rev.*, vol. 4, no. 4, pp. 257–272, 2017, doi: 10.1002/cben.201600023.

[11] M. Sabalza, P. Christou, and T. Capell, "Recombinant plant-derived pharmaceutical proteins: current technical and economic bottlenecks," *Biotechnol. Lett.*, vol. 36, no. 12, pp. 2367–2379, 2014, doi: 10.1007/s10529-014-1621-3.

[12] G. Markou and E. Nerantzis, "Microalgae for high-value compounds and biofuels production: A review with focus on cultivation under stress conditions," *Biotechnol. Adv.*, vol. 31, no. 8, pp. 1532–1542, 2013, doi: 10.1016/j.biotechadv.2013.07.011.

[13] Y. M. Dyo and S. Purton, "The algal chloroplast as a synthetic biology platform for production of therapeutic proteins," *Microbiol. (United Kingdom)*, vol. 164, no. 2, pp. 113–121, 2018, doi: 10.1099/mic.0.000599.

[14] F. Balique, H. Lecoq, D. Raoult, and P. Colson, "Can plant viruses cross the kingdom border and be pathogenic to humans?," *Viruses*, vol. 7, no. 4, pp. 2074–2098, 2015, doi: 10.3390/v7042074.

[15] T. L. Walker, S. Purton, D. K. Becker, and C. Collet, "Microalgae as bioreactors," *Plant Cell Rep.*, vol. 24, no. 11, pp. 629–641, 2005, doi: 10.1007/s00299-005-0004-6.

[16] N. Yan, C. Fan, Y. Chen, and Z. Hu, "The potential for microalgae as bioreactors to produce pharmaceuticals," *Int. J. Mol. Sci.*, vol. 17, no. 6, pp. 1–25, 2016, doi: 10.3390/ijms17060962.

[17] J. Yao, Y. Weng, A. Dickey, and K. Wang, "Plants as Factories for Human Pharmaceuticals: Applications and Challenges," *Int. J. Mol. Sci.*, vol. 16, no. 12, pp. 28549–28565, Dec. 2015, doi: 10.3390/ijms161226122.

[18] S. Y. Teng, G. Y. Yew, K. Sukačová, P. L. Show, V. Máša, and J.-S. Chang, "Microalgae with artificial intelligence: A digitalized perspective on genetics, systems and products," *Biotechnol. Adv.*, vol. 44, no. September, p. 107631, Nov. 2020, doi: 10.1016/j.biotechadv.2020.107631.

[19] J. D. Rochaix and J. Van Dillewijn, "Transformation of the green alga Chlamydomonas reinhardii with yeast DNA," *Nature*, vol. 296, no. 5852, pp. 70–72, 1982, doi: 10.1038/296070a0.

[20] C. M. Vega, *Advanced Technologies for Protein Complex Production and Characterization*, 1st ed. Springer International Publishing AG Switzerland, 2016.

[21] B. A. Rasala and S. P. Mayfield, "Photosynthetic biomanufacturing in green algae; production of recombinant proteins for industrial, nutritional, and medical uses," *Photosynth. Res.*, vol. 123, no. 3, pp. 227–239, Mar. 2015, doi: 10.1007/s11120-014-9994-7.

[22] Walsh G, "Biopharmaceutical benchmarks 2010," *Nat. Biotechnol.*, vol. 28, no. 9, pp. 917–924,

2010, doi: http://dx.doi.org/10.1038/nbt0706-769.

[23] Market Research Engine, "Erythropoietin (EPO) Drugs Market By Product (Darbepoetin-alfa, Epoetin-beta); By Application (Anemia, Kidney Disorders) and by Regional Analysis - Global Forecast by 2018 – 2024," 2018. https://www.marketresearchengine.com/erythropoietin-epo-drugs-market (accessed Apr. 09, 2019).

[24] A. Eichler-Stahlberg, W. Weisheit, O. Ruecker, and M. Heitzer, "Strategies to facilitate transgene expression in Chlamydomonas reinhardtii," *Planta*, vol. 229, pp. 873–883, 2009, doi: 10.1007/s00425-008-0879-x.

[25] A. Zemella *et al.*, "Cell-free protein synthesis as a novel tool for directed glycoengineering of active erythropoietin," *Sci. Rep.*, vol. 8, no. 1, pp. 1–12, 2018, doi: 10.1038/s41598-018-26936-x.

[26] G. Vanier *et al.*, "Alga-Made Anti-Hepatitis B Antibody Binds to Human Fcγ Receptors," *Biotechnol. J.*, vol. 13, no. 4, pp. 1–10, 2018, doi: 10.1002/biot.201700496.

[27] J. A. Gregory and S. P. Mayfield, "Developing inexpensive malaria vaccines from plants and algae," *Appl. Microbiol. Biotechnol.*, vol. 98, no. 5, pp. 1983–1990, 2014, doi: 10.1007/s00253-013-5477-6.

[28] G. Potvin and Z. Zhang, "Strategies for high-level recombinant protein expression in transgenic microalgae: A review," *Biotechnol. Adv.*, vol. 28, no. 6, pp. 910–918, 2010, doi: 10.1016/j.biotechadv.2010.08.006.

[29] J. A. Gregory *et al.*, "Algae-produced pfs25 elicits antibodies that inhibit malaria transmission," *PLoS One*, vol. 7, no. 5, 2012, doi: 10.1371/journal.pone.0037179.

[30] S. Kumar, "GM Algae for Biofuel Production: Biosafety and Risk Assessment," *Collect. Biosaf. Rev.*, vol. 9, pp. 52–75, 2015.

[31] S. V. V. Bharadwaj, S. Ram, I. Pancha, and S. Mishra, "Recent Trends in Strain Improvement for Production of Biofuels From Microalgae," in *Microalgae Cultivation for Biofuels Production*, A. B. T.-M. C. for B. P. Yousuf, Ed. Elsevier, 2020, pp. 211–225.

[32] D. Eriksson *et al.*, "Scandinavian perspectives on plant gene technology: applications, policies and progress," *Physiol. Plant.*, vol. 162, no. 2, pp. 219–238, 2018, doi: 10.1111/ppl.12661.

[33] International service for the acquisition of agri-biotech Applications, "GM approval database," 2019. https://www.isaaa.org/gmapprovaldatabase/default.asp (accessed Jun. 12, 2019).

[34] Australian government Department of Health, "Table of authorisations for commercial releases of GM plants (subset of list of licences involving Intentional Release)," 2019. http://www.ogtr.gov.au/internet/ogtr/publishing.nsf/Content/cr-1 (accessed Jun. 13, 2019).

[35] R. Van Acker, M. Rahman, S. Z. H. Cici, R. Van Acker, M. Rahman, and S. Z. H. Cici, "Pros and Cons of GMO Crop Farming," *Oxford Res. Encycl. Environ. Sci.*, no. August, pp. 1–26, 2017, doi: 10.1093/acrefore/9780199389414.013.217.

[36] A. Spicer and A. Molnar, "Gene Editing of Microalgae: Scientific Progress and Regulatory Challenges in Europe," *Biology (Basel).*, vol. 7, no. 1, p. 21, Mar. 2018, doi: 10.3390/biology7010021.

[37] D. Eriksson *et al.*, "A comparison of the EU regulatory approach to directed mutagenesis with that of other jurisdictions, consequences for international trade and potential steps forward," *New Phytol.*, vol. 222, no. 4, pp. 1673–1684, 2019, doi: 10.1111/nph.15627.

[38] S. M. Schmidt, M. Belisle, and W. B. Frommer, "The evolving landscape around genome editing in agriculture," *EMBO Rep.*, vol. 21, no. 6, pp. 19–22, 2020, doi: 10.15252/embr.202050680.

[39] Office of Parliamentary Counsel Canberra, "Gene Technology Regulations 2001," 2016.

[40] R. R. Singhania, A. K. Patel, L. Thomas, M. Goswami, B. S. Giri, and A. Pandey, "Industrial Enzymes," in *Industrial Biorefineries & White Biotechnology*, A. Pandey, R. Höfer, M. Taherzadeh, K. M. Nampoothiri, and C. Larroche, Eds. Amsterdam: Elsevier, 2015, pp. 473–497.

[41] W. Fu *et al.*, "Algal cell factories: Approaches, applications, and potentials," *Mar. Drugs*, vol. 14, no. 12, pp. 1–19, 2016, doi: 10.3390/md14120225.

[42] Q. Shi *et al.*, "Transgenic eukaryotic microalgae as green factories: providing new ideas for the production of biologically active substances," *J. Appl. Phycol.*, Feb. 2021, doi: 10.1007/s10811-020-02350-7.

[43] L. Lin and Y. Luo, "Tracking CRISPR's Footprints," in *CRISPR Gene Editing*, 2019, pp. 13–28.

[44] European food safety authroity, "GMO," 2019. https://www.efsa.europa.eu/en/topics/topic/gmo (accessed Jun. 12, 2019).

[45] "A CRISPR definition of genetic modification.," *Nat. plants*, vol. 4, no. 5, p. 233, May 2018, doi: 10.1038/s41477-018-0158-1.

[46] Australian government Department of Health, "Record of GMO dealings," 2019. http://www.ogtr.gov.au/internet/ogtr/publishing.nsf/Content/gmorec-index-1 (accessed Aug. 14, 2019).

[47] Federation of American Scientists, "USDA Regulation of Pharma Crops," 2011. https://fas.org/biosecurity/education/dualuse-agriculture/2.-agricultural-biotechnology/usda-regulation-of-pharma-crops.html (accessed Aug. 08, 2019).

[48] R. Dronov and W. Howard, “Gene editing and CRISPR,” 2017.

[49] Australian Goverment Department of Health Office of the Gene Technology Regulator, “Technical Review of the Gene Technology Regulations 2001,” 2016.

[50] J. D. Wolt and C. Wolf, “Policy and Governance Perspectives for Regulation of Genome Edited Crops in the United States,” *Front. Plant Sci.*, vol. 9, no. November, pp. 1–12, Nov. 2018, doi: 10.3389/fpls.2018.01606.

[51] E. Waltz, “Gene-edited CRISPR mushroom escapes US regulation,” *Nature*, vol. 532, no. 7599, pp. 293–293, Apr. 2016, doi: 10.1038/nature.2016.19754.

[52] U.S. Department of Agriculture, “Petitions for Determination of Nonregulated Status,” 2019. https://www.aphis.usda.gov/aphis/ourfocus/biotechnology/permits-notifications-petitions/petitions/petition-status (accessed Aug. 23, 2019).

[53] PIC/S Secretariat, “Guide to Good Manufacturing Practice for Medicinal Products,” 2017.

[54] C. G. Lee, “Calculation of light penetration depth in photobioreactors,” *Biotechnol. Bioprocess Eng.*, vol. 4, no. 1, pp. 78–81, 1999, doi: 10.1007/BF02931920.

[55] H. Qiang and A. Richmond, “Productivity and photosynthetic efficiency of Spirulina platensis as affected by light intensity, algal density and rate of mixing in a flat plate photobioreactor,” *J. Appl. Phycol.*, vol. 8, no. 2, pp. 139–145, 1996, doi: 10.1007/BF02186317.

[56] A. P. Carvalho, L. A. Meireles, and F. X. Malcata, “Microalgal reactors: A review of enclosed system designs and performances,” *Biotechnol. Prog.*, vol. 22, no. 6, pp. 1490–1506, 2006, doi: 10.1021/bp060065r.

[57] S. Mobin and F. Alam, “Some Promising Microalgal Species for Commercial Applications: A review,” *Energy Procedia*, vol. 110, no. December 2016, pp. 510–517, 2017, doi: 10.1016/j.egypro.2017.03.177.

[58] P. Waller, R. Ryan, M. Kacira, and P. Li, “The algae raceway integrated design for optimal temperature management,” *Biomass and Bioenergy*, vol. 46, pp. 702–709, 2012, doi: 10.1016/j.biombioe.2012.06.025.

[59] R. D. Ryan, P. M. Waller, M. Kacira, and P. Li, “AQUACULTURE RACEWAY INTEGRATED DESIGN / US 8.245,440 B2,” 2012.

[60] B. Ketheesan and N. Nirmalakhandan, “Feasibility of microalgal cultivation in a pilot-scale airlift-driven raceway reactor,” *Bioresour. Technol.*, vol. 108, pp. 196–202, 2012, doi: 10.1016/j.biortech.2011.12.146.

[61] R. C. McBride *et al.*, “Contamination Management in Low Cost Open Algae Ponds for Biofuels Production,” *Ind. Biotechnol.*, vol. 10, no. 3, pp. 221–227, 2014, doi: 10.1089/ind.2013.0036.

[62] B. R. Holtz *et al.*, "Commercial-scale biotherapeutics manufacturing facility for plant-made pharmaceuticals," *Plant Biotechnol. J.*, vol. 13, no. 8, pp. 1180–1190, 2015, doi: 10.1111/pbi.12469.

[63] J. K.-C. Ma *et al.*, "Regulatory approval and a first-in-human phase I clinical trial of a monoclonal antibody produced in transgenic tobacco plants," *Plant Biotechnol. J.*, vol. 13, pp. 1106–1120, 2015, doi: 10.1111/pbi.12416.

[64] M. Sack *et al.*, "From gene to harvest: insights into upstream process development for the GMP production of a monoclonal antibody in transgenic tobacco plants," *Plant Biotechnol. J.*, vol. 13, no. 8, pp. 1094–1105, Oct. 2015, doi: 10.1111/pbi.12438.

[65] European Medicines Agency, "Guideline on the quality of biological active substances produced by stable transgene expression in higher plants," *Eur. Med. Agency Eval. Med. Hum. Use*, no. February, pp. 1–11, 2008, [Online]. Available: http://www.ema.europa.eu/docs/en_GB/document_library/Scientific_guideline/2009/09/WC500003154.pdf.

[66] J. Weissman and G. Radaelli, "Systems and methods for maintaining the dominance of Nannochloropsis in an algae cultivation system," US9187778B2, 2009.

[67] M. M. Loera-Quezada *et al.*, "A novel genetic engineering platform for the effective management of biological contaminants for the production of microalgae," *Plant Biotechnol. J.*, vol. 14, no. 10, pp. 2066–2076, 2016, doi: 10.1111/pbi.12564.

[68] Y. Tapia-Torres and G. Olmedo-Álvarez, "Life on Phosphite: A Metagenomics Tale," *Trends Microbiol.*, vol. 26, no. 3, pp. 170–172, 2018, doi: 10.1016/j.tim.2018.01.002.

[69] V. Bougault, J. Turmel, J. St-Laurent, M. Bertrand, and L.-P. Boulet, "Asthma, airway inflammation and epithelial damage in swimmers and cold-air athletes," *Eur. Respir. J.*, vol. 33, no. 4, pp. 740–746, Apr. 2009, doi: 10.1183/09031936.00117708.

[70] J. G. Day, S. P. Slocombe, and M. S. Stanley, "Overcoming biological constraints to enable the exploitation of microalgae for biofuels," *Bioresour. Technol.*, vol. 109, pp. 245–251, 2012, doi: 10.1016/j.biortech.2011.05.033.

[71] A. A. Snow and V. H. Smith, "Genetically Engineered Algae for Biofuels : A Key Role for Ecologists," *Bioscience*, vol. 62, no. 8, pp. 765–768, 2012, doi: 10.1525/bio.2012.62.8.9.

[72] R. H. Wijffels, *Biosafety and the Environmental Uses of Micro-Organisms*, no. 2012. OECD, 2015.

[73] S. J. Szyjka *et al.*, "Evaluation of phenotype stability and ecological risk of a genetically engineered alga in open pond production," *Algal Res.*, vol. 24, no. May, pp. 378–386, 2017, doi:

10.1016/j.algal.2017.04.006.

[74] K. J. Flynn, H. C. Greenwell, R. W. Lovitt, and R. J. Shields, "Selection for fitness at the individual or population levels: Modelling effects of genetic modifications in microalgae on productivity and environmental safety," *J. Theor. Biol.*, vol. 263, no. 3, pp. 269–280, 2010, doi: 10.1016/j.jtbi.2009.12.021.

[75] K. Motomura *et al.*, "Synthetic Phosphorus Metabolic Pathway for Biosafety and Contamination Management of Cyanobacterial Cultivation," *ACS Synth. Biol.*, vol. 7, no. 9, pp. 2189–2198, 2018, doi: 10.1021/acssynbio.8b00199.

[76] H. Čelešnik *et al.*, "Biosafety of biotechnologically important microalgae: intrinsic suicide switch implementation in cyanobacterium Synechocystis sp . PCC 6803," *Biol. Open*, vol. 5, no. 4, pp. 519–528, Apr. 2016, doi: 10.1242/bio.017129.

[77] T. G. Kimman, E. Smit, and M. R. Klein, "Evidence-Based Biosafety: a Review of the Principles and Effectiveness of Microbiological Containment Measures," *Clin. Microbiol. Rev.*, vol. 21, no. 3, pp. 403–425, Jul. 2008, doi: 10.1128/CMR.00014-08.

[78] W. J. Henley, R. W. Litaker, L. Novoveská, C. S. Duke, H. D. Quemada, and R. T. Sayre, "Initial risk assessment of genetically modi fi ed (GM) microalgae for commodity-scale biofuel cultivation ☆," *ALGAL*, vol. 2, no. 1, pp. 66–77, 2013, doi: 10.1016/j.algal.2012.11.001.

[79] J. C. Ogbonna, T. Soejima, and H. Tanaka, "An integrated solar and artificial light system for internal illumination of photobioreactors," *J. Biotechnol.*, vol. 70, no. 1–3, pp. 289–297, Apr. 1999, doi: 10.1016/S0168-1656(99)00081-4.

[80] M. Heining, A. Sutor, S. C. Stute, C. P. Lindenberger, and R. Buchholz, "Internal illumination of photobioreactors via wireless light emitters: a proof of concept," *J. Appl. Phycol.*, vol. 27, no. 1, pp. 59–66, 2014, doi: 10.1007/s10811-014-0290-x.

[81] S. Xue, Q. Zhang, X. Wu, C. Yan, and W. Cong, "A novel photobioreactor structure using optical fibers as inner light source to fulfill flashing light effects of microalgae," *Bioresour. Technol.*, vol. 138, pp. 141–147, 2013, doi: 10.1016/j.biortech.2013.03.156.

[82] A. K. Pegallapati and N. Nirmalakhandan, "Internally illuminated photobioreactor for algal cultivation under carbon dioxide-supplementation: Performance evaluation," *Renew. Energy*, vol. 56, pp. 129–135, 2013, doi: 10.1016/j.renene.2012.09.052.

[83] K. van't Riet and R. G. J. M. van der Lans, *Mixing in Bioreactor Vessels*, Second Edi., vol. 2. Elsevier B.V., 2011.

[84] M. R. Bilad, H. A. Arafat, and I. F. J. Vankelecom, "Membrane technology in microalgae cultivation and harvesting: A review," *Biotechnol. Adv.*, vol. 32, no. 7, pp. 1283–1300, Nov.

2014, doi: 10.1016/j.biotechadv.2014.07.008.

[85] C. Posten, "Design principles of photo-bioreactors for cultivation of microalgae," *Eng. Life Sci.*, vol. 9, no. 3, pp. 165–177, Jun. 2009, doi: 10.1002/elsc.200900003.

[86] R. Slade and A. Bauen, "Micro-algae cultivation for biofuels: Cost, energy balance, environmental impacts and future prospects," *Biomass and Bioenergy*, vol. 53, no. 0, pp. 29–38, 2013, doi: 10.1016/j.biombioe.2012.12.019.

[87] A. G. Lopes, "Single-use in the biopharmaceutical industry: A review of current technology impact, challenges and limitations," *Food Bioprod. Process.*, vol. 93, no. November, pp. 98–114, 2015, doi: 10.1016/j.fbp.2013.12.002.

[88] K. M. Jenkins, A. J. Vanderwielen, J. A. Armstrong, L. M. Leonard, G. P. Murphy, and N. A. Piros, "Application of total organic carbon analysis to cleaning validation.," *PDA J. Pharm. Sci. Technol.*, vol. 50, no. 1, pp. 6–15, Jan. 1996, [Online]. Available: http://journal.pda.org/content/50/1/6.abstract.

[89] R. Brecht, "Disposable Bioreactors: Maturation into Pharmaceutical Glycoprotein Manufacturing," in *Advances in Biochemical Engineering / Biotechnology*, vol. 115, 2009, pp. 1–31.

[90] J. B. Schultz, "Reaction to demand: Broad adoption of single-use bioreactors awaits fully scalable GMP systems, improved and less costly disposables, better analytics, greater process automation and low shear mixing," *Pharma*, pp. 26–34, 2011.

[91] T. Sandle and M. R. Saghee, "Some considerations for the implementation of disposable technology and single-use systems in biopharmaceuticals," *J. Commer. Biotechnol.*, vol. 17, no. 4, pp. 319–329, 2011, doi: 10.1057/jcb.2011.21.

[92] R. Jacquemart, M. Vandersluis, M. Zhao, K. Sukhija, N. Sidhu, and J. Stout, "A Single-use Strategy to Enable Manufacturing of Affordable Biologics," *Comput. Struct. Biotechnol. J.*, vol. 14, pp. 309–318, 2016, doi: 10.1016/j.csbj.2016.06.007.

[93] M. Pietrzykowski, W. Flanagan, V. Pizzi, A. Brown, A. Sinclair, and M. Monge, "An environmental life cycle assessment comparison of single-use and conventional process technology for the production of monoclonal antibodies," *J. Clean. Prod.*, vol. 41, pp. 150–162, 2013, doi: 10.1016/j.jclepro.2012.09.048.

[94] B. A. Sinclair, L. Leveen, M. Monge, J. Lim, and S. Cox, "The Environmental Impact of Disposable Technologies Can disposables reduce your facility's environmental," *BioPharm Int.*, pp. 1–11, 2008.

[95] T. Hahne, B. Schwarze, M. Kramer, and B. Frahm, "Disposable algae cultivation for high-value

products using all around LED-illumination directly on the bags," *J. Algal Biomass Util.*, vol. 5, no. 2, pp. 66–73, 2014.

[96] N. Lehmann, H. Rischer, D. Eibl, and R. Eibl, "Wave-mixed and orbitally shaken single-use photobioreactors for diatom algae propagation," *Chemie-Ingenieur-Technik*, vol. 85, no. 1–2, pp. 197–201, 2013, doi: 10.1002/cite.201200137.

[97] S. Cires, C. Alvarez-Roa, and K. Heimann, "First use of the WAVE disposable rocking bioreactor for enhanced bioproduct synthesis by N2-fixing cyanobacteria," *Biotechnol. Bioeng.*, vol. 112, no. 3, pp. 621–626, 2015, doi: 10.1002/bit.25455.

[98] S. Ahmad and A. U. Malik, "Corrosion behaviour of some stainless steels in chlorinated Gulf seawater," *J. Appl. Electrochem.*, vol. 31, no. 9, pp. 1009–1016, 2001, doi: 10.1023/A:1017945713331.

[99] Greenovation, "First preclinical data show full bioactivity of greenovations moss." www.greenovation.com (accessed Aug. 22, 2019).

[100] R. Reski, J. Parsons, and E. L. Decker, "Moss-made pharmaceuticals: From bench to bedside," *Plant Biotechnol. J.*, vol. 13, no. 8, pp. 1191–1198, 2015, doi: 10.1111/pbi.12401.

[101] N. Dorival-García *et al.*, "Large-Scale Assessment of Extractables and Leachables in Single-Use Bags for Biomanufacturing," *Anal. Chem.*, vol. 90, no. 15, pp. 9006–9015, Aug. 2018, doi: 10.1021/acs.analchem.8b01208.

[102] M. A. Jordi *et al.*, "Qualitative assessment of extractables from single-use components and the impact of reference standard selection," *J. Pharm. Biomed. Anal.*, vol. 150, pp. 368–376, Feb. 2018, doi: 10.1016/j.jpba.2017.12.029.

[103] ISPE, *Good Practice Guide: Single-Use Technology*. 2018.

[104] T. Sandle, *EU GMP Annex 1 : The New Draft and the Implications for Sterile Products Manufacturing*, no. April. 2020.

[105] C. Gustafsson, S. Govindarajan, and J. Minshull, "Codon bias and heterologous protein expression," *Trends Biotechnol.*, vol. 22, no. 7, pp. 346–353, 2004, doi: 10.1016/j.tibtech.2004.04.006.

[106] S. E. Franklin and S. P. Mayfield, "Prospects for molecular farming in the green alga Chlamydomonas reinhardtii," *Curr. Opin. Plant Biol.*, vol. 7, no. 2, pp. 159–165, 2004, doi: 10.1016/j.pbi.2004.01.012.

[107] S. Wu, L. Xu, R. Huang, and Q. Wang, "Improved biohydrogen production with an expression of codon-optimized hemH and lba genes in the chloroplast of Chlamydomonas reinhardtii," *Bioresour. Technol.*, vol. 102, no. 3, pp. 2610–2616, 2011, doi: 10.1016/j.biortech.2010.09.123.

[108] S. Purton, J. B. Szaub, T. Wannathong, R. Young, and C. K. Economou, "Genetic Engineering of Algal Chloroplasts: Progress and Prospects," *Russ. J. Plant Physiol.*, vol. 60, no. 4, pp. 491–499, 2013, doi: 10.7868/S0015330313040155.

[109] L. Doron, N. Segal, and M. Shapira, "Transgene Expression in Microalgae—From Tools to Applications," *Front. Plant Sci.*, vol. 7, no. April, pp. 1–24, Apr. 2016, doi: 10.3389/fpls.2016.00505.

[110] E. J. Kim, X. Ma, and H. Cerutti, "Gene silencing in microalgae: Mechanisms and biological roles," *Bioresour. Technol.*, vol. 184, pp. 23–32, 2015, doi: 10.1016/j.biortech.2014.10.119.

[111] M. Nymark, A. K. Sharma, T. Sparstad, A. M. Bones, and P. Winge, "A CRISPR/Cas9 system adapted for gene editing in marine algae," *Sci. Rep.*, vol. 6, no. 1, p. 24951, Jul. 2016, doi: 10.1038/srep24951.

[112] D. Stukenberg, S. Zauner, G. Dell'Aquila, and U. G. Maier, "Optimizing CRISPR/Cas9 for the Diatom Phaeodactylum tricornutum," *Front. Plant Sci.*, vol. 9, 2018, doi: 10.3389/fpls.2018.00740.

[113] A. K. Sharma, M. Nymark, T. Sparstad, A. M. Bones, and P. Winge, "Transgene-free genome editing in marine algae by bacterial conjugation – comparison with biolistic CRISPR/Cas9 transformation," *Sci. Rep.*, vol. 8, no. 1, p. 14401, Dec. 2018, doi: 10.1038/s41598-018-32342-0.

[114] K. H. Schneider, "GMP requirements for Master and Working Cell Bank," *Pharm. Ind.*, vol. 67, pp. 1366–1369, Jan. 2005.

[115] R. Taylor and R. L. Fletcher, "Cryopreservation of eukaryotic algae - A review of methodologies," *J. Appl. Phycol.*, vol. 10, no. 5, pp. 481–501, 1998, doi: 10.1023/A:1008094622412.

[116] D. Gonzalez-Ballester *et al.*, "Reverse genetics in Chlamydomonas: A platform for isolating insertional mutants," *Plant Methods*, vol. 7, no. 1, p. 24, 2011, doi: 10.1186/1746-4811-7-24.

[117] R. V. Kapoore *et al.*, "Effects of cryopreservation on viability and functional stability of an industrially relevant alga," *Sci. Rep.*, vol. 9, no. 1, p. 2093, Dec. 2019, doi: 10.1038/s41598-019-38588-6.

[118] F. Durrenberger, "Double strand break-induced recombination in Chlamydomonas reinhardtii chloroplasts," *Nucleic Acids Res.*, vol. 24, no. 17, pp. 3323–3331, Sep. 1996, doi: 10.1093/nar/24.17.3323.

[119] D. Guzmán-Zapata, K. S. Macedo-Osorio, A. L. Almaraz-Delgado, N. Durán-Figueroa, and J. A. Badillo-Corona, "Production of Recombinant Proteins in the Chloroplast of the Green Alga

Chlamydomonas reinhardtii," in *Methods in Molecular Biology*, vol. 1385, 2016, pp. 69–85.

[120] P. Neofotis, A. Huang, W. Chang, F. Joseph, and J. Polle, "Microalgae Strain Isolation, Screening, and Identification for Biofuels and High-Value Products," in *Microalgal Production for Biomass and High-Value Products*, CRC Press, 2016, pp. 63–89.

[121] J.-W. F. Zijffers, K. J. Schippers, K. Zheng, M. Janssen, J. Tramper, and R. H. Wijffels, "Maximum Photosynthetic Yield of Green Microalgae in Photobioreactors," *Mar. Biotechnol.*, vol. 12, no. 6, pp. 708–718, Nov. 2010, doi: 10.1007/s10126-010-9258-2.

[122] M. Benedetti, V. Vecchi, S. Barera, and L. Dall'Osto, "Biomass from microalgae: the potential of domestication towards sustainable biofactories," *Microb. Cell Fact.*, vol. 17, no. 1, p. 173, Dec. 2018, doi: 10.1186/s12934-018-1019-3.

[123] T. Granata, "Dependency of Microalgal Production on Biomass and the Relationship to Yield and Bioreactor Scale-up for Biofuels: a Statistical Analysis of 60+ Years of Algal Bioreactor Data," *Bioenergy Res.*, vol. 10, no. 1, pp. 267–287, 2017, doi: 10.1007/s12155-016-9787-2.

[124] S. Khanra, M. Mondal, G. Halder, O. N. Tiwari, K. Gayen, and T. K. Bhowmick, "Downstream processing of microalgae for pigments, protein and carbohydrate in industrial application: A review," *Food Bioprod. Process.*, vol. 110, pp. 60–84, 2018, doi: 10.1016/j.fbp.2018.02.002.

[125] J. F. Buyel and R. Fischer, "Flocculation increases the efficacy of depth filtration during the downstream processing of recombinant pharmaceutical proteins produced in tobacco," *Plant Biotechnol. J.*, vol. 12, no. 2, pp. 240–252, 2014, doi: 10.1111/pbi.12132.

[126] J. L. Corchero *et al.*, "Unconventional microbial systems for the cost-efficient production of high-quality protein therapeutics," *Biotechnol. Adv.*, vol. 31, no. 2, pp. 140–153, 2013, doi: 10.1016/j.biotechadv.2012.09.001.

[127] A. I. Barros, A. L. Gonçalves, M. Simões, and J. C. M. Pires, "Harvesting techniques applied to microalgae: A review," *Renew. Sustain. Energy Rev.*, vol. 41, pp. 1489–1500, 2015, doi: 10.1016/j.rser.2014.09.037.

[128] F. Fasaei, J. H. Bitter, P. M. Slegers, and A. J. B. van Boxtel, "Techno-economic evaluation of microalgae harvesting and dewatering systems," *Algal Res.*, vol. 31, no. November 2017, pp. 347–362, 2018, doi: 10.1016/j.algal.2017.11.038.

[129] B. G. Gouveia, P. Rijo, T. S. Gonçalo, and C. P. Reis, "Good manufacturing practices for medicinal products for human use," *J. Pharm. Bioallied Sci.*, vol. 7, no. 2, pp. 87–96, 2015, doi: 10.4103/0975-7406.154424.

[130] GE Healthcare Life Sciences, "Xcellerex™ XDR cell culture bioreactor systems, Data file 29-0929-25 AA," 2014.

[131] E. Specht, S. Miyake-Stoner, and S. Mayfield, "Micro-algae come of age as a platform for recombinant protein production," *Biotechnol. Lett.*, vol. 32, no. 10, pp. 1373–1383, 2010, doi: 10.1007/s10529-010-0326-5.

[132] L. A. Meireles, A. C. Guedes, C. R. Barbosa, J. L. Azevedo, J. P. Cunha, and F. X. Malcata, "On-line control of light intensity in a microalgal bioreactor using a novel automatic system," *Enzyme Microb. Technol.*, vol. 42, no. 7, pp. 554–559, Jun. 2008, doi: 10.1016/j.enzmictec.2007.12.002.

[133] G. Naderi, H. Znad, and M. O. Tade, "Investigating and modelling of light intensity distribution inside algal photobioreactor," *Chem. Eng. Process. Process Intensif.*, vol. 122, pp. 530–537, Dec. 2017, doi: 10.1016/j.cep.2017.04.014.

[134] M. D. Ooms, C. T. Dinh, E. H. Sargent, and D. Sinton, "Photon management for augmented photosynthesis," *Nat. Commun.*, vol. 7, p. 12699, 2016, doi: 10.1038/ncomms12699.

[135] J. Neidhardt, J. R. Benemann, L. Zhang, and A. Melis, "Photosystem-II repair and chloroplast recovery from irradiance stress: Relationship between chronic photoinhibition, light-harvesting chlorophyll antenna size and photosynthetic productivity in Dunaliella salina (green algae)," *Photosynth. Res.*, vol. 56, no. 2, pp. 175–184, 1998, doi: 10.1023/A:1006024827225.

[136] Q. Huang, F. Jiang, L. Wang, and C. Yang, "Design of Photobioreactors for Mass Cultivation of Photosynthetic Organisms," *Engineering*, vol. 3, no. 3, pp. 318–329, 2017, doi: 10.1016/J.ENG.2017.03.020.

[137] P. S. C. Schulze, L. A. Barreira, H. G. C. Pereira, J. A. Perales, and J. C. S. Varela, "Light emitting diodes (LEDs) applied to microalgal production," *Trends Biotechnol.*, vol. 32, no. 8, pp. 422–430, Aug. 2014, doi: 10.1016/j.tibtech.2014.06.001.

[138] T. de Mooij, G. de Vries, C. Latsos, R. H. Wijffels, and M. Janssen, "Impact of light color on photobioreactor productivity," *Algal Res.*, vol. 15, pp. 32–42, 2016, doi: 10.1016/j.algal.2016.01.015.

[139] R. J. Ritchie, A. W. D. Larkum, and I. Ribas, "Could photosynthesis function on Proxima Centauri b ?," *Int. J. Astrobiol.*, pp. 1–30, 2017, doi: 10.1017/S1473550417000167.

[140] E. Eroglu, P. K. Eggers, M. Winslade, S. M. Smith, and C. L. Raston, "Enhanced accumulation of microalgal pigments using metal nanoparticle solutions as light filtering devices," *Green Chem.*, vol. 15, pp. 3155–3159, 2013, doi: 10.1039/c3gc41291a.

[141] A. R. Grossman, M. Lohr, and C. S. Im, "Chlamydomonas reinhardtii in the landscape of pigments," *Annu. Rev. Genet.*, vol. 38, pp. 119–173, 2004, doi: 10.1146/annurev.genet.38.072902.092328.

[142] C.-H. Hung, K. Endo, K. Koichi, Y. Nakamura, and H. Wada, "Characterization of Chlamydomonas reinhardtii phosphatidylglycerophosphate synthase in Synechocystis sp . PCC 6803," *Front. Microbiol.*, vol. 6, no. August, p. 842, 2015, doi: 10.3389/fmicb.2015.00842.

[143] D. G. Kim, C. Lee, S. M. Park, and Y. E. Choi, "Manipulation of light wavelength at appropriate growth stage to enhance biomass productivity and fatty acid methyl ester yield using Chlorella vulgaris," *Bioresour. Technol.*, vol. 159, pp. 240–248, 2014, doi: 10.1016/j.biortech.2014.02.078.

[144] M. Hultberg, H. L. Jönsson, K. J. Bergstrand, and A. S. Carlsson, "Impact of light quality on biomass production and fatty acid content in the microalga Chlorella vulgaris," *Bioresour. Technol.*, vol. 159, pp. 465–467, 2014, doi: 10.1016/j.biortech.2014.03.092.

[145] K. Huang and C. F. Beck, "Phototropin is the blue-light receptor that controls multiple steps in the sexual life cycle of the green alga Chlamydomonas reinhardtii," *Proc. Natl. Acad. Sci. U. S. A.*, vol. 100, no. 10, pp. 6269–6274, 2003, doi: 10.1073/pnas.0931459100.

[146] Y. Zhao, J. Wang, H. Zhang, C. Yan, and Y. Zhang, "Effects of various LED light wavelengths and intensities on microalgae-based simultaneous biogas upgrading and digestate nutrient reduction process," *Bioresour. Technol.*, vol. 136, pp. 461–468, 2013, doi: 10.1016/j.biortech.2013.03.051.

[147] S. K. Wang, A. R. Stiles, C. Guo, and C. Z. Liu, "Microalgae cultivation in photobioreactors: An overview of light characteristics," *Eng. Life Sci.*, vol. 14, no. 6, pp. 550–559, 2014, doi: 10.1002/elsc.201300170.

[148] R. B. Rivkin, "Influence of irradiance and spectral quality on the carbon metabolism of phytoplankton. I. Photosynthesis, chemical composition and growth," *Mar. Ecol. Prog. Ser.*, vol. 55, pp. 291–304, 1989.

[149] A. Jungandreas, B. S. Costa, T. Jakob, M. Von Bergen, S. Baumann, and C. Wilhelm, "The acclimation of Phaeodactylum tricornutum to blue and red light does not influence the photosynthetic light reaction but strongly disturbs the carbon allocation pattern," *PLoS One*, vol. 9, no. 8, 2014, doi: 10.1371/journal.pone.0099727.

[150] P. Das, W. Lei, S. S. Aziz, and J. P. Obbard, "Enhanced algae growth in both phototrophic and mixotrophic culture under blue light," *Bioresour. Technol.*, vol. 102, no. 4, pp. 3883–3887, 2011, doi: 10.1016/j.biortech.2010.11.102.

[151] M. P. Sanchez-Saavedra, C. Jimenez, and F. L. Figueroa, "Far-red light inhibits growth but promotes carotenoid accumulation in the green microalga Duneliella bardawil," *Physiol. Plant.*, vol. 98, pp. 419–423, 1996.

[152] U. Schreiber, C. Klughammer, and J. Kolbowski, "Assessment of wavelength-dependent parameters of photosynthetic electron transport with a new type of multi-color PAM chlorophyll fluorometer," *Photosynth. Res.*, vol. 113, no. 1–3, pp. 127–144, Sep. 2012, doi: 10.1007/s11120-012-9758-1.

[153] B. D. Fernandes *et al.*, "Development of a novel user-friendly platform to couple light regime characterization with particle tracking - cells' light history determination during phototrophic cultivations," *Algal Res.*, vol. 24, no. April, pp. 276–283, 2017, doi: 10.1016/j.algal.2017.04.017.

[154] I. S. Suh and S. B. Lee, "A light distribution model for an internally radiating photobioreactor," *Biotechnol. Bioeng.*, vol. 82, no. 2, pp. 180–189, 2003, doi: 10.1002/bit.10558.

[155] A. Jacobi, C. Steinweg, R. R. Sastre, and C. Posten, "Advanced photobioreactor LED illumination system: Scale-down approach to study microalgal growth kinetics," *Eng. Life Sci.*, vol. 12, no. 6, pp. 621–630, 2012, doi: 10.1002/elsc.201200004.

[156] V. Loomba, G. Huber, and E. Von Lieres, "Single-cell computational analysis of light harvesting in a flat-panel photo-bioreactor," *Biotechnol. Biofuels*, vol. 11, no. 1, pp. 1–12, 2018, doi: 10.1186/s13068-018-1147-3.

[157] D. Fuente, J. Keller, J. A. Conejero, M. Rögner, S. Rexroth, and J. F. Urchueguía, "Light distribution and spectral composition within cultures of micro-algae: Quantitative modelling of the light field in photobioreactors," *Algal Res.*, vol. 23, pp. 166–177, 2017, doi: 10.1016/j.algal.2017.01.004.

[158] K. Kumar, A. Sirasale, and D. Das, "Use of image analysis tool for the development of light distribution pattern inside the photobioreactor for the algal cultivation," *Bioresour. Technol.*, vol. 143, pp. 88–95, 2013, doi: 10.1016/j.biortech.2013.05.117.

[159] T. C. Vogelmann and J. R. Evans, "Profiles of light absorption and chlorophyll within spinach leaves from chlorophyll fluorescence," *Plant. Cell Environ.*, vol. 25, no. 10, pp. 1313–1323, Oct. 2002, doi: 10.1046/j.1365-3040.2002.00910.x.

[160] A. Zavafer, H. Bates, L. Labeeuw, J. R. Kofler, and P. J. Ralph, "Normalized chlorophyll fluorescence imaging a method to determine irradiance and photosynthetically active radiation in phytoplankton cultures.," 2021.

[161] M. J. Griffiths, C. Garcin, R. P. van Hille, and S. T. L. Harrison, "Interference by pigment in the estimation of microalgal biomass concentration by optical density," *J. Microbiol. Methods*, vol. 85, no. 2, pp. 119–123, 2011, doi: 10.1016/j.mimet.2011.02.005.

[162] G. Govindjee and G. Papageorgiou, *Chlorophyll A Fluorescence: A Signature of Photosynthesis*,

no. January. 2004.

[163] J. Bialon and T. Rath, "Growth rates and photon efficiency of Chlorella vulgaris in relation to photon absorption rates under different LED-types," *Algal Res.*, vol. 31, no. February, pp. 204–215, 2018, doi: 10.1016/j.algal.2018.02.007.

[164] M. M. Margulies, "Changes in absorbance spectrum of the diatom Phaeodactylum tricornutum upon modification of protein structure," *J. Phycol.*, vol. 6, pp. 160–164, 1970.

[165] T. Le Costaouëc, C. Unamunzaga, L. Mantecon, and W. Helbert, "New structural insights into the cell-wall polysaccharide of the diatom Phaeodactylum tricornutum," *Algal Res.*, vol. 26, no. July, pp. 172–179, 2017, doi: 10.1016/j.algal.2017.07.021.

[166] R. R. L. Guillard, "Culture of Phytoplankton for Feeding Marine Invertebrates," in *Culture of Marine Invertebrate Animals*, 1975, pp. 29–60.

[167] C. A. Schneider, W. S. Rasband, and K. W. Eliceiri, "NIH Image to ImageJ: 25 years of image analysis," *Nat. Methods*, vol. 9, no. 7, pp. 671–675, 2012, doi: 10.1038/nmeth.2089.

[168] A. Stirbet and Govindjee, "The slow phase of chlorophyll a fluorescence induction in silico: Origin of the S–M fluorescence rise," *Photosynth. Res.*, vol. 130, no. 1–3, pp. 193–213, Dec. 2016, doi: 10.1007/s11120-016-0243-0.

[169] A. Zavafer, W. S. Chow, and M. H. Cheah, "The action spectrum of Photosystem II photoinactivation in visible light," *J. Photochem. Photobiol. B Biol.*, vol. 152, pp. 247–260, Nov. 2015, doi: 10.1016/j.jphotobiol.2015.08.007.

[170] I. IERMAK, M. SZABÓ, and A. ZAVAFER, "Special issue in honour of Prof. Reto J. Strasser - Analysis of OJIP transients during photoinactivation of photosystem II indicates the presence of multiple photosensitizers in vivo and in vitro," *Photosynthetica*, vol. 58, no. SPECIAL ISSUE, pp. 497–506, May 2020, doi: 10.32615/ps.2019.166.

[171] E. Tyystjärvi, "Photoinhibition of Photosystem II and photodamage of the oxygen evolving manganese cluster," *Coord. Chem. Rev.*, vol. 252, no. 3–4, pp. 361–376, 2008, doi: 10.1016/j.ccr.2007.08.021.

[172] J. C. Dunlap, O. Sostin, R. Widenhorn, and E. Bodegom, "Dark current behavior in DSLR cameras," in *Sensors, Cameras, and Systems for Industrial/Scientific Applications X*, Feb. 2009, vol. 7249, no. February, p. 72490N, doi: 10.1117/12.806128.

[173] R Core Team, "R: A Language and Environment for Statistical Computing." Vienna, Austria, 2019, [Online]. Available: https://www.r-project.org.

[174] C. Jurado-Verdu, V. Guerra, V. Matus, C. Almeida, and J. Rabadan, "Optical Camera Communication as an Enabling Technology for Microalgae Cultivation," *Sensors*, vol. 21, no.

5, p. 1621, Feb. 2021, doi: 10.3390/s21051621.

[175] B. D. Fernandes, G. M. Dragone, J. A. Teixeira, and A. A. Vicente, "Light regime characterization in an airlift photobioreactor for production of microalgae with high starch content," *Appl. Biochem. Biotechnol.*, vol. 161, no. 1–8, pp. 218–226, 2010, doi: 10.1007/s12010-009-8783-9.

[176] A. Richmond and Z. Cheng-Wu, "Optimization of a flat plate glass reactor for mass production of Nannochloropsis sp. outdoors," *J. Biotechnol.*, vol. 85, no. 3, pp. 259–269, 2001, doi: 10.1016/S0168-1656(00)00353-9.

[177] E. R. Mattos, M. Singh, M. L. Cabrera, and K. C. Das, "Enhancement of biomass production in Scenedesmus bijuga high-density culture using weakly absorbed green light," *Biomass and Bioenergy*, vol. 81, pp. 473–478, 2015, doi: 10.1016/j.biombioe.2015.07.029.

[178] J. E. Mann and J. Myers, "Photosynthetic Enhancement in the Diatom Phaeodactylum tricornutum.," *Plant Physiol.*, vol. 43, no. 1968, pp. 1991–1995, 1968, doi: 10.1104/pp.43.12.1991.

[179] H. Berberoglu, L. Pilon, and A. Melis, "Radiation characteristics of Chlamydomonas reinhardtii CC125 and its truncated chlorophyll antenna transformants tla1, tlaX and tla1-CW+," *Int. J. Hydrogen Energy*, vol. 33, no. 22, pp. 6467–6483, Nov. 2008, doi: 10.1016/j.ijhydene.2008.07.071.

[180] R. Kandilian, E. Lee, and L. Pilon, "Radiation and optical properties of Nannochloropsis oculata grown under different irradiances and spectra," *Bioresour. Technol.*, vol. 137, pp. 63–73, 2013, doi: 10.1016/j.biortech.2013.03.058.

[181] Y. Wang, D. J. Stessman, and M. H. Spalding, "The CO2 concentrating mechanism and photosynthetic carbon assimilation in limiting CO2: How Chlamydomonas works against the gradient," *Plant J.*, vol. 82, no. 3, pp. 429–448, 2015, doi: 10.1111/tpj.12829.

[182] F. Garcia-Ochoa and E. Gomez, "Bioreactor scale-up and oxygen transfer rate in microbial processes: An overview," *Biotechnol. Adv.*, vol. 27, no. 2, pp. 153–176, 2009, doi: 10.1016/j.biotechadv.2008.10.006.

[183] V. C. Srivastava, I. M. Mishra, and S. Suresh, *Oxygen Mass Transfer in Bioreactors*, Second Edi., vol. 2. Elsevier B.V., 2011.

[184] E. Kadic and T. J. Heindel, "Gas-Liquid Mass Transfer Models," in *An Introduction to Bioreactor Hydrodynamics and Gas-Liquid Mass Transfer*, Hoboken, NJ, USA: John Wiley & Sons, Inc., 2014, pp. 10–16.

[185] R. Putt, M. Singh, S. Chinnasamy, and K. C. Das, "An efficient system for carbonation of high-

rate algae pond water to enhance CO2 mass transfer," *Bioresour. Technol.*, vol. 102, no. 3, pp. 3240–3245, 2011, doi: 10.1016/j.biortech.2010.11.029.

[186] T. Temesgen, T. T. Bui, M. Han, T. il Kim, and H. Park, "Micro and nanobubble technologies as a new horizon for water-treatment techniques: A review," *Adv. Colloid Interface Sci.*, vol. 246, pp. 40–51, 2017, doi: 10.1016/j.cis.2017.06.011.

[187] W. Zimmerman, V. Tesar, S. Butler, and H. Bandulasena, "Microbubble Generation," *Recent Patents Eng.*, vol. 2, no. 1, pp. 1–8, Jan. 2008, doi: 10.2174/187221208783478598.

[188] T. il Kim, Y. ha Kim, and M. Han, "Development of novel oil washing process using bubble potential energy," *Mar. Pollut. Bull.*, vol. 64, no. 11, pp. 2325–2332, 2012, doi: 10.1016/j.marpolbul.2012.08.031.

[189] M. J. Barbosa, Hadiyanto, and R. H. Wijffels, "Overcoming Shear Stress of Microalgae Cultures in Sparged Photobioreactors," *Biotechnol. Bioeng.*, vol. 85, no. 1, pp. 78–85, 2004, doi: 10.1002/bit.10862.

[190] Y. Chisti, "Animal-cell damage in sparged bioreactors," *Trends Biotechnol.*, vol. 18, no. 10, pp. 420–432, Oct. 2000, doi: 10.1016/S0167-7799(00)01474-8.

[191] C. B. Alías, M. C. García-Malea López, F. G. Acién Fernández, J. M. Fernández Sevilla, J. L. García Sánchez, and E. Molina Grima, "Influence of power supply in the feasibility of Phaeodactylum tricornutum cultures," *Biotechnol. Bioeng.*, vol. 87, no. 6, pp. 723–733, 2004, doi: 10.1002/bit.20179.

[192] A. Kazbar *et al.*, "Effect of dissolved oxygen concentration on microalgal culture in photobioreactors," *Algal Res.*, vol. 39, no. January, p. 101432, 2019, doi: 10.1016/j.algal.2019.101432.

[193] D. Bilanovic, M. Holland, J. Starosvetsky, and R. Armon, "Co-cultivation of microalgae and nitrifiers for higher biomass production and better carbon capture," *Bioresour. Technol.*, vol. 220, pp. 282–288, 2016, doi: 10.1016/j.biortech.2016.08.083.

[194] T. Song, K. Jiang, J. Zhou, Z. Shen, and Y. Feng, "Cfd Impeller Speed Evaluation of an Industrial Scale Two-Phase," *11th Int. Conf. CFD Miner. Process Ind.*, no. December, pp. 1–5, 2015.

[195] J. Cheng, Z. Yang, Q. Ye, J. Zhou, and K. Cen, "Improving CO2 fixation with microalgae by bubble breakage in raceway ponds with up-down chute baffles," *Bioresour. Technol.*, vol. 201, pp. 174–181, 2016, doi: 10.1016/j.biortech.2015.11.044.

[196] M. Ndiaye, E. Gadoin, and C. Gentric, "CO 2 gas–liquid mass transfer and k L a estimation: Numerical investigation in the context of airlift photobioreactor scale-up," *Chem. Eng. Res.*

Des., vol. 133, no. 1998, pp. 90–102, May 2018, doi: 10.1016/j.cherd.2018.03.001.

[197] M. Raeisossadati, N. R. Moheimani, and D. Parlevliet, "Luminescent solar concentrator panels for increasing the efficiency of mass microalgal production," *Renew. Sustain. Energy Rev.*, vol. 101, no. November 2018, pp. 47–59, 2019, doi: 10.1016/j.rser.2018.10.029.

[198] A. Delafosse, S. Calvo, M. L. Collignon, and D. Toye, "Comparison of hydrodynamics in standard stainless steel and single-use bioreactors by means of an Euler-Lagrange approach," *Chem. Eng. Sci.*, vol. 188, pp. 52–64, 2018, doi: 10.1016/j.ces.2018.01.034.

[199] C. Wang and C. Q. Lan, "Effects of shear stress on microalgae – A review," *Biotechnol. Adv.*, vol. 36, no. 4, pp. 986–1002, 2018, doi: 10.1016/j.biotechadv.2018.03.001.

[200] A. Ellert and A. Grebe, "Process optimization made easy: design of experiments with multi-bioreactor system BIOSTAT® Qplus," *Nat. Methods*, vol. 8, no. 4, pp. i–ii, Apr. 2011, doi: 10.1038/nmeth.f.340.

[201] R. Bareither and D. Pollard, "A review of advanced small-scale parallel bioreactor technology for accelerated process development: Current state and future need," *Biotechnol. Prog.*, vol. 27, no. 1, pp. 2–14, Jan. 2011, doi: 10.1002/btpr.522.

[202] European Medicines Agency, "ICH Q11 on Development and Manufacture of Drug Substances (chemical entities and biotechnological/ biological entities)," 2012. [Online]. Available: www.ema.europa.eu.

[203] H. Noorman, "An industrial perspective on bioreactor scale-down: What we can learn from combined large-scale bioprocess and model fluid studies," *Biotechnol. J.*, vol. 6, no. 8, pp. 934–943, 2011, doi: 10.1002/biot.201000406.

[204] L. A. Palomares, A. R. Lara, and O. T. RamÍRez, "Bioreactor Scale-Down," in *Encyclopedia of Industrial Biotechnology*, vol. 7, Hoboken, NJ, USA: John Wiley & Sons, Inc., 2010.

[205] L. A. PALOMARES, A. R. LARA2, and O. T. RAM´IREZ, "BIOREACTOR SCALE-DOWN," in *Encyclopedia of Industrial Biotechnology: Bioprocess, Bioseparation, and Cell Technology*, vol. 3, no. 2, 2010.

[206] GE Healthcare, "Engineering characterization of the the single-use Xcellerex™ XDR-200 stirred-tank bioreactor system, 29268546 AA," 2017.

[207] N. T. Eriksen, "The technology of microalgal culturing," *Biotechnol. Lett.*, vol. 30, no. 9, pp. 1525–1536, Sep. 2008, doi: 10.1007/s10529-008-9740-3.

[208] K. Van't Riet, "Review of Measuring Methods and Results in Nonviscous Gas-Liquid Mass Transfer in Stirred Vessels," *Ind. Eng. Chem. Process Des. Dev.*, vol. 18, no. 3, pp. 357–364, Jul. 1979, doi: 10.1021/i260071a001.

[209] R. Higbie, "The rate of absorption of a pure gas into a still liquid during short periods of exposure," *Trans. Am. Inst. Chem. Eng*, vol. 31, pp. 365–388, 1935, [Online]. Available: https://books.google.be/books?id=vU3mmQEACAAJ.

[210] A. Contreras, F. García, E. Molina, and J. C. Merchuk, "Interaction between CO2-mass transfer, light availability, and hydrodynamic stress in the growth ofPhaeodactylum tricornutum in a concentric tube airlift photobioreactor," *Biotechnol. Bioeng.*, vol. 60, no. 3, pp. 317–325, Nov. 1998, doi: 10.1002/(SICI)1097-0290(19981105)60:3<317::AID-BIT7>3.0.CO;2-K.

[211] M. Jamnongwong, K. Loubiere, N. Dietrich, and G. Hébrard, "Experimental study of oxygen diffusion coefficients in clean water containing salt, glucose or surfactant: Consequences on the liquid-side mass transfer coefficients," *Chem. Eng. J.*, vol. 165, no. 3, pp. 758–768, 2010, doi: 10.1016/j.cej.2010.09.040.

[212] W. Klöckner *et al.*, "Correlation between mass transfer coefficient kLa and relevant operating parameters in cylindrical disposable shaken bioreactors on a bench-to-pilot scale," *J. Biol. Eng.*, vol. 7, no. 1, pp. 1–14, 2013, doi: 10.1186/1754-1611-7-28.

[213] C. Peña, C. P. Peter, J. Büchs, and E. Galindo, "Evolution of the specific power consumption and oxygen transfer rate in alginate-producing cultures of Azotobacter vinelandii conducted in shake flasks," *Biochem. Eng. J.*, vol. 36, no. 2, pp. 73–80, 2007, doi: 10.1016/j.bej.2007.02.019.

[214] M. P. C. Marques, J. M. S. Cabral, and P. Fernandes, "Bioprocess scale-up: Quest for the parameters to be used as criterion to move from microreactors to lab-scale," *J. Chem. Technol. Biotechnol.*, vol. 85, no. 9, pp. 1184–1198, 2010, doi: 10.1002/jctb.2387.

[215] A. Zhang, V. L. Tsang, R. Korke-Kshirsagar, and T. Ryll, "Effects of pH probe lag on bioreactor mixing time estimation," *Process Biochem.*, vol. 49, no. 6, pp. 913–916, 2014, doi: 10.1016/j.procbio.2014.03.005.

[216] C. J. Hulatt and D. N. Thomas, "Productivity, carbon dioxide uptake and net energy return of microalgal bubble column photobioreactors," *Bioresour. Technol.*, vol. 102, no. 10, pp. 5775–5787, 2011, doi: 10.1016/j.biortech.2011.02.025.

[217] G. Ascanio, "Mixing time in stirred vessels: A review of experimental techniques," *Chinese J. Chem. Eng.*, vol. 23, no. 7, pp. 1065–1076, 2015, doi: 10.1016/j.cjche.2014.10.022.

[218] P. Mavros, "Flow Visualization in Stirred Vessels," *Chem. Eng. Res. Des.*, vol. 79, no. 2, pp. 113–127, 2001, doi: 10.1205/02638760151095926.

[219] Y. Chisti and M. Moo-Young, "Improve the performance of airlift reactors," *Chemical Engineering Progress*, vol. 89, no. 6. pp. 38–45, 1993.

[220] D. Y. Hsiun and W. T. Wu, "Mass transfer and liquid mixing in an airlift reactor with a net draft

tube," *Bioprocess Eng.*, vol. 12, no. 5, pp. 221–225, 1995, doi: 10.1007/BF00369494.

[221] H. Zollner and R. Sablatnig, "A Method for Determining Geometrical Distortion of Off-The-Shelf Wide-Angle Cameras BT - Pattern Recognition," 2005, pp. 224–229.

[222] S. S. Sawant, H. P. Khadamkar, C. S. Mathpati, R. Pandit, and A. M. Lali, "Computational and experimental studies of high depth algal raceway pond photo-bioreactor," *Renew. Energy*, vol. 118, pp. 152–159, Apr. 2018, doi: 10.1016/j.renene.2017.11.015.

[223] J. C. Ogbonna and H. Tanaka, "Light requirement and photosynthetic cell cultivation – Development of processes for efficient light utilization in photobioreactors," *J. Appl. Phycol.*, vol. 12, pp. 207–218, 2000, doi: https://doi.org/10.1023/A:1008194627239.

[224] S. P. Singh and P. Singh, "Effect of temperature and light on the growth of algae species: A review," *Renew. Sustain. Energy Rev.*, vol. 50, pp. 431–444, 2015, doi: 10.1016/j.rser.2015.05.024.

[225] M. Huesemann *et al.*, "A validated model to predict microalgae growth in outdoor pond cultures subjected to fluctuating light intensities and water temperatures," *Algal Res.*, vol. 13, pp. 195–206, 2016, doi: 10.1016/j.algal.2015.11.008.

[226] C. U. Ugwu, H. Aoyagi, and H. Uchiyama, "Photobioreactors for mass cultivation of algae," *Bioresour. Technol.*, vol. 99, no. 10, pp. 4021–4028, 2008, doi: 10.1016/j.biortech.2007.01.046.

[227] S. Takahashi and N. Murata, "How do environmental stresses accelerate photoinhibition?," *Trends Plant Sci.*, vol. 13, no. 4, pp. 178–182, 2008, doi: 10.1016/j.tplants.2008.01.005.

[228] S. Abu-Ghosh, D. Fixler, Z. Dubinsky, and D. Iluz, "Flashing light in microalgae biotechnology," *Bioresour. Technol.*, vol. 203, pp. 357–363, 2016, doi: 10.1016/j.biortech.2015.12.057.

[229] K.-H. Park and C.-G. Lee, "Effectiveness of flashing light for increasing photosynthetic efficiency of microalgal cultures over a critical cell density," *Biotechnol. Bioprocess Eng.*, vol. 6, no. 3, pp. 189–193, Jun. 2001, doi: 10.1007/BF02932549.

[230] A. P. Carvalho, S. O. Silva, J. M. Baptista, and F. X. Malcata, "Light requirements in microalgal photobioreactors: An overview of biophotonic aspects," *Appl. Microbiol. Biotechnol.*, vol. 89, no. 5, pp. 1275–1288, 2011, doi: 10.1007/s00253-010-3047-8.

[231] P. S. C. Schulze *et al.*, "Flashing light does not improve photosynthetic performance and growth of green microalgae," *Bioresour. Technol. Reports*, vol. 9, no. October 2019, p. 100367, 2020, doi: 10.1016/j.biteb.2019.100367.

[232] J. U. Grobbelaar, "Turbulence in mass algal cultures and the role of light/dark fluctuations," *J. Appl. Phycol.*, vol. 6, no. 3, pp. 331–335, 1994, doi: 10.1007/BF02181947.

[233] G. Luzi, C. McHardy, C. Lindenberger, C. Rauh, and A. Delgado, "Comparison between different strategies for the realization of flashing-light effects – Pneumatic mixing and flashing illumination," *Algal Res.*, vol. 38, no. December 2018, p. 101404, 2019, doi: 10.1016/j.algal.2018.101404.

[234] J. Degen, A. Uebele, A. Retze, U. Schmid-Staiger, and W. Trösch, "A novel airlift photobioreactor with baffles for improved light utilization through the flashing light effect," *J. Biotechnol.*, vol. 92, no. 2, pp. 89–94, Dec. 2001, doi: 10.1016/S0168-1656(01)00350-9.

[235] M. J. Barbosa, M. Janssen, N. Ham, J. Tramper, and R. H. Wijffels, "Microalgae cultivation in air-lift reactors: Modeling biomass yield and growth rate as a function of mixing frequency," *Biotechnol. Bioeng.*, vol. 82, no. 2, pp. 170–179, 2003, doi: 10.1002/bit.10563.

[236] J. Huang *et al.*, "Improving performance of flat-plate photobioreactors by installation of novel internal mixers optimized with computational fluid dynamics," *Bioresour. Technol.*, vol. 182, pp. 151–159, 2015, doi: 10.1016/j.biortech.2015.01.067.

[237] I. Perner-Nochta and C. Posten, "Simulations of light intensity variation in photobioreactors," *J. Biotechnol.*, vol. 131, no. 3, pp. 276–285, 2007, doi: 10.1016/j.jbiotec.2007.05.024.

[238] H. C. P. Matthijs, H. Balke, U. M. Van Hes, B. M. A. Kroon, L. R. Mur, and R. A. Binot, "Application of light-emitting diodes in bioreactors: Flashing light effects and energy economy in algal culture (Chlorella pyrenoidosa)," *Biotechnol. Bioeng.*, vol. 50, no. 1, pp. 98–107, 1996, doi: 10.1002/(SICI)1097-0290(19960405)50:1<98::AID-BIT11>3.0.CO;2-3.

[239] J. C. M. Pires, M. C. M. Alvim-Ferraz, and F. G. Martins, "Photobioreactor design for microalgae production through computational fluid dynamics: A review," *Renew. Sustain. Energy Rev.*, vol. 79, no. November 2016, pp. 248–254, Nov. 2017, doi: 10.1016/j.rser.2017.05.064.

[240] J. P. Bitog *et al.*, "Application of computational fluid dynamics for modeling and designing photobioreactors for microalgae production: A review," *Comput. Electron. Agric.*, vol. 76, no. 2, pp. 131–147, May 2011, doi: 10.1016/j.compag.2011.01.015.

[241] A. K. Pegallapati and N. Nirmalakhandan, "Modeling algal growth in bubble columns under sparging with CO2-enriched air," *Bioresour. Technol.*, vol. 124, pp. 137–145, 2012, doi: 10.1016/j.biortech.2012.08.026.

[242] W. Blanken, P. R. Postma, L. de Winter, R. H. Wijffels, and M. Janssen, "Predicting microalgae growth," *Algal Res.*, vol. 14, pp. 28–38, 2016, doi: 10.1016/j.algal.2015.12.020.

[243] Y. S. Yun and J. M. Park, "Attenuation of monochromatic and polychromatic lights in Chlorella vulgaris suspensions," *Appl. Microbiol. Biotechnol.*, vol. 55, no. 6, pp. 765–770, 2001, doi:

10.1007/s002530100639.

[244] Y. Lei, J. Wang, and J. Wu, "Optimization of tubular microalgal photobioreactors with spiral ribs under single-sided and double-sided illuminations," *Processes*, vol. 7, no. 9, 2019, doi: 10.3390/pr7090619.

[245] P. Duhamel and M. Vetterli, "Fast fourier transforms: A tutorial review and a state of the art," *Signal Processing*, vol. 19, no. 4, pp. 259–299, 1990, doi: 10.1016/0165-1684(90)90158-U.

[246] J. C. Ogbonna, H. Yada, H. Masui, and H. Tanaka, "A novel internally illuminated stirred tank photobioreactor for large-scale cultivation of photosynthetic cells," *J. Ferment. Bioeng.*, vol. 82, no. 1, pp. 61–67, Jan. 1996, doi: 10.1016/0922-338X(96)89456-6.

[247] A. Bricaud and A. Morel, "Light attenuation and scattering by phytoplanktonic cells: a theoretical modeling," *Appl. Opt.*, vol. 25, no. 4, p. 571, Feb. 1986, doi: 10.1364/AO.25.000571.

[248] Q. Ye, J. Cheng, W. Guo, J. Xu, H. Li, and J. Zhou, "Numerical simulation on promoting light/dark cycle frequency to improve microalgae growth in photobioreactor with serial lantern-shaped draft tube," *Bioresour. Technol.*, vol. 266, no. June, pp. 89–96, 2018, doi: 10.1016/j.biortech.2018.06.055.

[249] A. Soman and Y. Shastri, "Optimization of novel photobioreactor design using computational fluid dynamics," *Appl. Energy*, vol. 140, pp. 246–255, 2015, doi: 10.1016/j.apenergy.2014.11.072.

[250] C. Brindley, F. G. Acién Fernández, and J. M. Fernández-Sevilla, "Analysis of light regime in continuous light distributions in photobioreactors," *Bioresour. Technol.*, vol. 102, no. 3, pp. 3138–3148, 2011, doi: 10.1016/j.biortech.2010.10.088.

[251] P. S. C. Schulze, R. Guerra, H. Pereira, L. M. Schüler, and J. C. S. Varela, "Flashing LEDs for Microalgal Production," *Trends Biotechnol.*, vol. 35, no. 11, pp. 1088–1101, 2017, doi: 10.1016/j.tibtech.2017.07.011.

[252] E. Lee, M. Jalalizadeh, and Q. Zhang, "Growth kinetic models for microalgae cultivation: A review," *Algal Res.*, vol. 12, pp. 497–512, 2015, doi: 10.1016/j.algal.2015.10.004.